



Norwegian University of
Science and Technology

Design and Optimization of Mooring Systems for Floating Wind Turbines

Rémi Marcel Borlet

Marine Technology

Submission date: June 2016

Supervisor: Kjell Larsen, IMT

Co-supervisor: Rune Yttervik, Statoil ASA

Norwegian University of Science and Technology
Department of Marine Technology



MASTER THESIS SPRING 2016

for

Stud. tech. Remi Marcel Borlet

Design and optimization of mooring systems for floating wind turbines

Design og optimalisering av forankringssystemer for flytende vindturbiner

Background

The purpose of the mooring system is to keep the floating wind turbine safely at a required position. It normally consists of three mooring lines of chain

The importance of the mooring system for a floating wind turbine is crucial. The moorings must be reliable enough to prevent any free drift where cable rupture and collisions are typical consequences and the cost of mooring must be as low as possible in order to make such developments profitable. Optimization of the mooring system is therefore an important task.

The overall objective of this thesis is to assess different design methods for moorings of floating wind turbines and to compare different mooring options. The HYWIND DEMO floating turbine shall be assessed in this thesis.

Analysis methods for estimating ultimate mooring line tension and vessel offset can be divided into frequency domain (FD) methods and time domain (TD) methods. Using FD methods, the low frequency (LF) load effects and the wave frequency (WF) load effects are analysed separately and then combined into characteristic values used in recipes for ULS and ALS design. The dynamic system describing the behavior of the vessel must be linearized and the maxima of vessel motions and line tensions are usually assumed to be statistically distributed according to the Rayleigh distribution. Sometimes empirical corrections for non-Rayleigh distributions are, however, performed. When using TD methods, all non-linearities in the dynamic system (stiffness and damping) and in the excitation may be taken into account. The first part of the thesis shall be to establish a TD model for the HYWIND DEMO and run selected cases in order to compare results with the FD models established in the project work. The second part shall focus on mooring system design with focus on improvement and reduction of cost using mooring line components of synthetic fibre.

Scope of Work

- 1) Establish and describe a coupled RIFLEX-SIMO time domain analysis model for HYWIND DEMO in the SIMA user interface.
- 2) Select cases for appropriate wind velocities and corresponding operation modes for the turbine. Compare TD and FD analysis results for turbine offsets and mooring line tensions. Discuss the observations and propose any improvements to the FD model.
- 3) Describe the tension-elongation behavior of synthetic ropes based on a literature review of relevant work performed for polyester and nylon fibre ropes.
- 4) Propose a mooring system configuration based on synthetic fibre ropes for the existing HYWIND DEMO wind turbine and compare with “as is”.
- 5) Perform a brief feasibility study on fibre mooring of HYWIND DEMO in water depths towards 100m
- 6) Conclusions and recommendations for further work.

General information

The work scope may prove to be larger than initially anticipated. Subject to approval from the supervisor, topics may be reduced in extent.

In the project the candidate shall present her's/his personal contribution to the resolution of problems within the scope of work.

Theories and conclusions should be based on mathematical derivations and/or logic reasoning identifying the various steps in the deduction.

The candidate should utilise the existing possibilities for obtaining relevant literature.

Thesis format

The thesis should be organised in a rational manner to give a clear exposition of results, assessments, and conclusions. The text should be brief and to the point, with a clear language. Telegraphic language should be avoided.

The thesis shall be written in English and edited as a research report including scope, preface, list of contents, summary, main body of thesis, conclusions with recommendations for further work, list of symbols and acronyms, references and (optional) appendices. All figures, tables and equations shall be numerated.

The supervisor may require that the candidate, in an early stage of the work, presents a written plan for the completion of the work.

The original contribution of the candidate and material taken from other sources shall be clearly defined. Work from other sources shall be properly referenced using an acknowledged referencing system.

The report shall be submitted in two copies:

- Signed by the candidate
- The text defining the scope included
- In bound volume(s)
- Drawings and/or computer prints which cannot be bound should be organised in a separate folder.

Ownership

NTNU has normally according to the present rules the ownership of the project results. But for this case, since the HYWIND DEMO is Statoil property, a confidentiality agreement must be signed.

Thesis supervisor:

Prof. II Kjell Larsen, NTNU/Statoil
Co-supervisor : Rune Yttervik, Statoil

Deadline: July 7th, 2016

Trondheim, June 26th, 2016

Kjell Larsen:



Remi Borlet:



Abstract

Hywind Demo is the world's first full scale floating offshore wind turbine, developed and operated by Statoil ASA. Throughout this thesis, a time domain model of Hywind Demo is used to design an optimized mooring system which can reduce the overall cost of floating wind turbines.

This thesis describes different mooring system design ideas, consisting of commonly used configurations such as catenary and taut mooring, and a less common configuration which uses buoyancy elements to increase the length of a fibre rope and increase flexibility without increasing the footprint.

Rules and regulations that govern the design of the mooring system for a floating offshore wind turbine are described to their full extent with respect to ULS, ALS and FLS.

In accordance with the rules and regulations, two environmental conditions were established. These correspond to rated wind velocity for the wind turbine and 50-year storm. For these two conditions the significant wave height and peak period; current velocity; and wind velocity were determined.

A time domain model of Hywind Demo with catenary mooring is established in SIMO-RIFLEX through SIMA, this model is compared against a correlating frequency domain model in MIMOSA. The results show that the SIMO-RIFLEX model and MIMOSA model are in correspondence, and that the MIMOSA model yield more conservative results.

With the aim of maintaining the station keeping properties of the catenary system, several fibre mooring designs were investigated, including plain taut mooring; fibre mooring with clump weights; and fibre mooring with buoyancy elements. It was found that by combining the elasticity of fibre ropes of 1000 m with the geometric flexibility added by a buoy with 30 t net buoyancy, the same restoring properties as the catenary system was achieved. Environmental response analyses on the fibre mooring system was conducted, verifying it's applicability and compliance with the governing rules and regulations.

The proposed fibre mooring system results in a cost reduction of 70% and a weight reduction of 60% for the mooring system, while maintaining similar floater motion responses, mooring utilization factors and footprint as the original, catenary mooring system.

A brief study on the use of fibre mooring in 130 m water depth was performed with regard to Statoil ASA's proposed relocation of Hywind Demo. The study yielded positive results, and the utilization of the fibre mooring system in shallow water is seen to be feasible, though further investigation should be performed.

Sammendrag

Hywind Demo er verdens første fullskala flytende vindturbin, utviklet og operert av Statoil ASA. Denne masteroppgaven tar i bruk en tidsplanmodell av Hywind Demo for å designe et optimalisert forankringssystem for flytende vindturbiner, som kan redusere den totale kostnaden av slike konstruksjoner.

Det er beskrevet ulike alternativer for forankring, inkludert ofte brukte systemer slik som slakk forankring og rene fibersystemer, og mindre brukte systemer slik som fibertau med klumpvekter eller flyteelementer som bidrar til geometrisk fleksibilitet.

Regelverk, gitt av Det Norske Veritas, for forankring av flytende vindturbiner er beskrevet i sin helhet med tanke på ULS, ALS og FLS. I henhold til regelverket er sjø-, strøm- og vindkondisjonen for to miljøforhold etablert, korresponderende til "rated" vindhastighet for vindturbinen og 50-års storm.

En tidsplanmodell av Hywind Demo med slakk forankring, tilsvarende dagens situasjon, er definert i SIMO-RIFLEX gjennom SIMA. Denne modellen er brukt i en sammenligning med en tilsvarende frekvensplanmodell i MIMOSA. Det er konkludert med at de to modellene gir korrelerende resultater, og at MIMOSA har mer konservative beregninger.

Med mål om å opprettholde egenskapene til det opprinnelige forankringssystemet ble flere ulike systemer baster på fibertau analysert. Dette inkluderte rene fibertausystemer og fibertau med enten klumpvekter eller flytelementer. Gjennom disse analysene ble det funnet at et system med taulengde på 1000 m og flyteelementer med 30 t oppdrift gir en kombinasjon av elastisk stivhet og geometrisk fleksibilitet som resulterer i samme stivhet som den opprinnelige forankringen. Dette forankringssystemet ble brukt i en analyse med de to miljøforholdene, og det ble verifisert at dette systemet gir ønsket systemrespons og at det er i henhold til regelverket.

Det foreslåtte fibertausystemet gir en kostnadsreduksjon på 70%, og reduserer vekten av forankringen med 60%. Det gir tilsvarende systemrespons, utnyttelsesgrad og horisontal utstrekning som slakk forankring.

En kort studie på bruk av det foreslåtte fibersystemet på 130 m vandyp er utført med bakgrunn i Statoil ASA sitt ønske om å flytte Hywind Demo til en annen plassering. Resultatene av studien er positive og det er sett på som gjennomførbart å bruke fibertausystemet på grunnere vann selv om ytterligere undersøkelser må gjøres.

Preface

This thesis has been carried out at the Department of Marine Technology at the Norwegian University of Science and Technology, and is the final work in a two-year master program, resulting in the degree Master of Science. This thesis was written during the spring semester of 2016 and comprises all 30 credits that forms the 10th term of the education plan.

The assignment has been to propose an optimized mooring system for the floating off-shore wind turbine, Hywind Demo, in order to reduce the overall cost of the system. The topic was provided by Rune Yttervik at Statoil ASA. My gratitude goes to Rune for the opportunity to work on this highly inspiring project.

I would also like to thank my supervisor, Kjell Larsen, who has provided excellent guidance, assistance and tutoring.

Finally, I would like to thank my fellow students in Trondheim for our time together, especially Mikal H. Espedal, Einar Lunde, Mohibb G. Malik, Jon C. Mossige and Petter A. Tvedt, who I have shared office with.



Rémi Marcel Borlet
Trondheim, June 26, 2016

Table of Contents

Table of Contents	xiv
List of Tables	xvi
List of Figures	xx
1 Introduction	25
1.1 Motivation	25
1.2 Previous work	26
2 Mooring system designs	27
2.1 Introduction	27
2.2 Mooring line components	27
2.2.1 Line materials	27
2.2.2 Line accessories	28
2.2.3 Anchors	29
2.3 Mooring system configurations	31
2.3.1 Slack mooring	31
2.3.2 Mooring with clump weights	32
2.3.3 Taut mooring with fibre rope	33
2.3.4 Fibre rope with buoyancy elements	34
2.4 Yaw stiffness	34
3 Hywind Demo	37
3.1 Introduction	37
3.2 Structural description	37
3.3 Mooring system	39
4 Rules and regulations	41
4.1 Ultimate and accidental loads	41
4.2 Resistance	43

4.3	Design criteria	43
4.3.1	ULS	43
4.3.2	ALS	43
4.3.3	FLS	44
5	Environmental loads on floating offshore wind turbines	45
5.1	Introduction	45
5.2	Wave forces	46
5.3	Current force	47
5.4	Wind force	48
5.5	Thrust force	49
5.6	Stiffness	50
5.6.1	Mooring stiffness	50
5.6.2	Hydrostatic stiffness	51
5.7	Damping	51
5.8	Inertia	52
6	Tension-elongation of sythetic fibre ropes	53
6.1	Introduction	53
6.2	Spring-dashpot model	53
6.3	Simplified, linear stiffness	56
7	SIMA and applied theory	61
7.1	Introduction	61
7.2	RIFLEX	61
7.2.1	Non-linear time domain simulation	62
7.2.2	Beam and bar elements	63
7.2.3	Blade element momentum	64
7.3	Dynamic time domain integration	73
7.4	SIMO	75
7.5	Statistics	75
7.5.1	Mean and standard deviation	75
7.5.2	Response confidence interval	75
7.5.3	Extreme value distribution	76
8	Establishment of Environmental Conditions	79
8.1	Introduction	79
8.2	Environmental data	79
8.3	Rated wind speed	82
8.4	50-year wind speed	82
8.5	Resulting environmental conditions	83
9	SIMO-RIFLEX Model	85
9.1	Modelling of spar and tower	85
9.1.1	Drag force coefficients	88
9.1.2	Added mass coefficients	90

9.2	Skin friction/Yaw damping	91
9.3	Polar moment of inertia of spar and tower	92
9.4	Modelling of wind turbine generator	92
9.5	Modelling of Mooring lines	95
9.6	Decay tests	96
10	Response analysis of original mooring system	99
10.1	Analytical differences between MIMOSA and SIMO-RIFLEX	100
10.2	MIMOSA results	101
10.3	SIMA results	102
10.3.1	Mean values	102
10.3.2	Maximum values	104
10.3.3	Comparison and discussion MIMOSA/SIMA	107
10.3.4	Surge and tension spectra	108
10.4	DNV compliance	109
11	Fibre rope mooring system design for Hywind Demo	111
11.1	Introduction	111
11.2	Goal	112
11.3	Stiffness combination	112
11.4	Challenges	114
11.4.1	Fibre rope challenges	114
11.4.2	Clump weight challenges	115
11.4.3	Buoys challenges	115
11.4.4	Summary of challenges	115
11.5	Investigation of line characteristics	115
11.5.1	Plain taut mooring	116
11.5.2	Taut mooring with clump weights	119
11.5.3	Taut mooring with buoyancy elements	121
11.5.4	Buoy size and position sensitivity test	126
11.6	Decay test	128
12	Response analysis of fibre mooring system	131
12.1	Environmental simulations	131
12.1.1	Mean values	131
12.1.2	Max values	133
12.2	Surge and tension spectra	135
12.3	Leeward line behaviour	136
12.4	DNV compliance	137
13	Comparison of mooring systems, additional aspects and discussion of results	139
13.1	Introduction	139
13.2	Natural periods and damping	140
13.3	Response comparisons	142
13.3.1	Surge	147
13.3.2	Heave	148

13.3.3	Pitch	149
13.3.4	Line tension	149
13.3.5	Distributions of largest maxima	150
13.3.6	Rotor air gap investigation	151
13.4	Leeward line of fibre mooring	151
13.5	Economic comparison	152
13.6	Footprint	154
13.7	Limitations to the analyses	154
14	Fibre mooring of Hywind Demo at 130m water depth	155
14.1	Introduction	155
14.2	Challenges	156
14.3	Design	156
14.4	Natural periods and damping	158
14.5	Feasibility	160
15	Conclusions and recommendations	161
15.1	Concluding remarks	161
15.2	Recommendation for further work	162
	Appendices	167
A	Bridle details	169
B	Original mooring response samples	171
C	Fibre mooring response samples	173

List of Tables

4.1	Load factor requirements for design of mooring lines	42
4.2	Design fatigue factors (DNV-OS-J103 2013)	44
6.1	Lanhorst Rope’s data of stiffness as a function of cyclic tension (Lankhorst Ropes 2015)	59
8.1	Current return periods corresponding to different wind velocities (DNV-OS-J103 2013)	80
8.2	Omni-directional extremes for the 10 minutes mean current speed (cm/s) versus depth for 1-, 10- and 100-year return period. Weibull parameters are given for 3 m above seabed. (Statoil 2004)	80
8.3	Sea states to be examined	83
9.1	Structural parameters for spar and tower	88
9.2	Numerical calculation of wind drag coefficient	89
9.3	Numerical calculation of water drag coefficient	90
9.4	KC number at top, middle and bottom of the spar with their respective diameters (including marine growth)	91
9.5	Mooring line input data to SIMA for Hywind Demo original mooring system	95
9.6	Mooring line drag coefficients for Hywind Demo original mooring system (DNV-OS-E301 2013)	96
9.7	Natural period of SIMO-RIFLEX model and full scale version	98
10.1	Equilibrium position in surge, heave and pitch	101
10.2	Wave frequency motions	101
10.3	Low frequency motions	101
10.4	Top tension of Line 3	102
10.5	Mimosa Results	102
10.6	Mean values and standard deviation for motions and line tension for rated and 50-year environment from time-domain simulations	104

10.7	Maximum values for surge, heave, pitch and line tension for rated and 50-year environment from time-domain simulations	106
10.8	Pitch response in 50-year environment with and without wind loads	108
11.1	Drag coefficients for fibre rope (DNV-OS-E301 2013)	117
11.2	Drag coefficients for in-line clump weight (based on DNV-OS-E301 2013)	119
11.3	Drag coefficients for rectangles in steady flow (DNV-RP-C205 2010)	122
11.4	Added mass coefficients for square prisms in steady flow (DNV-RP-C205 2010)	123
11.5	Possible taut mooring combinations with buoy	124
11.6	Combination 1 parameters	128
11.7	Natural period of Hywind Demo with fibre rope mooring system	129
12.1	Mean values and standard deviation for motions and line tension for rated and 50-year environment for fibre mooring	133
12.2	Maximum values for surge, heave, pitch and line tension for rated and 50-year environment for fibre mooring	135
12.3	Leeward buoy vertical position in 50-year environment	137
12.4	Leeward line tension in 50-year environment	137
13.1	Comparison of natural periods, original and fibre mooring	140
13.2	Comparison of damping coefficients, original and fibre mooring	141
13.3	Coefficient of variation, original mooring	150
13.4	Coefficient of variation, fibre mooring	150
13.5	Mean and standard deviation of air-gap process	151
13.6	Cost of mooring system elements	152
13.7	Cost of original mooring system	152
13.8	Cost of fibre rope mooring system with buoy	153
14.1	Natural period of Hywind Demo with fibre rope mooring system in 130 m water depth	159
14.2	Comparison of damping coefficients, original and fibre mooring	160
B.1	Response samples for Hywind Demo original mooring configuration	171
C.1	Response samples for Hywind Demo fibre mooring configuration	173

List of Figures

2.1	Sheated spiral strand rope (Bridon)	28
2.2	Six strand rope (Bridon)	28
2.3	Fibre rope (Larsen 2015)	28
2.4	Clumpweights attached to chain (AMC)	29
2.5	Byouancy elements (AMC)	29
2.6	Fluke anchor (Vryhof)	29
2.7	Plate anchor (Vryhof)	30
2.8	Suction anchor (Semar)	30
2.9	Deep penetrating anchor of 75 t (Deep Sea Anchors)	31
2.10	Slack mooring (Larsen 2015)	32
2.11	Slack mooring with clump weight (Larsen 2015)	32
2.12	Taut mooring (Larsen 2015)	33
2.13	Mooring with bouyancy elements (Larsen 2015)	34
2.15	Yaw stiffness from bridle (DNV-RP-H103 2014, modified)	35
2.14	Bridle configuration as seen from above (Moxnes 2009)	35
3.1	Structural drawing of Hywind Demo. The spar and tower are not drawn to scale. (Godø 2013)	38
3.2	Schematic drawing of a single mooring line on Hywind Demo (Godø 2013)	39
4.1	Most probable maximum in extreme value distribution (DNV-OS-E301 2013)	42
5.1	Wave particle velocity profile	47
5.2	Example of current particle velocity profile	48
5.3	Wind shear profile	48
5.4	Wind velocity spectrum (Green Rhino Energy, modified)	49
5.5	50
6.1	Spring-dashpot model for synthetic fibre rope (Flory, Ahjem, and Banfield 2007)	54

6.2	Harmonic and irregular tension tests, each test drawn in different colour (Falkenberg et al. 2011)	56
6.3	Working curves dependant on maximum tension history (Falkenberg et al. 2011)	57
6.4	Constant stiffness based on historic maximum tension	58
7.1	Definition of line, segment and element in RIFLEX (Godø 2013)	62
7.2	Beam element in RIFLEX (MARINTEK 2015)	64
7.3	Control volume shaped as an annular ring to be used in the BEM model (Hansen 2015)	65
7.4	66
7.5	69
7.6	Tower shadow coordinate system (MARINTEK 2015)	72
7.7	Constant average acceleration (Larsen 2014, modified)	74
7.8	Discrete and continous solution (Larsen 2014, modified)	75
7.9	95% confidence interval of a normal distribution (Hagen 2007, modified)	76
7.10	Broad banded process. O = local maxima, X= zero up-crossing (Myrhaug 2005)	77
7.11	Generation of extreme value distribution from processes (Larsen 2014)	77
8.1	All-year wind speed distribution at Heidrun (Statoil 2004)	81
8.2	Marginal (all year) distribution for the significant wave height at Heidrun (Statoil 2004)	81
8.3	Conditional characteristics for the spectral peak period versus significant wave height at Heidrun (Statoil 2004)	82
8.4	JONSWAP spectra for rated and 50-year environment	83
8.5	ISO wind spectra for rated and 50-year environment	84
9.1	Line 1, marked with pink color	86
9.2	Line 2, marked with pink color	87
9.3	SIMO bodies used in corporation with the RIFLEX model, visualized as red boxes	87
9.4	Drag coefficients for fixed circular cylinder for steady flow in critical flow regime for varying roughnesses (DNV-RP-C205 2010)	89
9.5	Mass coefficient as function of KC-number for smooth (solid line) and rough (dotted line) cylinder (DNV-RP-C205 2010)	90
9.6	Aerodynamic coefficients for airfoil segment 10 as a function of angle of attack	93
9.7	Rotor thrust force as a function of wind velocity	94
9.8	Generator power as a function of wind velocity	94
9.9	Blade pitch angle as a function of wind velocity	94
9.10	Rotor thrust force give in Bjørnsen 2015	95
9.11	Single mooring line characteristics for original mooring system	96
9.12	Decay tests, measured at center of gravity	97
9.13	Coordinate system for decay tests	97

10.1	Coordinate system used for response analysis	99
10.2	Time series of surge motion, original mooring	103
10.3	Time series of heave motion, original mooring	103
10.4	Time series of pitch motion, original mooring	103
10.5	Time series of line tension, original mooring	104
10.6	PDF of largeste maxima, surge, original mooring	105
10.7	PDF of largeste maxima, heave, original mooring	105
10.8	PDF of largeste maxima, pitch, original mooring	106
10.9	PDF of largeste maxima, line tension, original mooring	106
10.10	Response comparioson between MIMOSA and SIMA	107
10.11	Sepctrum of surge motion, rated environment, original mooring	108
10.12	Sepctrum of surge motion, 50-year environment, original mooring	109
10.13	Spectrum of line tension, rated environment, original mooring	109
11.1	Combination of elastic and geometric stiffness	113
11.2	Fibre rope subjected to large compression forces (Smith 2011)	114
11.3	Pretension aquired by anchor position	116
11.4	Line characteristics of plain taut mooring	118
11.5	Taut mooring with line on bottom, subjected to 1000 kN, orthographic view	119
11.6	Clump weight made of chains	120
11.7	Example of 2: 1 ratio of fibre mooring line on each side of a clump weight	120
11.8	Mooring buoyancy elements (Lankhorst Mouldings)	121
11.9	Example of 1: 2 ratio of fibre mooring line on each side of a bouyancy element	122
11.10	Isotropic view of combination 1 without horizontal load	125
11.11	Orthographic view of combination 1 at 3000 kN horizontal load	125
11.12	Orthographic view of combination 2 at 2000 kN horizontal load	125
11.13	Orthographic view of combination 4 at 2000 kN horizontal load	126
11.14	Single line characteristics of combination 1	126
11.15	Single line characteristics of taut mooring with 53 m ³ buoy	127
11.16	Orthographic view of taut mooring with 53 m ³ buoy without horizontal load	128
11.17	Decay tests, measured at center of gravity	129
12.1	Time series of surge motion, fibre mooring	132
12.2	Time series of heave motion, fibre mooring	132
12.3	Time series of pitch motion, fibre mooring	132
12.4	Time series of line tension, fibre mooring	133
12.5	PDF of largeste maxima, surge, fibre mooring	133
12.6	PDF of largeste maxima, heave, fibre mooring	134
12.7	PDF of largeste maxima, pitch, fibre mooring	134
12.8	PDF of largeste maxima, line tension, fibre mooring	135
12.9	Sepctrum of surge motion, rated environment, fibre mooring	135
12.10	Sepctrum of surge motion, 50-year environment, fibre mooring	136
12.11	Spectrum of line tension, 50-year environment, fibre mooring	136
13.1	Comparison of decay tests, original and fibre mooring	140

13.2	Illustration of amplitude notation for damping ratio	141
13.3	Response comparison, original and fibre mooring	143
13.4	Time series of surge motion, comparison, 50-year environment	144
13.5	Time series of heave motion, comparison, 50-year environment	144
13.6	Time series of pitch motion, comparison, 50-year environment	144
13.7	Time series of line tension, comparison, 50-year environment	145
13.8	PDF of largeste maxima, surge, comparison	145
13.9	PDF of largeste maxima, heave, comparison	145
13.10	PDF of largeste maxima, pitch, comparison	146
13.11	PDF of largeste maxima, line tension, comparison	146
13.12	Sepctrum comparison of surge motion, rated environment	146
13.13	Sepctrum comparison of surge motion, 50-year environment	147
13.14	Spectrum comparison of line tension, 50-year environment	147
13.15	Sepctrum comparison of heave motion, 50-year environment	148
14.1	1 : 5 ratio of fibre mooring line on each side of a buoyancy element	156
14.2	Single mooring line characteristics for 130 m water depth	158
14.3	Decay tests, measured at center of gravity	159
A.1	Bridle details (Larsen 2015)	169

Nomenclature

Abbreviations

AHTS	=	Anchor Handling Tug Supply
ALS	=	Accidental Limit State
AOA	=	Angle Of Attack
BEM	=	Blade Element Momentum
CAPEX	=	Capital Expenditure
COG	=	Centre of Gravity
COB	=	Centre of Buoyancy
COV	=	Coefficient Of Variation
DAF	=	Dynamic Amplification Factor
DNV	=	Det Norske Veritas
DOF	=	Degree Of Freedom
FE	=	Finite Element
FEM	=	Finite Element Method
FFT	=	Fast Fourier Transformation
FD	=	Frequency Domain
FLS	=	Fatigue Limit State
FOWT	=	Floating Offshore Wind Turbine
LF	=	Low Frequency
MBL	=	Minimum Breaking Load
MBS	=	Minimum Breaking Strength
MPM	=	Most Probable Maximum
PDF	=	Probability Density Function
TD	=	Time Domain
ULS	=	Ultimate Limit State
VIV	=	Vortex Induced Vibration
WF	=	Wave Frequency
WTG	=	Wind Turbine Generator

Greek letters and other symbols

∇	=	Volume displacement
α	=	Angle of attack
β	=	Time integration parameter
β_M	=	Local blade pitch angle from manufacturer
ε	=	Strain
γ	=	Time integration parameter
γ_{mean}	=	Load factor for characteristic mean line tension
γ_{dyn}	=	Load factor for characteristic dynamic line tension
θ	=	Blade pitch angle
θ_p	=	Blade pitch angle applied by control system
μ	=	Mean value
μ_s	=	Mean braking strength
ν	=	Viscosity
ρ	=	Density
ξ	=	Damping ratio
σ	=	Standard deviation
σ'	=	Solidity ratio
τ	=	Time constant
φ	=	Flow angle on airfoil
χ	=	Wake skew angle
Ψ	=	Rotor azimuth angle
Ω	=	Angular velocity of rotor
ω	=	Frequency

Roman letters

a	=	Distance from fairlead to attack point of the mooring line's suspended weight
a_A	=	Axial induction factor
a_T	=	Tangential induction factor
$a_{t,e}$	=	Material constant for tension-elongation model
A	=	Cross-section area
A_M	=	Added mass
A_{wl}	=	Water plane area
$b_{t,e}$	=	Material constant for tension-elongation model
B	=	Number of blades on rotor
$c_{t,e}$	=	Material constant for tension-elongation model
C	=	Damping coefficient
C_A	=	Added mass coefficient
C_D	=	Drag coefficient
C_L	=	Lift coefficient
C_M	=	Mass coefficient
C_N	=	Normal coefficient of airfoil
C_T	=	Tangential coefficient of airfoil
D	=	Diameter
COV	=	Coefficient of variation
D_D	=	Design cumulative fatigue damage
DFD	=	Design fatigue factor
D_c	=	Characteristic cumulative fatigue damage
E	=	Modulus of elasticity
$f_{Prandtl}$	=	Prandtl correction factor
f_s	=	Degree of stall
F	=	External force
g	=	Gravitational acceleration
GM	=	Metacentric height
H_s	=	Significant wave height
I	=	Moment of Inertia
K	=	Stiffness coefficient
K_E	=	Elastic stiffness
K_G	=	Geometric stiffness
K_{TOT}	=	Total stiffness
KC	=	Keulegan–Carpenter number
L	=	Line length
L'	=	Horizontal distance from fairlead to horizontal rotation point of mooring line
L_c	=	Airfoil chord length
M	=	Mass
p_N	=	Flow force normal to rotor plane
p_T	=	Flow force tangential to rotor plane
P	=	Period
Q	=	Torque

r	=	Rotor plane control volume radius
dr	=	Rotor plane control volume thickness
\mathbf{r}	=	displacement vector
$\dot{\mathbf{r}}$	=	velocity vector
$\ddot{\mathbf{r}}$	=	acceleration vector
$r_{spar,tower}$	=	Average radius of spar and tower
r_{WTG}	=	distance to centre of gravity of wind turbine generator
R	=	Rotor radius
\mathbf{R}	=	External force vector
R'	=	Bridle radius
R_{mean}	=	Mean response
R_{std}	=	Standard deviation of response
$R_{0,025}$	=	Lower limit of 95% confidence interval
$R_{0,975}$	=	Upper limit of 95% confidence interval
Re	=	Reynolds number
S_c	=	Characteristic capacity
S_{mbs}	=	Minimum breaking strength
t	=	time
T	=	Tension
T_0	=	Pretension of mooring lines
$T_{c,mean}$	=	Characteristic mean tension
$T_{c,dyn}$	=	Characteristic dynamic tension
T_d	=	Design line tension
T_H	=	Horizontal mooring line tension
T_p	=	Peak period
$u(t)$	=	Flow velocity
$\dot{u}(t)$	=	Flow acceleration
u_0	=	Flow velocity amplitude
u_i	=	Decay test amplitude
u_{i+1}	=	Decay test amplitude
U_{10m}	=	Wind velocity at 10 m height
$U_{ISO}(z)$	=	Wind profile for ISO wind spectrum
$U(t)$	=	Wind velocity
v_0	=	Air flow velocity in front of rotor
V_{rel}	=	Inflow velocity on airfoil
$V(t)$	=	Current velocity
W	=	Corrected induced velocity
W_{qs}	=	Quasi-static induced velocity
W_w	=	Weight in water
W_{air}	=	Weight in air
P	=	Period
$x(t)$	=	Displacement
$\dot{x}(t)$	=	Velocity
$\ddot{x}(t)$	=	Acceleration
z_G	=	Global z-coordinate fo centre of gravity

Introduction

1.1 Motivation

Floating offshore wind turbines (FOWT) are still a new technology without comprehensive experience and little full scale testing. In 2009 Statoil launched the world's first large-capacity FOWT, Hywind Demo, 10km outside of Stavanger (Statoil 2009). Since that day there has been little activity regarding FOWTs, one reason for this is that with today's designs and world situation, the FOWTs are not cost effective compared to other energy sources. In 2017 Statoil will be commissioning the world's first FOWT park, Hywind Scotland Pilot Park, with the expectation of demonstrating the feasibility of multiple FOWTs in one location.

Offshore wind energy has the benefit of steady wind at greater velocities than land based wind energy. In addition, the means of transport of the constructions has less limitations for offshore wind turbines. However, CAPEX for a FOWT is much higher than for a land based WT. The main contributions for the increase in CAPEX for a FOWT are the array cable and the support structure, which consist of the floater and mooring system.

Carbon Trust 2015 lists eleven key technical barriers that must be broken through in order for a FOWT project to become cost effective, one of which is the mooring system design. Today, the mooring designs used for FOTWs are imported from the oil and gas industry. These designs are based around projects that has been known to quickly become profitable, hence little work has been done in order to optimize mooring systems. A FOWT takes many years in operation before becoming profitable, and it is crucial to minimize CAPEX. An optimized mooring system design would help reduce CAPEX, which would in turn make the energy production from the FOWT more profitable.

This thesis aims to provide theoretical background regarding time domain simulations and tension-elongation behaviour of fibre ropes, and a mooring system for Hywind Demo based on fibre ropes that will reduce the cost of the system.

1.2 Previous work

The FOWT field of study has increased significantly in the last years due to the demonstration of feasibility, and several companies are producing their own design with the hope of reducing the CAPEX. Statoil ASA has been one of the front runners in the field of FOWT with Hywind Demo and Hywind Scotland.

Regarding mooring system optimization for FOWT, there have been several design studies related to tension leg mooring, but little with respect to catenary mooring, and even less related to fibre mooring. T. Hordvik did an optimization study on mooring systems for Hywind Demo, but focused on the use of chains and steel wire ropes (Hordvik 2011).

With the increase in activity regarding FOWT, rules and regulations are now available specifically for their design, such as DNV's "Design of Floating Wind Turbine Structures", which also incorporates mooring systems (DNV-OS-J103 2013).

Chapter 2

Mooring system designs

2.1 Introduction

In this chapter, the components of a mooring line as well as three different types of mooring systems are discussed: Slack mooring with chain, spiral strand rope and possibly clump weights; taut mooring with fibre rope; and fibre rope with buoyancy elements.

2.2 Mooring line components

2.2.1 Line materials

Chain

Chain is one of the most commonly used mooring line materials worldwide. Chain comes with and without studs, where the chains that have studs are commonly used for temporary operations since the studs help keep the chain from tangling when stored. Chain is the sturdiest mooring line material, with a high natural resistance against abrasion. However, this sturdiness comes at the cost of weight, as it is the heaviest mooring line material, and is therefore not commonly used alone due to the cost of the mooring line and the lowered payload capability of the floater. Chain is often used along the sea floor, due to the abrasion resistance, and topside since the chain links are easy to handle for the tension jacks and locking mechanisms.

Wire rope

Together with chain, wire ropes are one of the most common mooring line materials. There are two main variants of the wire rope, the spiral strand rope and the six strand rope. The six strand rope is more robust, but comes without plastic sheathing, making it vulnerable to corrosion. Due to this weakness against corrosion it is commonly used by mobile units. The spiral strand rope is often covered with a plastic sheath, which provides a barrier to the sea water, thereby extending its lifetime and making it the preferred choice for long-term installations.

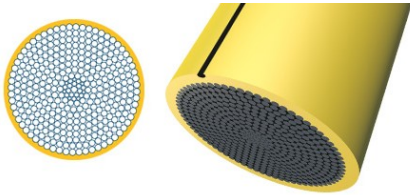


Figure 2.1: Sheathed spiral strand rope (Bridon)

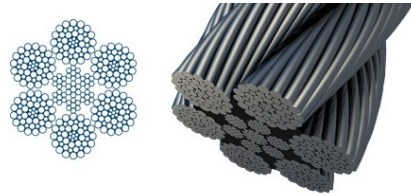


Figure 2.2: Six strand rope (Bridon)

Fibre rope

Fibre ropes consisting of polyester or nylon has a submerged weight close to zero, giving it little influence on the payload capabilities of the floater. It is therefore often used in deep water mooring configurations, either alone as taut mooring or as an insert between topside and bottom chain. Fibre rope has a relative high longitudinal elasticity, as opposed to that of chain and wire ropes. It does, however, have close to zero abrasion resistance and can easily be damaged. Similarly, it poses little threat to nearby structures, and can therefore be used close to risers and umbilicals.

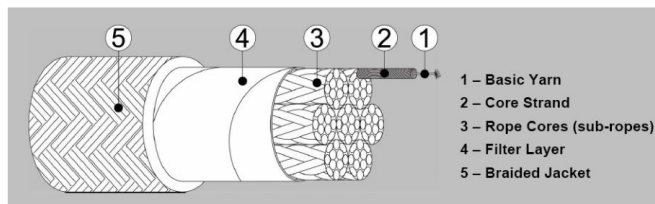


Figure 2.3: Fibre rope (Larsen 2015)

2.2.2 Line accessories

Accessories used along the mooring line are those used to combine different mooring line materials, such as rope-chain connectors; wire socket terminator; triplates; and shack-

les, and those used to alter the line geometry, such as clump weights and buoyancy elements.



Figure 2.4: Clumpweights attached to chain (AMC)



Figure 2.5: Buoyancy elements (AMC)

2.2.3 Anchors

Fluke anchors

Fluke anchors are the most basic anchor design used today, and are designed to dig into the seabed when the mooring line is tensioned. Both installation and retrieval is simple, but the anchor only supports lateral forces. A vertical force on a fluke anchor will pull the anchor up from the seabed.



Figure 2.6: Fluke anchor (Vryhof)

Plate anchors

A plate anchor share some design similarities with the fluke anchor with it's way of digging into the seabed. However, the design of the plate anchor make it possible to alter the angle between plate and mooring line, making it possible to apply a vertical force to the anchor and still keep the anchor in place.



Figure 2.7: Plate anchor (Vryhof)

Suction Anchor

Suction anchors are today widely used, especially in deep water installations that require taut or semi-taut mooring systems. A suction anchor uses a cylindrical caisson with an open bottom end. The caisson is embedded in the seabed by pumping out the water from within the cylinder. Both installation and retrieval is easy and fast compared to other anchor designs. Another advantage of the suction anchor is its ability to withstand large vertical forces, thereby reducing the footprint of the mooring system.



Figure 2.8: Suction anchor (Semar)

Deep penetrating anchors

The deep penetrating anchors, also called torpedo piles, are a result of the offshore industry needing a more cost-effective anchor designs. The anchor is released freely from a predetermined height above the seabed and uses gravity as installation force. A deep penetrating anchor of 75 t which is released 75 m above the seabed will have reached a velocity of 25 m s^{-1} when hitting the seabed, providing deep penetration into the sediments (Deep Sea Anchors). A deep penetrating anchor provides sufficient vertical resistance to be applied to taut mooring. Retrieval of the anchor is done by applying a vertical lifting force which exceeds the holding capacity of the anchor (Deep Sea Anchors).



Figure 2.9: Deep penetrating anchor of 75 t (Deep Sea Anchors)

2.3 Mooring system configurations

2.3.1 Slack mooring

A standard catenary mooring system consisting of chains and/or steel wire ropes where the stiffness is provided by the geometry of the line.

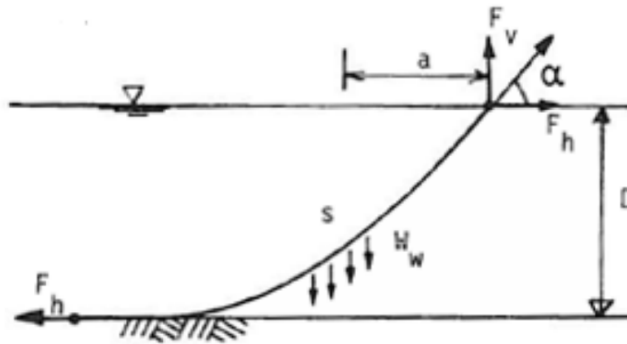


Figure 2.10: Slack mooring (Larsen 2015)

A slack mooring system with bottom chain provides a restoring force in the way that when the floater is given an offset, additional elements of the bottom chain is being lifted off the sea bed, increasing the suspended weight, W_w , while at the same time increasing the moment arm, a .

2.3.2 Mooring with clump weights

This mooring configuration is similar to the slack mooring in the way that the restoring force is provided by a geometric stiffness.

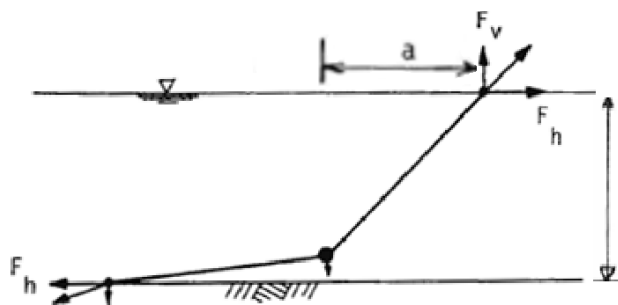


Figure 2.11: Slack mooring with clump weight (Larsen 2015)

This system can be used either with fibre rope or chain and steel wire configurations, and can be fitted with a bottom chain if needed. If bottom chain is not installed, the anchor must be capable of withstanding vertical loads, and the restoring force will only be derived from the increasing moment arm, a , and not from an increasing weight of suspended line.

If used with fibre ropes, care must be taken to ensure that there is no contact between the fibre rope and sea bed, as fibre ropes have little abrasion resistance.

2.3.3 Taut mooring with fibre rope

This design uses fibre ropes which are tensioned in a taut mooring configuration. Taut mooring is commonly used in deep water, where it becomes both a cheaper and lighter solution while providing a smaller footprint than catenary mooring. The stiffness in the system is provided by the elastic stiffness of the fibre ropes, given as

$$K_E = \frac{EA}{L} \quad (2.1)$$

where

- E = modulus of elasticity of the line
- A = cross-section area of the line
- L = line length

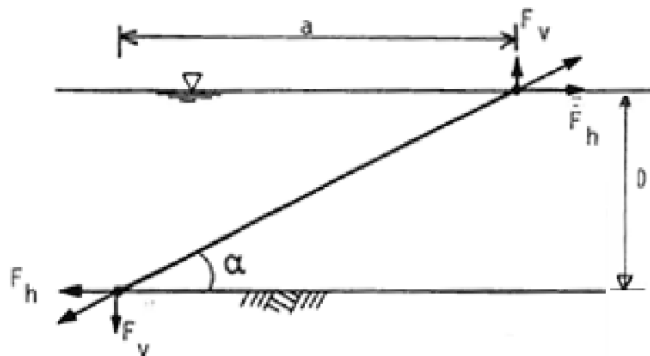


Figure 2.12: Taut mooring (Larsen 2015)

There are two large challenges with outfitting Hywind Demo with such a mooring system:

- Fibre ropes are known to creep, meaning that when a new fibre rope is installed it will suffer permanent elongation when subjected to tension. Since Hywind Demo does not have any anchor winches, any permanent elongation of the ropes must be present when the mooring is installed
- Hywind Demo is moored in shallow water, meaning that the lines would have to be unreasonably long to provide sufficient flexibility (as evident from Equation (2.1)), giving a large footprint.

2.3.4 Fibre rope with buoyancy elements

This design utilises the elastic stiffness of fibre ropes and introduces flexibility through geometry. By increasing the line length and adding a buoyancy element, the system is given the ability to accommodate offsets without stretching the line (by pulling the buoyancy element downwards). This provides flexibility with a smaller footprint than taut mooring and absorbs some of the low frequency (LF) and wave frequency (WF) motions, which would else have been absorbed by stretching the fibre rope.

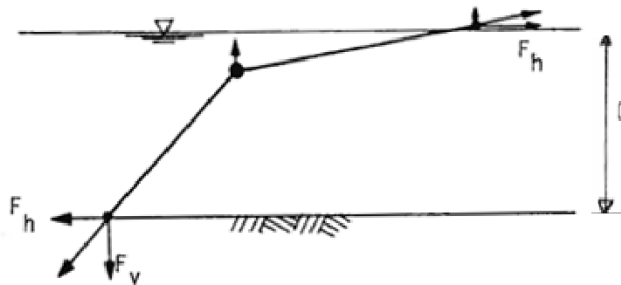


Figure 2.13: Mooring with buoyancy elements (Larsen 2015)

Note that the geometric stiffness will be reduced when the system is given an offset, as opposed to the slack moored system. This is because the moment arm of the geometric stiffness, a , will be reduced when an offset is introduced, as opposed to that of the slack moored system. However, since the line in this case is elastic, it is not possible to give a general comment on how much the stiffness in the system varies, as this will depend on the elastic stiffness.

2.4 Yaw stiffness

To ensure yaw stiffness of the spar, a bridle configuration as shown in Figure 2.14 is utilized for the different mooring systems. The yaw stiffness provided by the bridle is described in DNV-RP-H103 2014 as

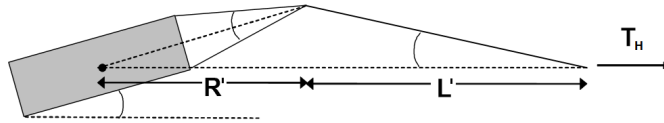


Figure 2.15: Yaw stiffness from bridle (DNV-RP-H103 2014, modified)

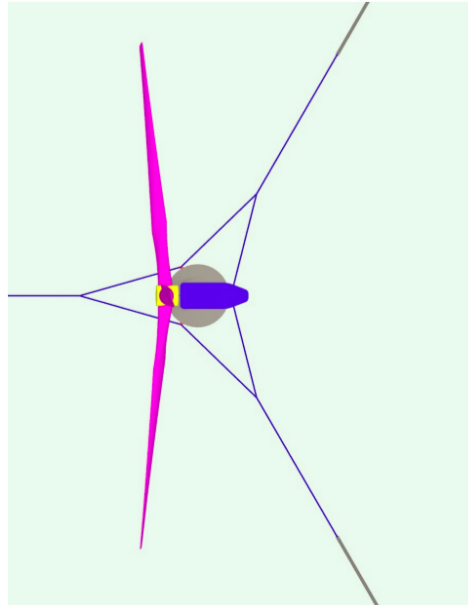


Figure 2.14: Bridle configuration as seen from above (Moxnes 2009)

$$K_{66} = T_H R' \left(1 + \frac{R'}{L'} \right) [\text{Nm/rad}] \quad (2.2)$$

where

- T_H = horizontal force in mooring line
- L' = horizontal distance from bridle to virtual anchor, lower horizontal pivot point
- R' = distance from center of gravity of the spar to end of bridle.

Illustration is given in Figure 2.15.

The components of the bridle is identical for all the different mooring systems, and the details of these are given in Appendix A.

Hywind Demo

3.1 Introduction

This chapter presents information and basic technical data regarding Hywind Demo.

Launched in 2009, Hywind Demo was the first full scale FOWT. It was designed and built by Statoil, and is located on the Norwegian coast outside Karmøy in 204 m water depth. Hywind Demo is fitted with a Siemens 2.3 MW wind turbine generator (WTG), and is producing electrical power to the Norwegian power grid. The main goal of Hywind Demo is not to produce energy for profit, but to be used as a tool in the research on how wind and waves affect a FOWT and its power production (Statoil 2009). The results have been greater than expected, and in 2011 Hywind Demo had a capacity factor of more than 50 % (NVE 2012), which is very high in both a national and international context.

In the following sections, a technical description of the structure and mooring system of Hywind Demo is given.

3.2 Structural description

The structural description of Hywind Demo is given in Godø 2013 and Bjørnsen 2015.

Hywind Demo can be divided into three main components: substructure, tower and WTG. The substructure on Hywind Demo is a spar buoy made of steel with 100 m draft and a diameter of 8.34 m, with a tapering to 6 m close to the water line. Above the water line, the spar extends about 15 m to the tower flange. The tower is mounted on top of the spar's tower flange, is 50 m high, and supports the WTG which is positioned at a total elevation of 65 m. The WTG has a three-bladed rotor with a diameter of 82.4 m. Stability of the total structure is achieved by having the centre of gravity (COG) beneath the centre of buoyancy

(COB). To obtain this low position of the COG, the bottom of the spar is ballasted with olivine and water. A technical drawing of Hywind Demo is given in Figure 3.1. However, one dimension is not given, which is the distance from the waterline to the base of the tower, which is 15 m. The total weight of Hywind Demo is 5 129 800 kg.

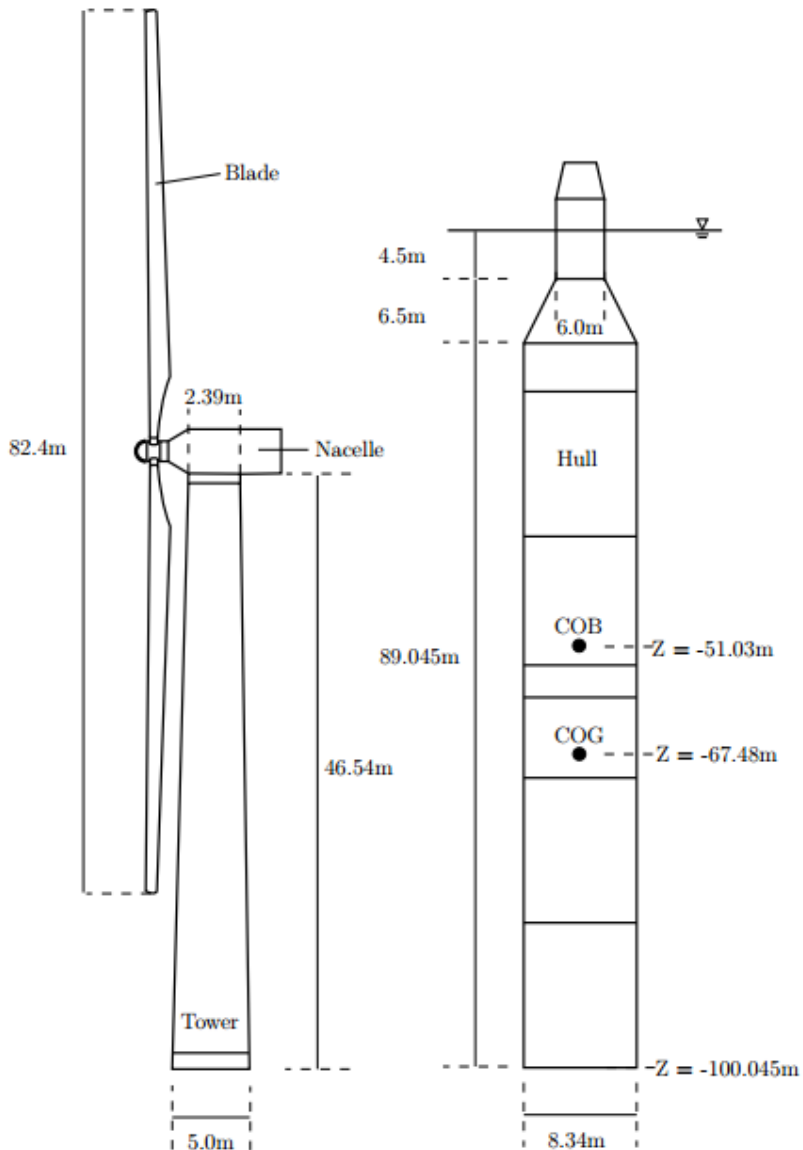


Figure 3.1: Structural drawing of Hywind Demo. The spar and tower are not drawn to scale. (Godø 2013)

3.3 Mooring system

The Hywind Demo mooring system details are given in Godø 2013 and Bjørnsen 2015.

Hywind Demo is moored with a traditional catenary mooring system, consisting of chains and spiral strand rope, with a length of approximately 1000 m. About 50 m from the spar, each mooring line is split into two, creating a bridle system. The bridle provides yaw stiffness, as described in Section 2.4. Pretension and geometric stiffness is increased by the addition of a clump weight of 45 t on each line, approximately 150 m from the spar. A schematic drawing of a single mooring line is given in Figure 3.2. An illustration of the bridle is seen in Figure 2.15, and a detailed list of the line components are given in Table 9.5.

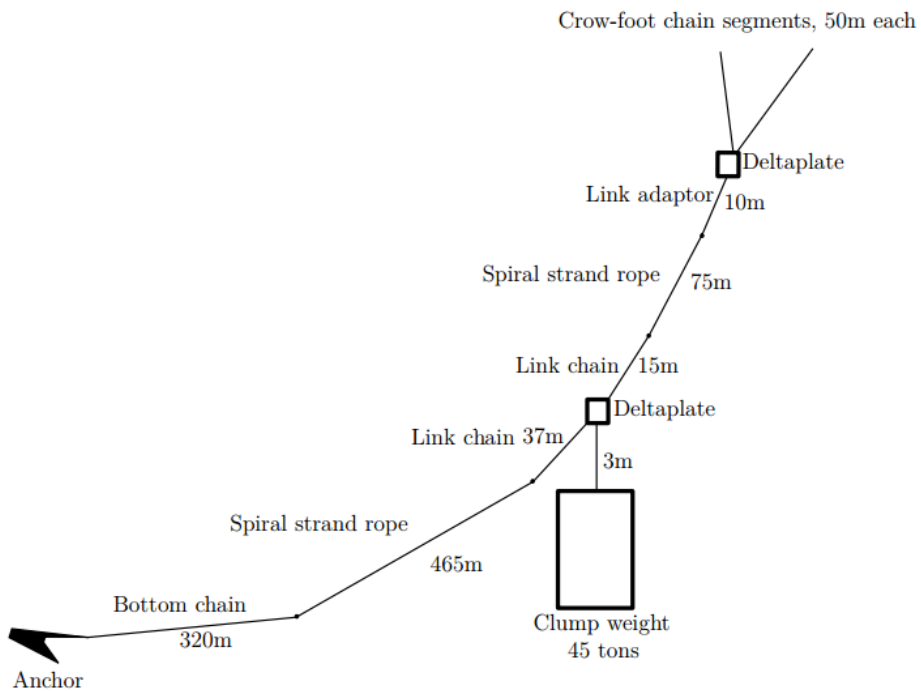


Figure 3.2: Schematic drawing of a single mooring line on Hywind Demo (Godø 2013)

Chapter 4

Rules and regulations

The rules and regulations for station keeping of FOWTs are given in DNV-OS-J103 2013.

4.1 Ultimate and accidental loads

Following DNV-OS-J103 2013, the design tension, T_d , can be calculated as

$$T_d = \gamma_{mean} \cdot T_{c,mean} + \gamma_{dyn} \cdot T_{c,dyn} \quad (4.1)$$

where $T_{c,mean}$ is the characteristic mean tension and $T_{c,dyn}$ is the characteristic dynamic tension. γ_{mean} and γ_{dyn} are load factors given in Table 4.1. For ultimate limit state (ULS), $T_{c,mean}$ should be taken as the worst line tension caused by pretension and mean static wind, current and wave drift with a 50 year return period. $T_{c,dyn}$ should be taken as the worst dynamic part of the line tension caused by oscillatory LF and WF excitation with a 50 year return period. For accidental limit state (ALS), the components are to be found through a similar deduction, but with a 1 year return period. It is to be assumed that the environment is direction-independent, and that the load is acting on the structure in the least favourable direction.

The method for determination of the worst line tension is given in DNV-OS-E301 2013, where it is stated that the *most probable maximum* (MPM) value shall be used.

Limit state	Load factor	Safety class	
		Normal	High
ULS	γ_{mean}	1.3	1.5
ULS	γ_{dyn}	1.75	2.2
ALS	γ_{mean}	1.00	1.00
ALS	γ_{dyn}	1.10	1.25

Table 4.1: Load factor requirements for design of mooring lines

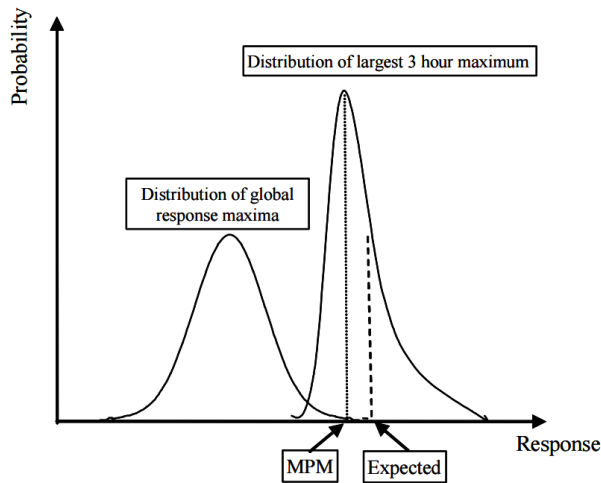


Figure 4.1: Most probable maximum in extreme value distribution (DNV-OS-E301 2013)

It is to be noted that due to the blade-pitch control system, the 50 year value of the line tension may not occur in an environment with 50 year return period. This is because the wind thrust on the blades decrease after the wind velocity has reached the turbine’s rated wind speed. At that point the turbine has reached it’s rated power, and starts pitching its blades to keep a constant RPM. It is therefore important to check the loads in the mooring system at both rated wind and along the 50-year contour line.

The load factors in Table 4.1 are split into two safety classes: Normal and high. The normal class can be utilized if there is no risk of collision with adjacent structure when in ALS condition. If such a risk is present, the high class should be utilized.

4.2 Resistance

The characteristic capacity of the mooring lines, S_C , is given in DNV-OS-J103 2013 as

$$S_C = \mu_S \cdot (1 - COV_S \cdot (3 - 6 \cdot COV_S)), COV_S < 0.10 \quad (4.2)$$

where μ_S is the mean breaking strength of the mooring line and COV_S is the *coefficient of variation* (COV) of the breaking strength.

If the strength statistics are based on test results, statistical uncertainty is accounted for in the following manner

$$S_C^* = S_C \cdot (1 - 2 \cdot \frac{COV_S}{n}) \quad (4.3)$$

where n is the number of test, which is not to be less than 5.

If there is no statistics available for the breaking strength of the mooring line, the characteristic capacity can be calculated as

$$S_C = 0.95 \cdot S_{mbs} \quad (4.4)$$

where S_{mbs} is the *minimum breaking strength* (MBS).

4.3 Design criteria

4.3.1 ULS

The design criterion for ULS is given in DNV-OS-J103 2013 as

$$S_C > T_d \quad (4.5)$$

where S_C should be replaced with S_C^* when the mooring line strength statistics are based on tests. T_d is calculated using the ULS safety factors in Table 4.1.

4.3.2 ALS

The design criterion for ALS is given in DNV-OS-J103 2013 as

$$S_C > T_d \quad (4.6)$$

where S_C should be replaced with S_C^* when the mooring line strength statistics are based on tests. T_d is calculated using the ALS safety factors in Table 4.1 and with one broken mooring line.

4.3.3 FLS

According to DNV-OS-J103 2013 the mooring lines shall be designed for a fatigue limit state (FLS), where the design cumulative fatigue damage is given as

$$D_D = DFF \cdot D_C \quad (4.7)$$

where D_C is the characteristic cumulative fatigue damaged caused by the stress history in the line, and DFF is the design fatigue factor. D_C can be calculated by Miner's sum by the use of SN-curves given in DNV-OS-E301 2013 or may be calculated by the "combined spectrum approach", which is also given in DNV-OS-E301 2013. DFF is dependant on safety class, and is given in Table 4.2.

Structural element	Safety class		
	Low	Medium	High
Internal structure, accessible and not welded directly to the submerged part.	1	2	3
External structure, accessible for regular inspection and repair in dry clean conditions	1	2	3
Internal structure, accessible and welded directly to the submerged part	2	3	6
External structure not accessible for inspection and repair in dry and clean conditions ¹⁾	2	3	6
Non-accessible areas, areas not planned to be accessible for inspection and repair during operation, and structures with permanent ballast ²⁾	3	6	10

1) Regular inspection, preferably by NDT.

2) No planned inspection.

Table 4.2: Design fatigue factors (DNV-OS-J103 2013)

The design criterion for FLS is

$$D_D \leq 1.0 \quad (4.8)$$

Environmental loads on floating offshore wind turbines

5.1 Introduction

Floating offshore wind turbines are subject to one of the most complex load systems of any offshore installation. In addition to wind, wave and current loads that all offshore installations are subjected to, FOWTs are also influenced by the thrust force from the rotor.

The complex load system is absorbed by the system through inertia, damping and stiffness, described by the generalized dynamic equilibrium equation as

$$(M + A_M)\ddot{x}(t) + C(x, \dot{x})\dot{x}(t) + K(x, \dot{x})x(t) = F(t) \quad (5.1)$$

where

- M = mass of system [kg]
- A_M = added mass [kg]
- $C(x, \dot{x})$ = non-linear damping coefficient [N s m^{-1}]
- $K(x, \dot{x})$ = non-linear stiffness coefficient [N m^{-1}]
- $F(t)$ = external force [N]
- x, \dot{x}, \ddot{x} = displacement, velocity and acceleration

The left side of Equation (5.1) represents the physical properties of the system, the right side represents the external loading, where force, $F(t)$, can be separated into the different

load contributions as

$$F(t) = F_{wave}(t) + F_{current}(t) + F_{wind}(t) + F_{thrust}(t) \quad (5.2)$$

5.2 Wave forces

The hydrodynamic forces on a slender structure are determined using the Morison Equation, given in Equation (5.3), where the inertia term is in phase with the local acceleration of the water particles, and the drag force is proportional to the square of the instantaneous flow velocity.

The Morison equation for a cylinder, per unit length, is in general given as

$$dF_{Morison}(t) = \underbrace{\rho C_M \frac{1}{4} \pi D^2 \dot{u}(t)}_{F_{Inertia}} + \underbrace{\frac{1}{2} \rho C_D D u(t) |u(t)|}_{F_{Drag}} \quad (5.3)$$

where

- ρ = density of water
- C_M = mass coefficient, given as $C_M = 1 + C_A$
- C_A = added mass coefficient
- D = diameter of cylinder
- $\dot{u}(t)$ = flow acceleration
- C_D = drag coefficient
- $u(t)$ = flow velocity

For floating bodies, such as a FOWT, the velocity and acceleration need to be taken as relative between the body and the flow. The wave force expressed with the Morison equation can then be written as

$$dF_{wave}(t) = \underbrace{\rho \frac{1}{4} \pi D^2 \dot{u}(t)}_{F_{FK}} + \underbrace{\rho \frac{1}{4} \pi D^2 C_A (\dot{u}(t) - \ddot{x}(t))}_{F_{Inertia}} + \underbrace{\frac{1}{2} \rho C_D D (u(t) - \dot{x}(t)) |u(t) - \dot{x}(t)|}_{F_{Drag}} \quad (5.4)$$

where

- F_{FK} = Froude-Krylov force
- $\dot{x}(t), \ddot{x}(t)$ = floater velocity and acceleration

The wave-induced particle velocity decays exponentially with depth, resulting in a potential for large horizontal offset as well as large pitch motions.

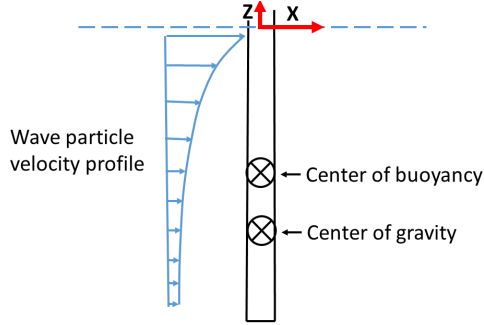


Figure 5.1: Wave particle velocity profile

5.3 Current force

The hydrodynamic forces from current are, similarly to the viscous wave forces, calculated from the Morison equation. However, due to the current's approximately steady flow, the Morison equation can be reduced to the drag term. Also, due to lack of accelerations, the current force can be to a large extent be regarded as a force contributing only to the mean offsets. The current force on a section of the spar is given per unit length as

$$dF_{current}(t) = \frac{1}{2}\rho C_D D(V(t) - \dot{x}(t)|V(t) - \dot{x}(t)|) \quad (5.5)$$

where $V(t)$ is the current velocity.

The velocity profile of the current is difficult to establish without measurements, and is often taken to be constant. In reality, the profile will change with depth, and can have sections along the z-axis with larger velocities than others.

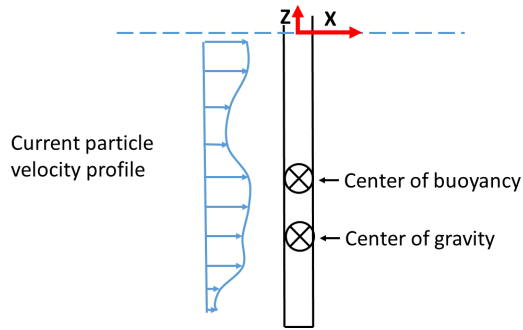


Figure 5.2: Example of current particle velocity profile

5.4 Wind force

The wind force represents the force on the air particles flowing around the tower. This flow is similar to the current flow with its slow variation, and can be calculated with the drag term from the Morison equation. Unlike current, the wind does have a time variation in the form of gusts, which can excite LF motions, and can have a larger velocity variation along the z-axis. The wind force on a section of the tower is thus given by the drag term in the Morison equation per unit length as

$$dF_{wind}(t) = \frac{1}{2} \rho C_D D (U(t) - \dot{x}(t)) |U(t) - \dot{x}(t)| \quad (5.6)$$

where $U(t)$ is the wind velocity.

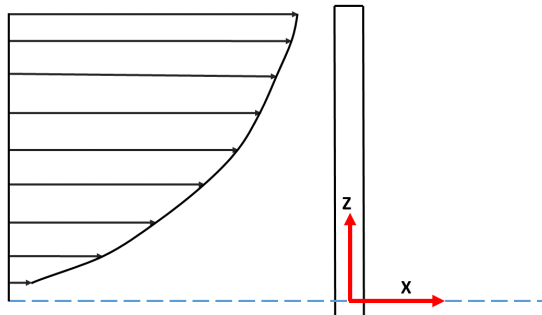


Figure 5.3: Wind shear profile

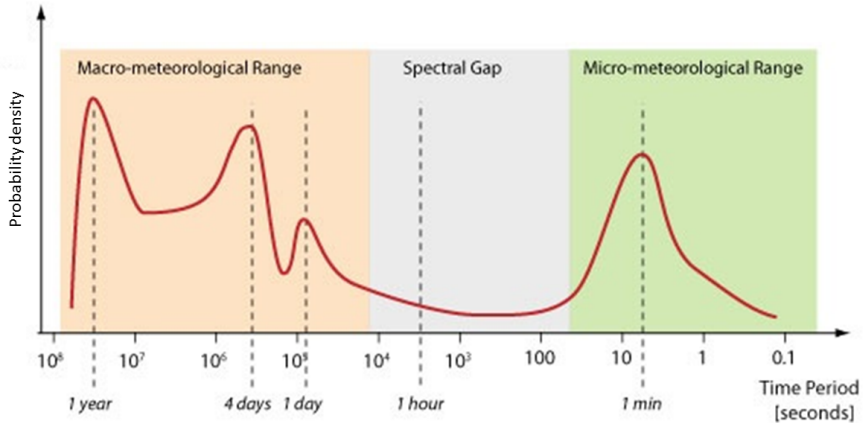
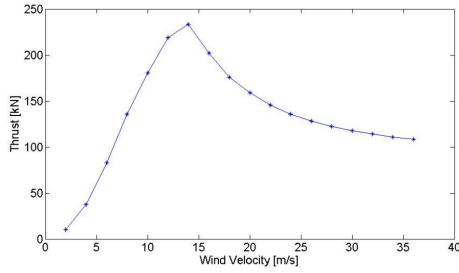


Figure 5.4: Wind velocity spectrum (Green Rhino Energy, modified)

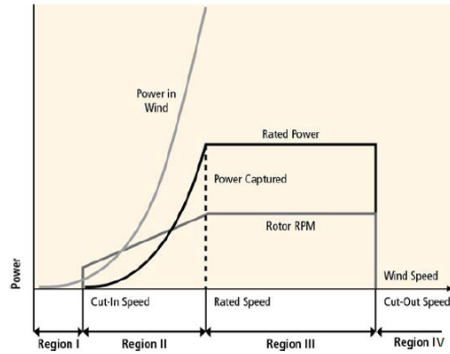
The wind force will contribute to both horizontal offset and pitch due to the exponentially increasing wind velocity with elevation, and large moment arm.

5.5 Thrust force

The thrust force is the one main element that separates FOWTs from other floating units. The thrust force is the force caused by the air flow on the rotor blades. The wind turbine's control system is, for operational environments, trying to keep the power output at its rated output. For wind velocities lower than the rated wind speed, the blades remain un-pitched, giving the rotor maximum lift force on the blades in order to maximize the rotational velocity of the rotor and generator. When the wind reaches the rated wind speed, the generator reaches its rated power, and the control system starts to pitch the rotor blades to avoid any further increase in rotational velocity, effectively reducing the force on the blades from the airflow. This, in practice, means that for low wind velocities, the thrust force increases with the wind velocities, while for large wind velocities, the thrust force is actually decreasing with increasing wind velocity. An illustration of the thrust force for Hywind Demo is given in Figure 5.5 together with a definition of wind velocity regions.



(a) Rotor thrust force for Hywind Demo (Bjørnsen 2015)



(b) Wind velocity regions (Ghao 2015)

Figure 5.5

The variation of thrust force with incoming wind at region 3 give rise to a problem with pitch and surge motion due to negative damping. When the rotor is moving towards the wind, either from surge or pitch motion, the turbine control system will sense an increase in rotor velocity from the increased relative velocity between wind and rotor. To account for the increased rotor velocity, the control system will increase the blade pitch angle, reducing the thrust force. Similarly, when the turbine is moving away from the wind, the relative velocity will be reduced, and the control system will reduce the blade pitch angle, increasing the thrust force. Moving towards the wind with decreasing thrust force will result in a larger motion amplitude, similarly with moving with the wind with increasing thrust force. The problem is identified as negative damping in pitch and surge from the varying rotor thrust force. This problem is only present for FOWT, and require special configurations to the control system that take the floater's motion into account.

5.6 Stiffness

Hywind Demo has stiffness contributions in surge, sway and yaw from the mooring system, and hydrostatic stiffness in pitch, roll and heave. Mooring systems can provide stiffness in heave and pitch, but this is dependant on the mooring configurations.

5.6.1 Mooring stiffness

The mooring system is designed to minimize the mean and LF offset, while at the same time absorb the WF motions. The horizontal stiffness is achieved by the mooring systems geometric or elastic properties, as discussed in Section 2.3. For a FOWT, it is important to minimize the mean offset of the spar to reduce the necessary length of the power cable.

5.6.2 Hydrostatic stiffness

The hydrostatic stiffness in heave is given as

$$K_{33} = \rho g A_{wl} \quad (5.7)$$

where

- ρ = density of water
- g = gravitational acceleration
- A_{wl} = water plane area

The hydrostatic stiffness in pitch and roll is identical for Hywind Demo, since the spar and tower are axis symmetric. These stiffness' are given as

$$K_{44} = K_{55} = \rho g \nabla GM \quad (5.8)$$

where

- ρ = density of water
- g = gravitational acceleration
- ∇ = volume displacement
- GM = metacentric height

5.7 Damping

There are several damping contributions on a FOWT. The most important ones are viscous damping in water and air and wave-radiation damping. There are also damping contributions from skin friction, but this is seen to be of little importance compared to the viscous effects.

There are viscous damping contributions to the surge, sway, pitch and roll motions from the air drag force on the tower and the water drag force on the spar. In addition, surge, sway, yaw and heave motions also have viscous damping from the drag force on the mooring lines that are set into motion. Hence, by increasing the line length that is suspended in the water, the damping is also increased. In addition to the viscous mooring line damping force, heave motion also has damping from vortex shedding on the bottom of the spar. The viscous damping forces from drag on tower, spar and mooring lines are calculated using the drag force term in the Morison equation.

Damping forces from the mooring lines are also a possibility in roll and pitch, but this is dependant on where the mooring lines are connected to the structure.

Dependant on the configuration of the WTG control system, the rotor thrust force may also contribute to damping in surge and pitch, i.e. motions parallel to the wind direction.

5.8 Inertia

A FOWT has inertia about all axis, as well as coupled inertias, which can be described with the mass matrix given in Equation (5.9) (Faltinsen 1990).

$$M_{jk} = \begin{bmatrix} M & 0 & 0 & 0 & Mz_G & 0 \\ 0 & M & 0 & -Mz_G & 0 & 0 \\ 0 & 0 & M & 0 & 0 & 0 \\ 0 & -Mz_G & 0 & I_4 & 0 & -I_{46} \\ Mz_G & 0 & 0 & 0 & I_5 & 0 \\ 0 & 0 & 0 & -I_{46} & 0 & I_6 \end{bmatrix} \quad (5.9)$$

where

- M = mass of the system
- z_G = z-coordinate of COG
- I_j = moment of inertia in the j th mode
- I_{jk} = product of inertia with respect to the coordinate system (x,y,z)

As defined in Equation(5.1), the system counter external loading by, amongst others, inertia responses in the six DOFs following Newton's law. The most prominent inertias are the mass of the systems itself, M , and the rotational inertia in pitch and roll, I_5 and I_6 , which has large contributions from the heavy WTG in one end and ballast in the other end. Due to the relatively small diameter of Hywind Demo, the rotational inertia in yaw has a relatively small contribution from the spar and tower themselves, and also from the WTG with the shaft and blades.

Tension-elongation of sythetic fibre ropes

6.1 Introduction

This chapter explains the theory behind the mechanical behaviour of synthetic ropes, which is more complex than the corresponding behaviour of steel wire ropes and chains. The complexity comes from the synthetic rope's visco-elastic and visco-plastic properties, giving it the ability to gradually develop permanent increases in length dependant on the load history. In practice this means that the length and mechanical properties of a synthetic rope may be different prior to and after a severe loading. These challenging behaviours set aside, the use of fibre ropes in mooring systems has several advantages compared to steel wire and chain, such as:

- Fibre ropes are close to neutrally buoyant, increasing the floater payload capability
- Lower material cost
- Potential reduction in installation cost due to the lighter weight of the mooring system
- Better endurance in cyclic load

6.2 Spring-dashpot model

A standard gravity based catenary system with steel wire or chain is usually modelled using a finite element (FE) model. Due to the catenary shape, several elements are needed to describe the curved shape. The smaller the curvatures are, the more elements are needed.

Therefore, a mooring systems based on synthetic fibre ropes, which under normal application will give straighter lines, will need less elements. On the other hand, the elements are more complex for synthetic fibre than for steel. A steel element is defined by the cross-sectional properties and a linear elasticity which is defined, per unit length, by the Young's modulus and cross-sectional area as

$$\frac{1}{EA}$$

Where

- E = Young's modulus [Pa]
- A = Cross-sectional area [m²]

A true FE model of fibre ropes need to include the complex behaviour of how the element changes due to the axial loading. Such a model is described in Flory, Ahjem, and Banfield 2007, with four submodels in a series connection:

1. A spring to model instantaneous elongation
2. A spring and dashpot in parallel to model slow elongation response
3. A spring and ratchet in parallel to model irreversible, instantaneous elongation
4. A dashpot to model long term elongation, or creep

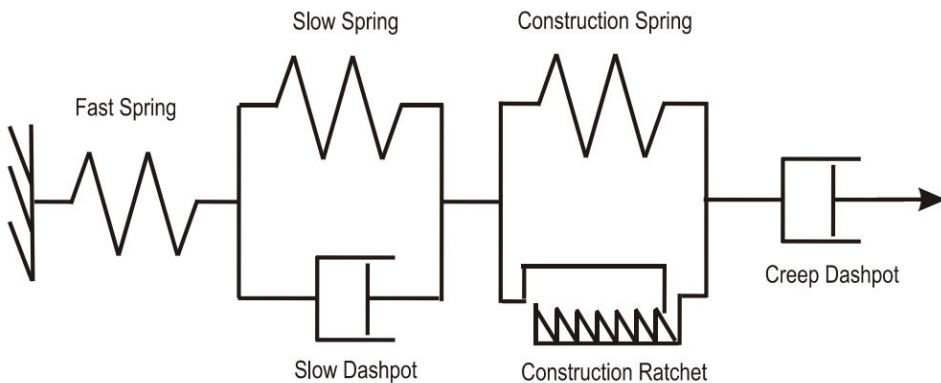


Figure 6.1: Spring-dashpot model for synthetic fibre rope (Flory, Ahjem, and Banfield 2007)

As described, and seen from Figure 6.1, the model is non-linear in the way that the springs and dashpots are not constant components. The visco-elastic behaviour of the rope is modelled in submodel 2, where the damping effect of the dashpot inhibits an immediate change in length from a sudden change in tension. Submodel 3 represents the permanent, irreversible elongation, caused by compaction of the fibres in the rope whenever the tension reaches a new maximum. Submodel 4 models the creep behaviour, i.e. polymer strain yielding irreversible elongation whenever the rope is under tension.

The use of such a spring-dashpot model would provide a detailed and accurate response in the fibre rope behaviour from dynamic tension. However, the mathematical model behind the spring-dashpot system requires detailed knowledge of the different submodels which are only accessible through empirical studies. In Kaasen et al. 2014, the mathematical model of the elongation in the spring-dashpot system is described as

$$\begin{aligned}
 x &= x_i + x_q + x_s + x_c + x_p \\
 x_i &= c_{i,1}F + c_{i,2}F^2 \\
 \dot{x}_q &= -\frac{1}{T_q}x_q + \frac{b_q}{T_q}F \\
 \dot{x}_s &= -\frac{1}{T_s}x_s + \frac{b_s}{T_s}F \\
 x_c &= c_{c,1}F_m + c_{c,2}F_m^2 \\
 \dot{x}_p &= -\frac{1}{T_p}x_p + \frac{b_p}{T_p}F \quad \dot{x}_p \geq 0
 \end{aligned} \tag{6.1}$$

where

- x = total elongation
- x_i = instantaneous elongation
- x_q = quick visco-elastic elongation
- x_s = slow visco-elastic elongation
- x_c = irreversible, instantaneous elongation
- x_p = irreversible, visco-plastic polymer elongation, creep
- F = axial load
- F_m = historical maximum load
- T = tension, time constants
- c and b are coefficients representing the physical properties of the rope

Through empirical data, the material properties can be found using numerical methods, as performed and explained in Kaasen et al. 2014. To this day, manufacturers of fibre ropes do not provide these parameters, so there is no easy way of utilizing the spring-dashpot model without perform the tension-elongation experiment for the fibre rope of interest. To be able to do simulations on a mooring system comprised of synthetic fibre ropes, a simplified model has to be utilized.

6.3 Simplified, linear stiffness

In Falkenberg et al. 2011, an experiment with fibre ropes using a test machine capable of applying both harmonic and irregular load cycles is described. The results from both the harmonic and irregular tests, five in total, are shown in Figure 6.2.

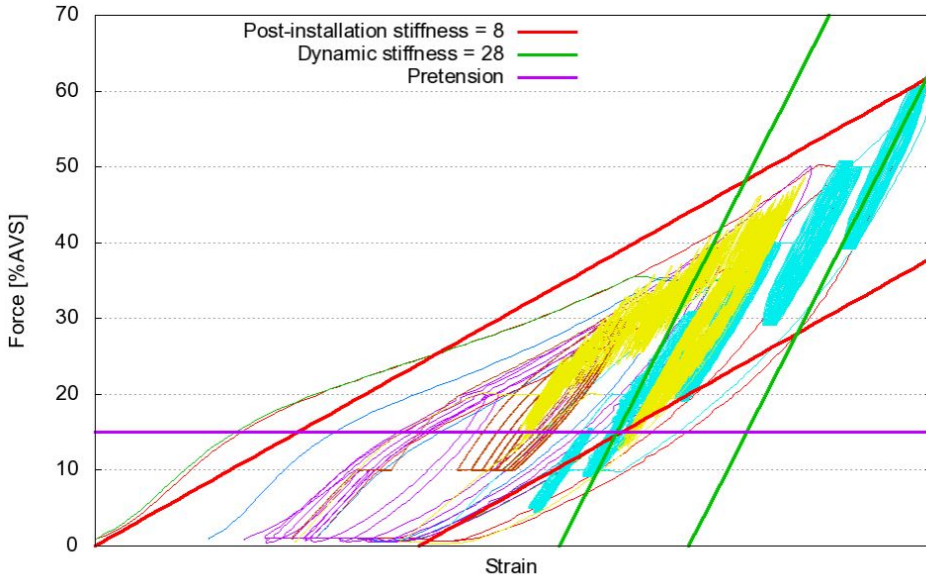


Figure 6.2: Harmonic and irregular tension tests, each test drawn in different colour (Falkenberg et al. 2011)

From Figure 6.2 it is seen that for cyclic loads, both regular and irregular, the tension-elongation is cycling around a curve. Falkenberg et al. 2011 proposes a change-in-length behaviour as shown in Figure 6.3, where the *original curve* represents the tension-elongation for a new rope tensioned rapidly for the first time. The *maximum curve* represents the *working points* for a rope that is cycled around a historical maximum tension level. After the tension has reached a maximum, the elongation will retract along a *working curve*, and when tensioned again the elongation will cycle back up to the working point, as illustrated in Figure 6.4. Note that the new working point can be on the maximum curve if the tension is cycling up to the historical maximum, or it can be on the working curve if it is below the historical maximum.

From this behaviour it is seen that the tension-elongation behaviour can be simplified into a model that is easier to adapt than the spring-dashpot model. The dynamic stiffness can be expressed as a linear function of the mean tension as

$$K_{dyn} = a_{t,e} + b_{t,e} \cdot F_{mean} \quad (6.2)$$

where

- $a_{t,e}$ and $b_{t,e}$ are material constants

The mean tension is given as a non-linear function of the strain as

$$T_{mean} = c_{t,e} \cdot \varepsilon^2 \quad (6.3)$$

where

- $c_{t,e}$ is a material constant
- ε = strain

The model thus consist of linear stiffness for LF and WF motions and tensions, and non-linear characteristics for mean tension.

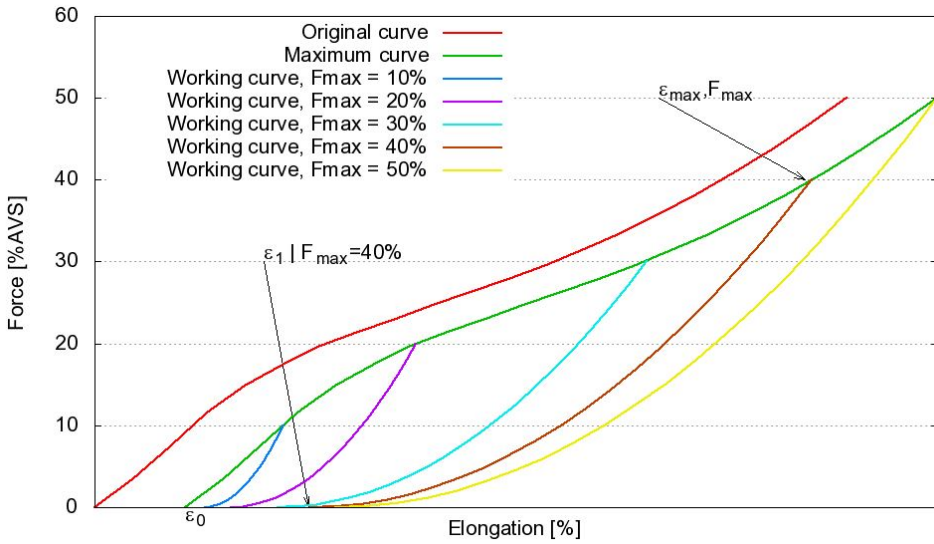


Figure 6.3: Working curves dependant on maximum tension history (Falkenberg et al. 2011)

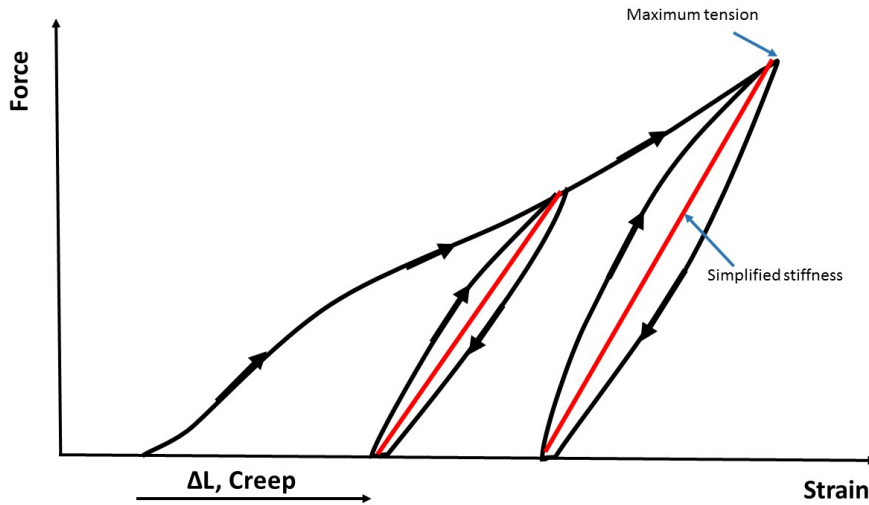


Figure 6.4: Constant stiffness based on historic maximum tension

This simplified model is the one that is commonly used today, and several fibre rope manufacturers lists their ropes stiffness' as a function of cycling tension. An example from Lankhorst Ropes is given in Table 6.1. Today, common practice in the industry is to adopt a stiffness that corresponds to 20 times the MBS (Larsen 2016), given as

$$EA = 20 \cdot S_{mbs} \tag{6.4}$$

which is the model that will be used in this thesis.

Minimum Breaking Load	ø	Mass in air	Mass in water	Stiffness		
				Cycling between 10-30% MBL	Cycling between 20-30% MBL	Cycling between 40-50% MBL
				MN	MN	MN
(TF)	(mm)	(kg/m)	(kg/m)			
450	125	10,8	2,8	68	100	121
500	132	12,2	3,1	76	111	134
600	144	14,4	3,7	91	134	161
700	156	16,7	4,3	106	156	187
800	167	19,3	4,9	121	178	214
900	177	21,6	5,5	136	200	241
1000	186	24,0	6,2	151	223	268
1100	196	26,5	6,8	166	245	295
1200	201	28,3	7,3	181	267	321
1250	203	29,0	7,4	189	278	335
1300	208	30,4	7,8	196	289	348
1400	217	33,0	8,5	212	312	375
1500	223	34,8	8,9	227	334	402
1600	232	37,7	9,7	242	356	429
1700	238	39,5	10,1	257	379	455
1800	246	42,4	10,9	272	401	482
1900	251	44,2	11,3	287	423	509
2000	259	46,8	12,0	302	445	536
2100	266	49,7	12,7	317	468	562
2200	274	52,5	13,5	332	490	589
2300	279	54,6	14,0	347	512	616
2400	286	57,4	14,7	363	534	643
2500	290	59,2	15,2	378	557	670

Table 6.1: Lanhorst Rope's data of stiffness as a function of cyclic tension (Lankhorst Ropes 2015)

SIMA and applied theory

7.1 Introduction

This chapter gives a introduction to the software used in this thesis, as well as the theory applied in this software.

SIMA is a workbench software that provides a graphical user interface for the use of, amongst other, SIMO and RIFLEX. This way SIMO and RIFLEX models can be developed and modified without the use of input-files. SIMA also has a built-in tool for the setup of calculations using combinations of different variables, and thus a simple way of running multiple analysis in parallel. Since TD simulations are solved step-by-step, only a single logical processor can be utilized per simulation. If multiple simulations are to be run, it is very time-saving to be able run several simulations simultaneously. In that case, the number of processors are the limiting factor for how many simulations that can be run in parallel.

7.2 RIFLEX

RIFLEX is a computational software for structural analysis based on the *finite element method* (FEM). It was designed to perform static and dynamic analysis of the internal forces and responses on slender systems such as mooring lines and risers. To do these analyses RIFLEX utilizes dynamic time-domain (TD) computation that follow a step-by-step integration of the incremental dynamic equilibrium equation (MARINTEK 2015). For each of the time steps in the integration, RIFLEX updates the mass, stiffness and damping matrices. A more detailed explanation of the TD simulation is given in Section 7.2.1.

A RIFLEX model is built with supernodes and lines, where the supernodes functions as the

connections in the system. They are position by coordinates and can be given constraints in any of the 6 DOFs as well as prescribed offsets that they are moved to when RIFLEX runs the static analysis. The supernodes are connected to each other by lines, which are defined by line types which again are composites of one or more segments. Each segment can contain a single set of cross-sectional properties, and different cross-sectional properties can be included by dividing a line into several segments. Each segment can be split into multiple elements that are used for the FEM formulation. The relation between line, segment and element is given in Figure 7.1.

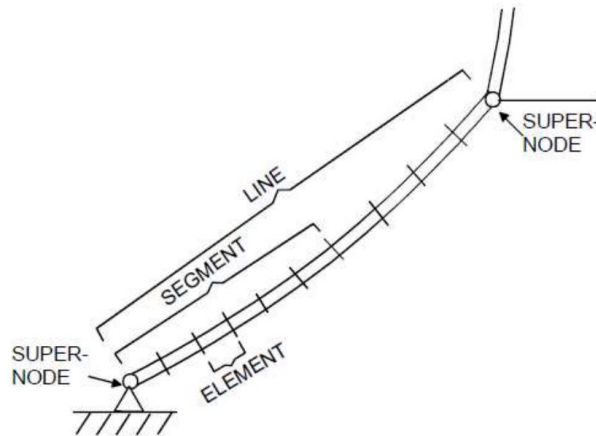


Figure 7.1: Definition of line, segment and element in RIFLEX (Godø 2013)

A line type can be used to define multiple identical lines, such as the three mooring lines of Hywind Demo.

7.2.1 Non-linear time domain simulation

The most important advantage of running a TD simulation is the treatment of non-linearities, the most important of which are

- Geometric stiffness (i.e contribution from axial force to transverse stiffness)
- Non-linear material properties
- Hydrodynamic loading according to the generalized Morison equation expressed by relative velocities
- Integration of loading to the actual surface elevation
- Contact problems (bottom contact, riser collision, other collisions or contacts)

The step-by-step numerical integration of the incremental dynamic equilibrium equations allows for the incorporation of these non-linearities. The numerical integration is solved

with a Newton-Raphson equilibrium at each time step. The downside of a TD simulation is that it is time consuming due to the repeating generation of the stiffness, mass and damping matrices.

The hydrodynamic loading on the elements are computed using 2D strip theory to calculate the hydrodynamic responses from potential flow and the drag term in Morison's equation as shown in Equation (7.1)

$$F_H = F_{Pot} + F_D = F_{FK} + F_S + F_R + F_D \quad (7.1)$$

where

- F_H = Total hydrodynamic forces
- F_{Pot} = Sum of potential flow forces
- F_D = Drag force
- F_{FK} = Potential flow force contribution from Freude-Kriloff
- F_S = Potential flow force contribution from diffraction
- F_R = Potential flow force contribution from added mass and damping

7.2.2 Beam and bar elements

Elements in RIFLEX can be modelled as either beam or bar elements. The beam element is based on the following assumptions:

- A plane cross-section that is initially normal to the x-axis remain plane and normal to the x-axis during deformations
- Lateral contractions due to elongations are neglected
- No large strains in the system
- Shear deformations from lateral loading are neglected. St. Venant torsion is accounted for.
- Coupling between torsion and bending is neglected.

The beam element has 6 degrees of freedom at each end/node, which is defined in relation to the beam's local coordinate system. The local x-axis is oriented between the two end nodes, from node 1 to node 2. An illustration of the beam element is given in Figure 7.2.

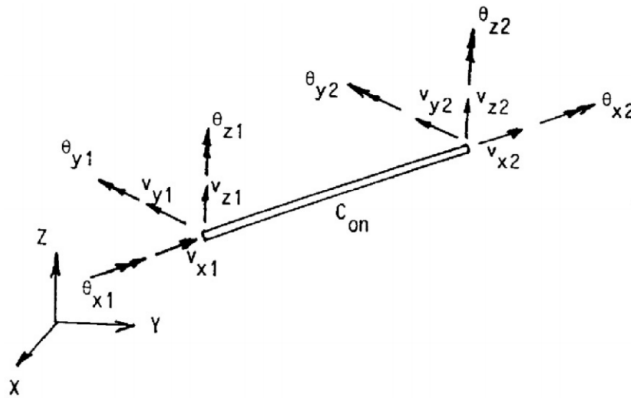


Figure 7.2: Beam element in RIFLEX (MARINTEK 2015)

The bar element has, unlike the beam element, only three translational degrees of freedom, i.e. no rotational degrees of freedom. Thus, the bar element is not capable of account for bending, or warping.

Due to the reduced amount of DOFs in a system built on bar elements, the computation time is reduced if the bar element is used where applicable, such as mooring lines with negligible bending stiffness.

7.2.3 Blade element momentum

The wind loads on the airfoils are calculated using *blade element momentum* (BEM) theory. BEM is a combination of blade element theory and momentum theory. In BEM, the airfoil is divided into elements, and it is assumed that these element do not influence one another. The force on each element are calculated using 2D foil theory, while 3D effect are accounted for by correction factors. In the following sections, the classic BEM method and the correction factors are discussed.

Classic blade element momentum method

The principle behind BEM is to calculate the *induction factors*, a_A and a_T . The axial induction factor, a_A , specify the ratio between the wind velocity in front of and far behind the rotor. The torque exerted on the air flow from the rotor blades causes the flow to rotate in the opposite direction of the rotor. The tangential induction factor, a_T , gives the ratio between the angular velocity imparted to the free stream and the angular velocity of the rotor.

The classic BEM method are based on the two following assumptions for annular elements:

1. There are no dependency between the blade elements, the forces on the elements do not affect another
2. The force from the blades exerted on the flow is constant for each annular element. This means that the rotor has an infinite number of blades

From momentum theory, the expressions for thrust and torque for an annular ring is given as

$$dF_{thrust} = 4a_A(1 - a_A)\frac{1}{2}\rho v_0^2 \pi r dr \quad (7.2)$$

$$dQ = 4a_T(1 - a_A)\frac{1}{2}\rho v_0 \Omega r^2 2\pi r dr \quad (7.3)$$

where

- dF_{thrust} = incremental contribution to thrust force
- dQ = incremental contribution to torque
- a_A = axial induction factor
- a_T = tangential induction factor
- ρ = density of air
- v_0 = flow velocity in front of rotor
- Ω = angular velocity of rotor
- r = distance from centre of rotor plane to control volume
- dr = thickness of control volume

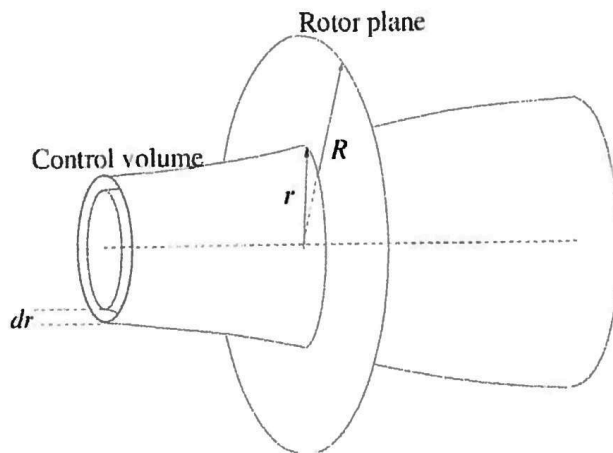


Figure 7.3: Control volume shaped as an annular ring to be used in the BEM model (Hansen 2015)

The *angle of attack* (AOA) of flow against an airfoil is defined as the angle between the relative wind and *chord line*, where the chord line is defined as a straight line connecting the leading and trailing edge, illustrated as α in Figure 7.4a. Figure 7.4a also illustrates the drag and lift force, F_D and F_L , on the airfoil from the airflow, as well as the pitching moment M .

The forces on the airfoil section can be split into two components; one normal to the the rotor plane, p_N ; and one tangential to the rotor plane, p_T , as illustrated in Figure 7.4b.

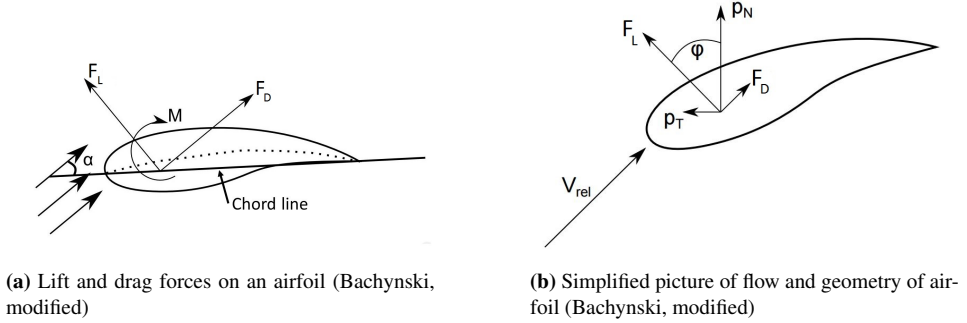


Figure 7.4

In Figure 7.4b, V_{rel} represents the inflow velocity from a combination of the incoming wind, angular rotor velocity, induced axial velocity and induced tangential velocity. The flow angle, φ , comes from the angle of attack and the angle of the blade. The angle φ can be calculated through the inductions factors as

$$\tan(\varphi) = \frac{(1 - a_A)v_0}{(1 + a_T)\Omega r} \quad (7.4)$$

The relation between the angle of attack and the flow angle, α and φ , is defined as

$$\alpha = \varphi - \theta = \varphi - \theta_p + \beta_m \quad (7.5)$$

where

- θ = blade pitch angle
- θ_p = blade pitch applied by control system
- β_m = local blade twist from manufacturer

From Figure 7.4b the following expressions can be formed

$$p_N = F_L \cos(\varphi) + F_D \sin(\varphi) \quad (7.6)$$

$$p_T = F_L \sin(\varphi) - F_D \cos(\varphi) \quad (7.7)$$

$$dF_{thrust} = B p_N dr = B [F_L \cos(\varphi) + F_D \sin(\varphi)] dr \quad (7.8)$$

$$dQ = Br p_T dr = Br [F_L \sin(\varphi) - F_D \cos(\varphi)] dr \quad (7.9)$$

where

- B = number of blades

In addition, the normal and tangential coefficients, C_N and C_T , can be expressed from the airfoil's drag and lift coefficients as

$$C_N = C_L \cos(\varphi) + C_D \sin(\varphi) \quad (7.10)$$

$$C_T = C_L \sin(\varphi) - C_D \cos(\varphi) \quad (7.11)$$

and the solidity ratio can be defined as

$$\sigma' = \frac{BL_c}{2\pi r} \quad (7.12)$$

where

- L_c = chord length of airfoil

The solidity ratio accounts for the fact that the rotor does not have an infinite amount of blades, as assumed in the blade momentum theory.

By combining the expressions for thrust, Equation (7.2) and (7.8), the axial induction factor can be found as

$$a_A = \frac{1}{\frac{4 \sin^2(\varphi)}{\sigma' C_N} + 1} \quad (7.13)$$

Similarly, by combining the expressions for torque, Equation (7.3) and (7.9), the tangential induction factor can be written as

$$a_T = \frac{1}{\frac{4 \sin(\varphi) \cos(\varphi)}{\sigma' C_T} + 1} \quad (7.14)$$

Using the equations developed in this section, the BEM model can be solved with an iterative process. Since the different blade elements used in the strip model are assumed to be independent, the solution for the different control volumes can be solved independently. The iterative process can be divided into the following eight steps (Hansen 2015) :

1. Set initial a_A and a_T , typically $a_A = a_T = 0$
2. Calculate the flow angle, φ , using Equation (7.4)
3. Compute the local angle of attack, α , using Equation (7.5)

4. Read the drag and lift coefficients for the airfoils that corresponds to the angle of attack, $C_D(\alpha)$ and $C_L(\alpha)$
5. Compute C_N and C_T using Equation (7.10) and (7.11)
6. Calculate the induction factors, a_A and a_T , from Equation (7.13) and (7.14)
7. Check difference between new and previous induction factors. If not within tolerance, go to step 2. If within tolerance, continue to step 8.
8. Compute local load on blade strip

By summing the forces on all elements for all blades, the total force from the rotor on the rest of the structure is found.

Prandtl's tip loss correction factor

Prandtl's tip loss factor accounts for the assumption of an infinite number of blades. A rotor with a finite amount blades will generate a different vortex system in the wake then a rotor with an infinite number of blades. This is because the air at the tip of the blade tends to flow around the blade-tip, following the pressure gradient. As seen in Figure 7.3, the classic BEM method is based on an axis-symmetric streamtube which does not exist in reality, making the momentum equations more complicated. Prandtl introduced a correction factor, $F_{Prandtl}$, to the aerodynamic loads so that when the loads are corrected and evenly distributed azimuthally, they yield results for induction at the blades which are similar to that of a rotor with an infinite number of blades.

The correction factor, $f_{Prandtl}$, is computed as

$$f_{Prandtl} = \frac{2}{\pi} \cos^{-1}(\exp(-f)) \quad (7.15)$$

where

$$f = \frac{B}{2} \frac{R-r}{r \sin(\varphi)} \quad (7.16)$$

where

- B = number of blades
- R = total radius of the rotor
- r = local radius of rotor for the strip
- φ = flow angle

The correction factor, $F_{Prandtl}$, is introduced into Equation (7.2) and (7.3) as

$$dF_{thrust} = 4a_A(1 - a_A)\frac{1}{2}\rho v_0^2 \pi r F_{Prandtl} dr \quad (7.17)$$

$$dQ = 4a_T(1 - a_A)\frac{1}{2}\rho v_0 \Omega r^2 2\pi r F_{Prandtl} dr \quad (7.18)$$

By using Equation (7.17) and (7.18) instead of Equation (7.2) and (7.3) when calculating the induction factors the following is found

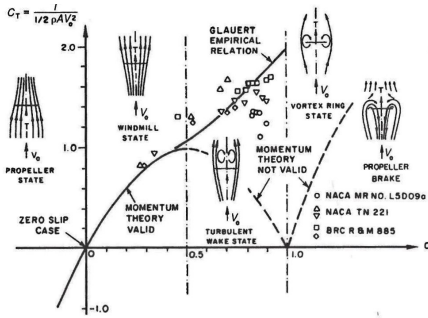
$$a_A = \frac{1}{\frac{4f_{Prandtl} \sin^2(\varphi)}{\sigma' C_N} + 1} \quad (7.19)$$

$$a_T = \frac{1}{\frac{4f_{Prandtl} \sin(\varphi) \cos(\varphi)}{\sigma' C_T} - 1} \quad (7.20)$$

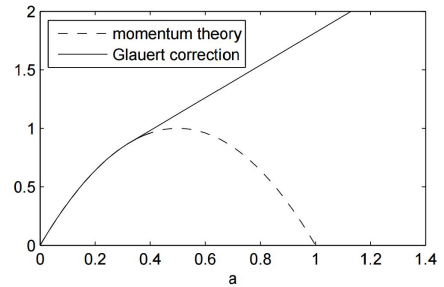
Hence, Equation (7.19) and (7.20) should be used in the BEM iteration instead of Equation (7.13) and (7.14). This will add an extra step in the BEM iteration, which would be to compute Prandtl's tip loss factor using Equation (7.15) after performing step 2.

Glauert correction

Classic BEM theory is only valid for axial induction factors lower than 0.4. Above this value, the simple momentum theory is not valid, as illustrated in Figure 7.5a.



(a) Classic BEM validity range (Hansen 2015)



(b) Glauert correction (MARINTEK 2015)

Figure 7.5

There are several relations, found through empirical data, between the axial induction factor and the thrust curve. The one used in RIFLEX is taken from Burton et al. 2011 and gives a thrust curve for $a_A > 0.4$ that is expressed as

$$a_A = \frac{\frac{C_T}{f_{Prandtl}} - C_{T1}}{C_{T2} - C_{T1}}(a_2 - a_1) + a_1 \quad (7.21)$$

where

- $C_{T1} = 4a_1(1 - a_1)$
- $C_{T2} = 1.82$
- $a_1 = 1.0 - 0.5\sqrt{C_{T2}}$

- $a_2 = 1.0$
- $f_{Prandtl} = \text{Prandtl correction factor}$

An illustration of the thrust curve with and without Glauert correction with $f_{Prandtl} = 1.0$ is given in Figure 7.5b.

Dynamic wake

The BEM procedure and corrections discussed so far can be seen as quasi-static in the way that any change in incoming wind velocity, blade pitch angle or angular rotor velocity will give an immediate change of the induction factors. In reality, the flow field will experience a time delay due to its large size. The *dynamic wake effect* is the time lag in the induced velocities as an effect of the vortex shedding from the blades and the convection of these vortices in the downstream. This dynamic wake effects are more distinct for heavily loaded rotors, i.e. high induction factors. In RIFLEX, this is taken care of by the *Stig Øye dynamic inflow model* (MARINTEK 2015) which filters the induced velocities. The model is given as

$$W = \tau_2 \frac{dW}{dt} = W_{int} \quad (7.22)$$

$$W_{int} + \tau_1 \frac{dW_{int}}{dt} = W_{qs} + 0.6\tau_1 \frac{dW_{qs}}{dt} \quad (7.23)$$

where

- $W = \text{corrected induced velocity}$
- $W_{qs} = \text{quasi-static induced velocity}$
- $\tau_1 = \text{time constant}$
- $\tau_2 = \text{time constant}$

Dynamic stall

The classic BEM method uses the static drag and lift coefficients for the airfoil in order to calculate the drag and lift forces on the blades, which give a steady-state solution to the forces given a certain AOA. However, a rotating blade on a WTG is subjected to dynamic changes of the AOA from wind shear, tower passage, atmospheric turbulence and yaw/tilt misalignment. Due to the dynamic nature of the incoming wind, the coefficients may not follow the static values. As a consequence, an airfoil may experience a high lift coefficient after a sudden increase in wind velocity. In RIFLEX, the Stig Øye model is, as previously stated, implemented, which gives unsteady lift by filtering the separation point on the

trailing edge with a time constant that is found empirically (MARINTEK 2015). For flow that is not completely stalled, the lift coefficient is corrected as

$$C_L = \frac{1}{4} \frac{dC_L}{d\alpha} (\alpha - \alpha_0) \left(1 + \sqrt{1 - |f_s|}\right)^2 \quad (7.24)$$

$$f_s(t + \Delta t) = f_s^{st} + (f_s(t) - f_s^{st}) \exp\left(-\frac{\Delta t}{\tau}\right) \quad (7.25)$$

where

- $\frac{dC_L}{d\alpha}$ is computed at the limit for full stall
- α_0 = angle of attack that gives zero lift
- f_s = degree of stall
- f_s^{st} = static value of degree of stall
- τ = time constant

The degree of stall, f_s is assumed to follow the static value, f_s^{st} , as

$$\frac{df_s}{dt} = \frac{f_s^{st} - f_s}{\tau} \quad (7.26)$$

For a completely stalled flow, the corrected lift coefficient is calculated as

$$C_L = C_{L,qs} \left(1 + \sqrt{1 - |f_s|}\right)^2 \quad (7.27)$$

where

- $C_{L,qs}$ = the quasi-static lift coefficient
- f_s = degree of stall, given in Equation (7.25)

Skewed inflow

Skewed inflow means that the rotor is either tilted or yawed at an angle against the wind. For a FOWT, this would be the case in pitch and yaw motion. A basic formulation developed by Glauert corrects the axial induction factor due to skewed inflow.

$$a_{A,skew} = a_A \left[1 + \tan\left(\frac{\chi}{2}\right) \frac{r}{R} \cos(\Psi)\right] \quad (7.28)$$

where

- a_A = axial induction factor
- χ = wake skew angle
- R = total radius of the rotor

- r = local radius of rotor for the strip
- Ψ = azimuth angle, equal to zero when rotor is faced directly downwind

Tower shadow

The influence from the tower on the blades, called *tower shadow*, is calculated using potential flow theory. Since the wind has to flow around the tower, the area in front of the tower will have a flow with reduced velocity. This reduction in flow velocity is calculated using the 2D potential solution for constant flow around a circle. The coordinate system used in the solution is given in Figure 7.6, and the non-dimensional solution to the tower influence at a point given by the coordinates (x, y, z) is given in Equation (7.29)-(7.32)

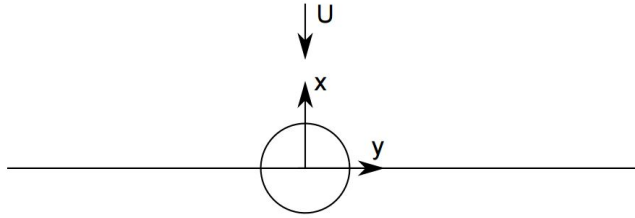


Figure 7.6: Tower shadow coordinate system (MARINTEK 2015)

$$x_w = \frac{2x}{D_{tower}} \quad (7.29)$$

$$y_w = \frac{2y}{D_{tower}} \quad (7.30)$$

$$x_{inflow} = \left[1 - \frac{x_w^2 - y_w^2}{x_w^2 + y_w^2} \right] \quad (7.31)$$

$$y_{inflow} = 2 \left[\frac{x_w y_w}{x_w^2 + y_w^2} \right] \quad (7.32)$$

where

- D_{tower} = tower diameter at z-level

The procedure for using the tower shadow correction is to calculate the horizontal wind velocity and direction at point (x, y, z) , then the velocity is multiplied with the factors, x_{inflow} and y_{inflow} , and transported back to the initial direction (Moriarty and Hansen 2005).

Hub Loss

It is important to note that hub loss correction is not implemented in RIFLEX.

Similar to the tip-loss correction, the hub-loss correction corrects the induced velocity from vortices being shed near the hub of the WTG.

7.3 Dynamic time domain integration

The governing dynamic equilibrium equation can be written as

$$\mathbf{R}^I(\mathbf{r}, \dot{\mathbf{r}}, \ddot{\mathbf{r}}, t) + \mathbf{R}^D(\mathbf{r}, \dot{\mathbf{r}}, t) + \mathbf{R}^S(\mathbf{r}, t) = \mathbf{R}^E(\mathbf{r}, \dot{\mathbf{r}}, t) \quad (7.33)$$

where

- \mathbf{R}^I = inertia force vector
- \mathbf{R}^D = damping force vector
- \mathbf{R}^S = internal structural reaction force vector
- \mathbf{R}^E = external force vector
- $\mathbf{r}, \dot{\mathbf{r}}, \ddot{\mathbf{r}}$ = structural displacement, velocity and acceleration vectors
- t = time

For the model used in this thesis, the external force vector accounts for weight and buoyancy; drag and mass force from Morison equation; and the aerodynamic force from the BEM solution.

The dynamic equilibrium equation are solved in TD using Newmark- β step-by-step integration. By the use of a constant time step throughout the simulation, this method uses following relation between displacement, velocity and acceleration at time t and $t + \Delta\tau$

$$\begin{aligned} \dot{\mathbf{r}}_{t+\Delta\tau} &= \dot{\mathbf{r}}_t + (1 - \gamma)\ddot{\mathbf{r}}_t\Delta\tau + \gamma\ddot{\mathbf{r}}_{t+\Delta\tau}\Delta\tau \\ \mathbf{r}_{t+\Delta\tau} &= \mathbf{r}_t + \dot{\mathbf{r}}_t\Delta\tau + \left(\frac{1}{2} - \beta\right)\ddot{\mathbf{r}}_t(\Delta\tau)^2 + \beta\ddot{\mathbf{r}}_{t+\Delta\tau}(\Delta\tau)^2 \end{aligned} \quad (7.34)$$

where γ and β are parameters that define the functional change in displacement, velocity and acceleration in the integration method.

The numerical damping of the method is determined by γ , where

- $\gamma > 0.5$ gives positive damping
- $\gamma < 0.5$ gives negative damping
- $\gamma = 0.5$ gives no damping

The integration method is unconditionally stable for $\gamma > \frac{1}{2}$ and $\beta \geq \frac{1}{4}(\gamma + \frac{1}{2})^2$.

This thesis has utilized the constant average acceleration method with $\gamma = 0.256$ and $\beta = 0.505$, introducing a small amount numerical damping to the simulation. This numerical damping does not provide any significant damping to the system when performing the analyses, but avoids numerical instability in the calculations. The time step utilized is 0.005 s, as recommended in SIMA for FOWTs. The constant acceleration method is based on taking the acceleration to be constant in the time step, as illustrated in Figure 7.7.

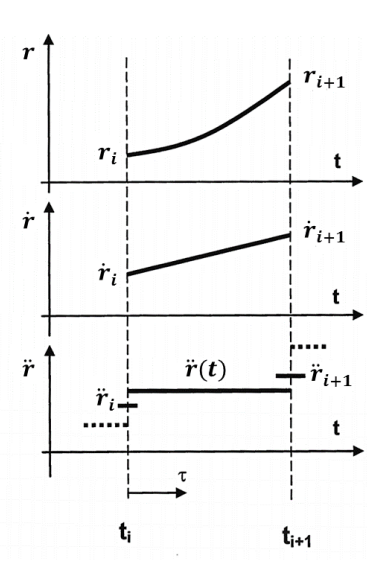


Figure 7.7: Constant average acceleration (Larsen 2014, modified)

Note that the dynamic time domain solution is only correct for the time steps used in the calculations. The solution does not yield the response as a continuous function, but as values for discrete time steps.

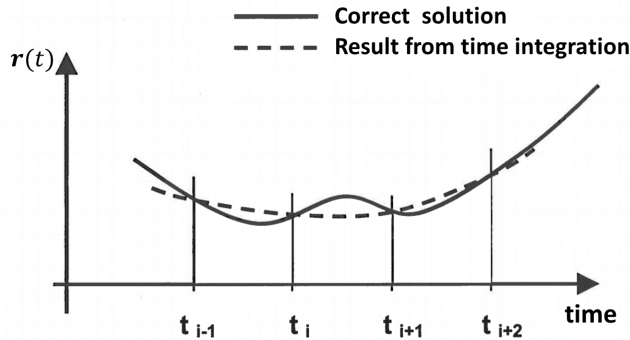


Figure 7.8: Discrete and continuous solution (Larsen 2014, modified)

7.4 SIMO

SIMO (Simulation of Marine Operations), is a software developed to simulate motions and behaviour of complex floating vessels and suspended loads, such as an offshore crane loading operation. SIMO uses TD simulation of the motions of *SIMO bodies* and the forces that act on these bodies. In addition to response calculation, SIMO also have the ability of generating time series of wind, waves and current. For this thesis, SIMO is used to output the pitch and yaw motion of the COG as well as the generation of environment.

7.5 Statistics

7.5.1 Mean and standard deviation

The mean values and standard deviations for the responses used in this thesis are calculated using a single time series realization of the responses. To avoid any transient behaviour, an analysis duration of 12 000 s is utilized, and the first 1200 s is disregarded, leaving a total of 10 800 s or 3 h to be used for the analysis.

7.5.2 Response confidence interval

By using the mean and standard deviations, and by assuming that the responses are normal distributed, a 95% confidence interval can be established.

The 95% confidence interval is based on a single environmental seed realization and is calculated from the mean value and standard deviation. A 95% confidence interval will contain 95% of the response values, meaning that for a 3-hour time series, there will be two time periods of 4.5 min, corresponding to 2.5% of 3-hours, that will have response

values above the upper limit and below the lower limit of the interval. The response values for the upper and lower limit of confidence interval, at the 97.5 and 2.5 percentile, are found as

$$\begin{aligned} R_{0.975} &= R_{mean} + 1.96R_{std}. \\ R_{0.025} &= R_{mean} - 1.96R_{std}. \end{aligned} \tag{7.35}$$

where

- R_{mean} = mean response value
- $R_{std.}$ = standard deviation of response

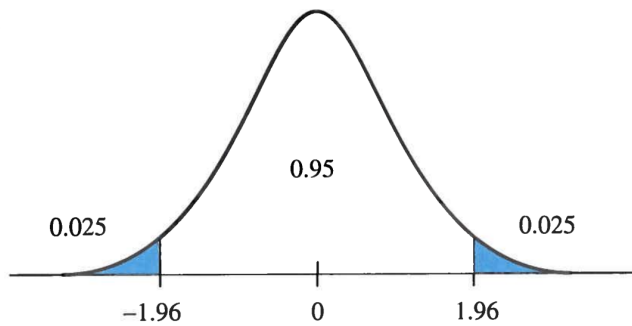


Figure 7.9: 95% confidence interval of a normal distribution (Hagen 2007, modified)

7.5.3 Extreme value distribution

To determine the maxima that fall outside the upper limit of the confidence interval, described in Section 7.5.2, the maxima of the time series were utilized. Due to the nature of TD simulations, a single seed of a 3-hour simulation is by itself not representative to determine the maximum responses. This is because a single 3-hour period may not contain the maximum environmental forces that can be associated with the environment, or may not include the dynamic behaviour of the system that results in the largest responses. Therefore, several seeds of 3-hour are used to generate a distribution of the largest responses.

This thesis utilized SIMA's post processor to generate the extreme value distributions for motion and line tension responses using the Gumbel distribution. If the largest value of many underlying values are selected for distribution fitting, the Gumbel distribution is a correct asymptotic distribution for most practical problems.

For each simulation run in SIMA, time series for each of the responses was generated, each having a set of maxima. An illustration of such a broad banded process is given in Figure 7.10.

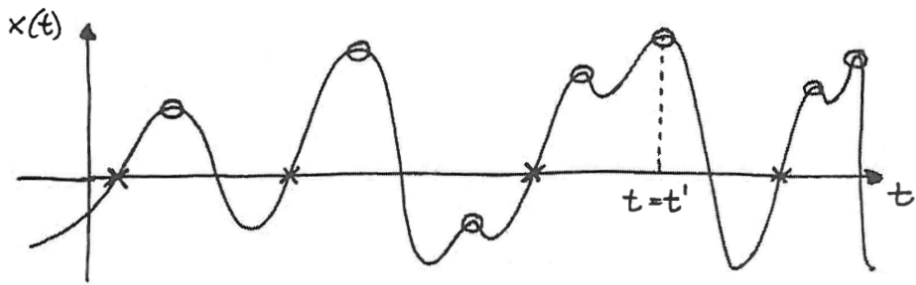


Figure 7.10: Broad banded process. O = local maxima, X= zero up-crossing (Myrhaug 2005)

From each of the time series, the largest of the maxima was used to generate a distribution of largest maxima. Therefore, it is necessary to run several simulations, each giving a single maximum response value, in order to generate a proper distribution. An illustration of several time series with their corresponding largest maxima and a distribution of largest maxima is given in Figure 7.11.

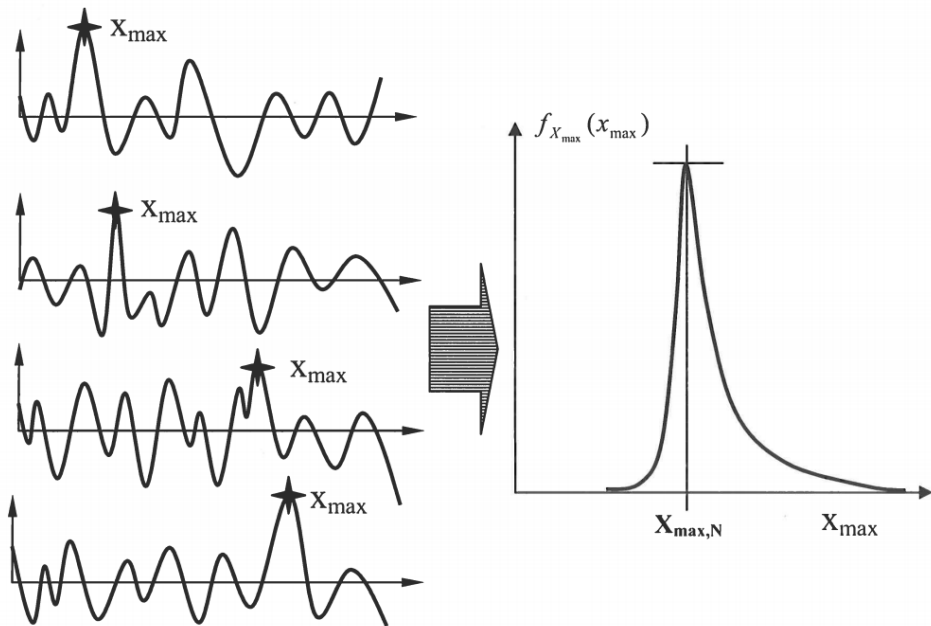


Figure 7.11: Generation of extreme value distribution from processes (Larsen 2014)

Establishment of Environmental Conditions

8.1 Introduction

This chapter defines the environmental conditions that are to be used in the motion and line tension response analysis. As defined in Chapter 4, the ULS environmental conditions are the one that correspond to rated wind velocity of the WTG and the one that has a return period of 50-year.

The resulting environmental conditions are given in Table 8.3, the procedure to define these conditions are given in the following sections.

8.2 Environmental data

To define the environmental conditions Statoil 2004, DNV-OS-J103 2013 and the wind profile for the ISO wind (MARINTEK 2012), given in Equation 8.1 was utilized.

$$U_{ISO}(z) = U_{w0} \left[1 + C_{ISO} \ln \left(\frac{z}{z_{ref}} \right) \right] \quad (8.1)$$

where

- $C_{ISO} = 0.0573\sqrt{1 + 0.15U_{w0}}$
- $U_{w0} = U_{10\text{ m}} [\text{m s}^{-1}]$, for this application
- $z_{ref} = 10\text{ m}$, for this application

Wind velocity	Corresponding current return period
Rated	1 year
50 year	10 year

Table 8.1: Current return periods corresponding to different wind velocities (DNV-OS-J103 2013)

1 year return period													
Depth (m)	0°	30°	60°	90°	120°	150°	180°	210°	240°	270°	300°	330°	Omni
Surface													82
50													55
150													49
3 m above seabed	No directional current data available												40
10 years return period													
Depth (m)	0°	30°	60°	90°	120°	150°	180°	210°	240°	270°	300°	330°	Omni
Surface													94
50													63
150													55
3 m above seabed	No directional current data available												45
100 years return period													
Depth (m)	0°	30°	60°	90°	120°	150°	180°	210°	240°	270°	300°	330°	Omni
Surface													105
50													70
150													60
3 m above seabed	No directional current data available												50
Weibull parameters 3 m above seabed													
Shape (-)													1.750
Scale (cm/s)													10.980
Location (cm/s)	No directional current data available												-2.740

Table 8.2: Omni-directional extremes for the 10 minutes mean current speed (cm/s) versus depth for 1-, 10- and 100-year return period. Weibull parameters are given for 3 m above seabed. (Statoil 2004)

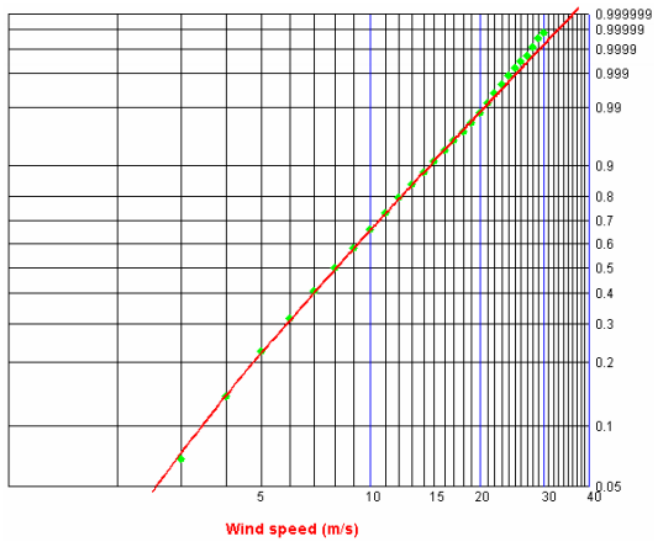


Figure 8.1: All-year wind speed distribution at Heidrun (Statoil 2004)

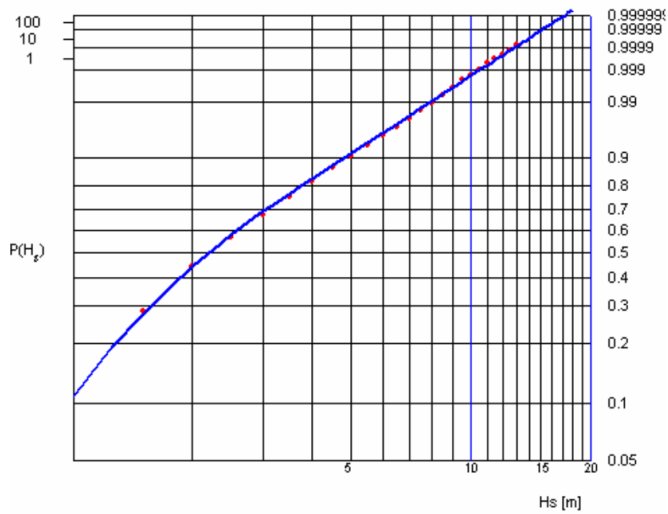


Figure 8.2: Marginal (all year) distribution for the significant wave height at Heidrun (Statoil 2004)

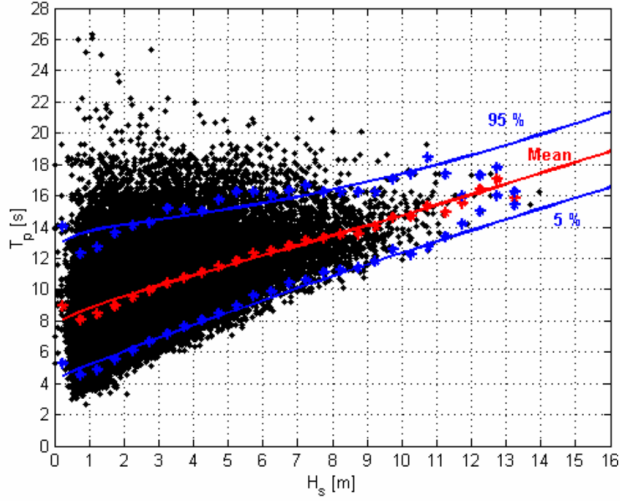


Figure 8.3: Conditional characteristics for the spectral peak period versus significant wave height at Heidrun (Statoil 2004)

8.3 Rated wind speed

The rated wind speed of Hywind Demo is 13 m s^{-1} (Bjørnsen 2015). Using Equation (8.1), the corresponding U_{10m} is found to be 11.3 m s^{-1} . By using Figure 8.1, the corresponding probability for rated wind speed is 0.75. Using this probability and Figure 8.2, the corresponding H_s , is found to be 3.5 m. The mean T_p is found to be 11 s using Figure 8.3.

From Table 8.1 it is seen that the return period for current associated with the rated wind speed is 1 year. Using data given in Statoil 2004 for the current speed, shown in Table 8.2, the mean current velocity, V , along the spar was calculated to be 0.61 m s^{-1} .

8.4 50-year wind speed

A return period of 50 years has an annual probability of

$$\text{Prob}(U_{10m} > U_{50y}) = 1 - \frac{1}{50 \text{ years} \frac{24 \text{ hours} \cdot 365 \text{ days}}{3 \text{ hours}}} = 0.999993 \quad (8.2)$$

Using the probability found in Equation (8.2) together with Figure 8.1 and 8.2 yields the 50-year return period wind of $U_{10m} = 34 \text{ m s}^{-1}$ and $H_s = 15.8 \text{ m}$. The mean T_p is found from Figure 8.3 as 18.8 s.

From Table 8.1 it is seen that the return period for current associated with the 50-year wind and sea state is 10 year. Using data given in Statoil 2004 for the current speed, shown in Table 8.2, the mean current velocity, V , along the spar was calculated to be 0.70 m s^{-1} .

8.5 Resulting environmental conditions

	$U_{10\text{m}}$ [m s^{-1}]	Prob.	H_s [m]	T_p [s]	V [m s^{-1}]
Rated	11.3	0.75	3.5	11.0	0.61
50-year	34.0	0.999993	15.8	18.8	0.70

$U_{10\text{m}}$ is the reference wind velocity, at 10 m height

H_s is the significant wave height

T_p is the peak period of the waves

V is the current velocity, which is taken as constant. $V = \bar{V}$

Table 8.3: Sea states to be examined

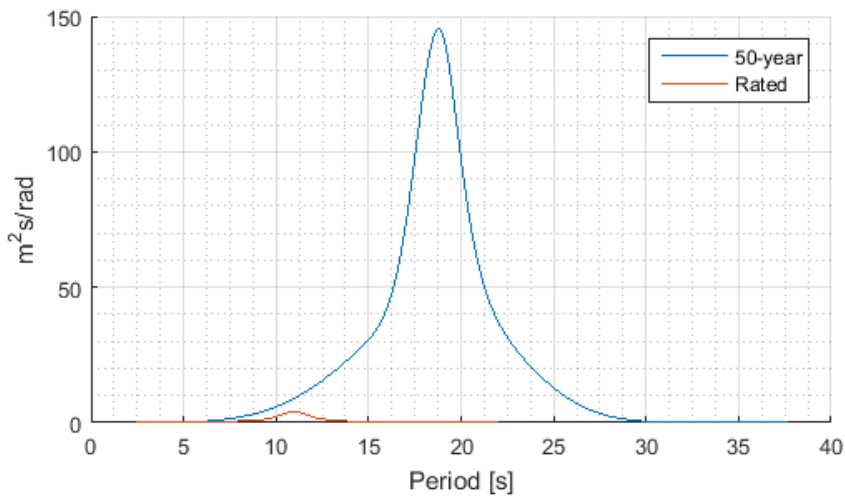


Figure 8.4: JONSWAP spectra for rated and 50-year environment

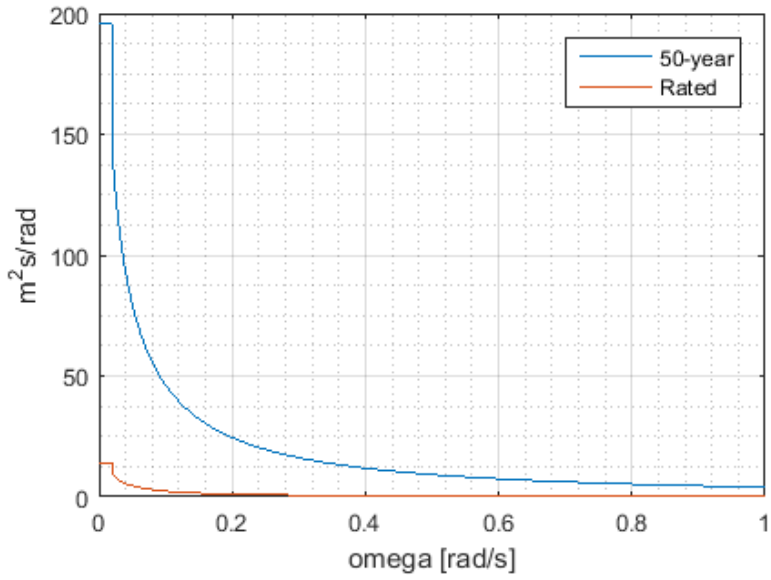


Figure 8.5: ISO wind spectra for rated and 50-year environment

SIMO-RIFLEX Model

A SIMO-RIFLEX model of Hywind Demo developed by Statoil ASA was used as a basis for the one developed in this thesis. The model provided by Statoil ASA was designed to be used for structural analysis of the spar and tower, and thus contained a large amount of degrees of freedom (DOFs) and consisted of a large variety of cross-sections to account for internal stiffeners, flanges, platforms, etc. Since the structural force responses is not a topic in this thesis, the model was severely simplified to reduce the computational complexity. There were also made some modifications to the physical properties of the global structure.

9.1 Modelling of spar and tower

The SIMO-RIFLEX model of Hywind Demo developed in this thesis is in practice a pure RIFLEX model. However, three dummy SIMO bodies are used to extract SIMO results for pitch and yaw motion and wind data, and also to implement some physical properties. These bodies are positioned at the COG, at the waterplane and at the WTG. The spar and tower are modelled using a set of RIFLEX cross-sections that build two lines between three supernodes. The reason for using three supernodes is that in order to have nodes that represent the mooring connections to the spar, it is needed to have a supernode at the same z-coordinate inside the spar, which serves as the mooring connections nodes' master. The three supernodes that build the spar and tower are hence positioned at $z = -100.045$ m, $z = -53.174$ m and $z = 65.0$ m. A graphic view of the two RIFLEX line that make the spar and tower, and the three SIMO bodies, are given in Figure 9.1-9.3.

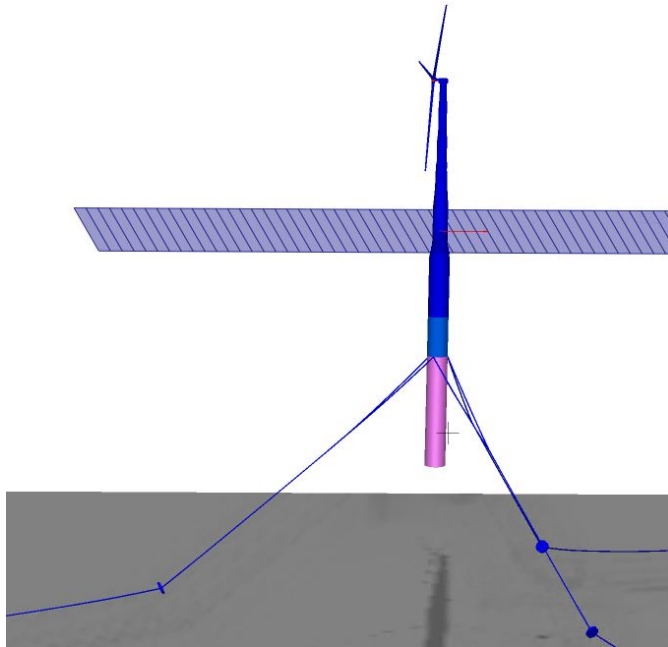


Figure 9.1: Line 1, marked with pink color

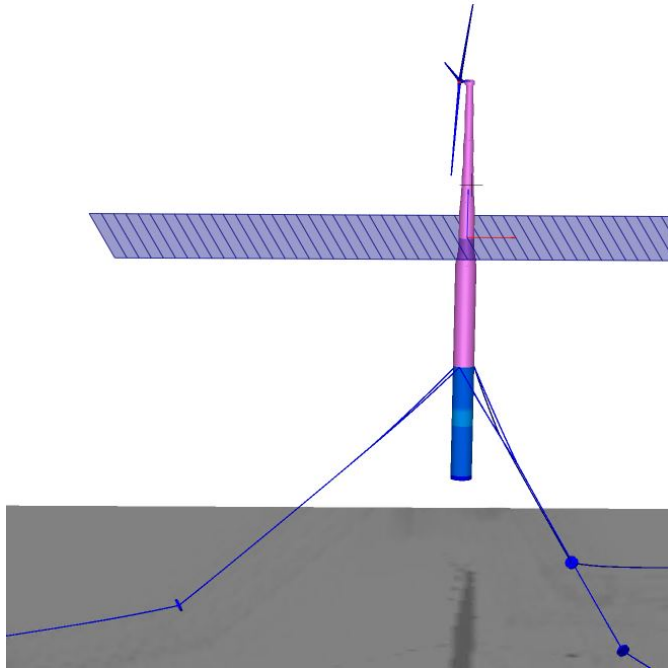


Figure 9.2: Line 2, marked with pink color

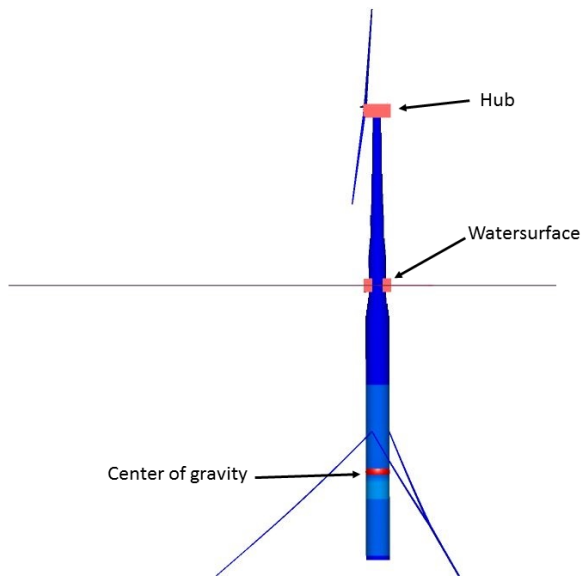


Figure 9.3: SIMO bodies used in corporation with the RIFLEX model, visualized as red boxes

In the original model, provided by Statoil ASA, the structure from top to bottom was modelled using 82 different cross-sections. The original model was built with a large amount of cross-sections to accurately model alternating internal stiffeners, flanges and material thickness' along the length of the spar and tower so that the model could be used for calculations of internal stresses in the structure. Since this thesis is only concerned with the mooring system and global response of the floater, the amount of cross-sections could be severely reduced. However, the model would have to accurate enough so that the external forces would be calculated correctly. Therefore, it was necessary to keep a relative large amount of cross-sections along the tower to model the tapering. The model used in this thesis was simplified to one that contains 22 cross-sections. This was done by merging neighbouring cross-sections with similar properties. After the merging, a fine tuning of the lower cross-section's mass coefficients were done in order to maintain the correct draft and COG. A generalized set of data for the spar and tower cross-section parameters is given in Table 9.1, this thesis does not discuss the structural properties of the spar and tower in detail due to confidentiality agreements with Statoil ASA.

	Vertical pos. [m]	Number of segments	Mass [$t m^{-1}$]	Ext. Area [m^2]
Line 1	-100.045 – -53.174	4	162 – 11	54.6
Line 2	-53.174 – 65.000	18	10.7 – 43.3	54.6 – 4.5

Table 9.1: Structural parameters for spar and tower

9.1.1 Drag force coefficients

Each of the cross-sections have to be defined with a drag coefficient, which RIFLEX will use for the response calculations. Two drag force coefficients are needed, one that represent the air drag on the tower, and one for the water drag on the spar.

Drag force coefficients for wind

To get the most accurate value for the tower's drag force coefficient, hand calculations were done for both environmental conditions and for three different tower diameters, corresponding to top, middle and bottom on the tower. The drag force coefficients were established using DNV-RP-C205 2010. First, Equation (8.1) was used to define the two environments' wind velocity at three different elevations, corresponding to the three diameters. Then, Reynolds numbers were established using a viscosity of $\nu_{air} = 1.29E-5 m^2 s^{-1}$. The surface roughness is given in DNV-RP-C205 2010 as $1.79E-5 m$ for painted steel. Using this information, the drag coefficients were found using Figure 9.4. The results are given in Table 9.2, where it is seen that there is not much variation in the drag coefficient. Therefore, an average drag coefficient of $C_{D_{wind}} = 0.63$ is used for the all sections of the tower for both environments.

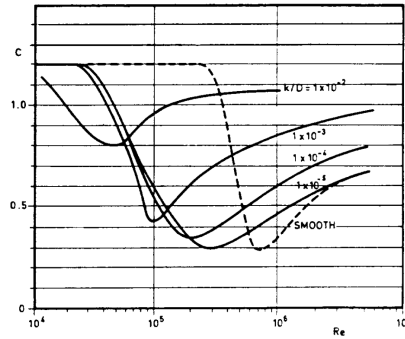


Figure 9.4: Drag coefficients for fixed circular cylinder for steady flow in critical flow regime for varying roughnesses (DNV-RP-C205 2010)

		Diameter [m]		
U_{10m} [m s ⁻¹]		5	3.7	2.39
11.3	$U(z)$	10.6	12.4	13.0
	Re	2.96E6	2.56E6	1.74E6
	Δ	1.00E-6	1.35E-6	2.10E-6
	$C_{D_{wind}}$	0.61	0.6	0.5
34	$U(z)$	30.7	39.0	41.9
	Re	8.56E6	8.06E6	5.59E6
	Δ	1.00E-6	1.35E-6	2.10E-6
	$C_{D_{wind}}$	0.7	0.69	0.67
Averaged $C_{D_{wind}} = 0.63$				

Table 9.2: Numerical calculation of wind drag coefficient

where

- $U(z)$ = Windspeed at height corresponding to given diameter [ms⁻¹]
- Re = Reynolds number [-]
- $\Delta = \frac{k}{D}$ [-]
- k = Surface roughness [m], given in DNV-RP-C205 2010
- D = Diameter [m]
- $C_{D_{wind}}$ = Drag coefficient for wind [-]

Drag force coefficients for water

The drag force coefficients in water was found using DNV-RP-C205 2010, in the same manner as for the drag force coefficients for wind, using a marine growth of 0.12 m, a

surface roughness of $k = 2.75\text{E-}2\text{ m}$ and a viscosity of $\nu_{water} = 1.26\text{E-}6\text{ m}^2\text{ s}^{-1}$. The resulting drag coefficients are given in Table 9.3, where it is seen that the results are stable around $C_{D_{water}} = 1.0$.

V [m s^{-1}]		Diameter [m]	
		6.12	8.46
0.61	Re	2.96E6	4.10E6
	Δ	4.5E-3	3.3E-3
	C_D	1.0	1.0
0.70	Re	3.4E6	4.7E6
	Δ	4.5E-3	3.3E-3
	C_D	1.0	1.1
Average $C_{D_{water}} = 1.0$			

Table 9.3: Numerical calculation of water drag coefficient

9.1.2 Added mass coefficients

Added mass coefficients for the spar were established in conjuncture with DNV-RP-C205 2010. The added mass coefficient is dependant on the Keulegan-Carpenter (KC) number as shown in Figure 9.5

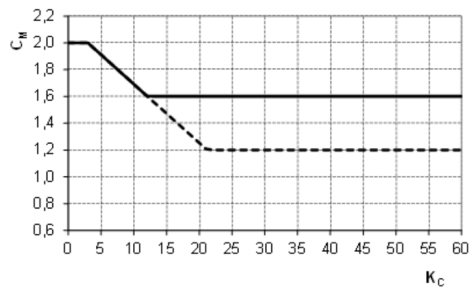


Figure 9.5: Mass coefficient as function of KC-number for smooth (solid line) and rough (dotted line) cylinder (DNV-RP-C205 2010)

KC number is defined as

$$KC = \frac{u_0 P}{D} \quad (9.1)$$

where

- u_0 = particle velocity amplitude [m s^{-1}]
- P = period [s]

- $D =$ diameter of cross section [m]

Inputting the data from the three environmental conditions in questions into Equation (9.1) gives KC numbers reaching a maximum of $KC = 8.1$, as shown in Table 9.4.

Env. condition	Top, $D = 6.12\text{m}$	Middle, $D = 8.4\text{m}$	Bottom, $D = 8.4\text{m}$
Rated	1.8	0	0
50-year	8.1	0	0
Before cut-off	4.1	0	0

Table 9.4: KC number at top, middle and bottom of the spar with their respective diameters (including marine growth)

Since the spar will move with the waves, the relative velocity between the particles and the spar will diverge from u_0 . However, from the results in Table 9.4 and from Figure 9.5, it is seen that the added mass coefficient can with reasonable certainty be chosen to be $C_{A_{spar}} = 1.0$.

9.2 Skin friction/Yaw damping

Hywind Demo has four effects that dampens yaw motion: air-foils that move through the air with the tower; mooring lines that are being pulled through the water from the bridle connections; and skin friction from the air around the tower and water around the spar. The damping effect from the air-foils are taken care of by the aerodynamic calculations done in RIFLEX, the damping from the mooring lines is also calculated in RIFLEX from the drag forces on the lines. RIFLEX can, however, not calculate skin friction on its elements. Therefore, this is added manually into the SIMO body in the waterplane. The skin friction from the air around the tower is neglected.

Since this thesis is focused around the mooring system of Hywind Demo, the yaw motions will not be of any significance. It is therefore concluded that to introduce a damping that is 5% of the critical damping is a sufficient approximation.

The critical damping is given as

$$C_{6_{crit}} = 2\sqrt{I_{66}K_{66}} \quad (9.2)$$

The total rotational inertia in yaw, I_{66} , is found by combining the polar moment of inertias of spar, tower and rotor.

$$I_{66} = I_{66_{spar,tower}} + I_{66_{WTG}} = M_{spar,tower}r_{spar,tower}^2 + M_{WTG}r_{WTG}^2 \quad (9.3)$$

where

- $M_{spar,tower}$ = combined mass of spar and tower

- M_{WTG} = mass of rotor
- $r_{spar,tower}$ = average radius of spar and tower, taken as 3 m
- r_{WTG} = distance from center of tower to weight-center of WTG.

From the SIMA model provided by Statoil ASA, the mass and COG of the rotor is found by combining all the RIFLEX elements' length, position and mass coefficients together. From this it is found that the WTG has a mass of $M_{WTG} = 138\,000$ kg with a mass center of $r_{WTG} = 2.3$ m. Knowing that the total weight of Hywind Demo is 5 150 829 kg, the weight of spar and tower is found to be $M_{spar,tower} = 5\,150\,829$ kg $- 138\,000$ kg = 5 012 829 kg.

The total rotational inertia of Hywind Demo in yaw is then found to be $I_{66} \approx 215E6$ kg m².

The stiffness in yaw, K_{66} , is found by using Equation (2.2). Inserting a tension of $T_H = 1E6$ N, which is the pretension, a distance $L' = 550$ m and bridle length $R' = 35$ m gives an approximate answer, resulting in a stiffness in yaw of $K_{66} \approx 37E6$ N m rad⁻¹.

The damping in yaw is then calculated as 5% of the critical damping as

$$C_{66} = 0.05C_{66,crit} \approx 9E6 \text{ N m s}$$

9.3 Polar moment of inertia of spar and tower

In addition to skin friction, polar moment of inertia of the spar and tower is not carried in RIFLEX due to their symmetry in the horizontal plane. The polar moment of inertia of spar and tower is included in the SIMO body at waterplane by

$$I_{66_{spar,tower}} = M_{spar,tower} r_{spar,tower}^2 \quad (9.4)$$

where

- $M_{spar,tower} \approx 5E6$ kg m², as defined in the previous paragraph
- $r_{spar,tower} \approx 3$ m, taken as a rough estimate

Solving Equation (9.4), yield a polar moment of inertia of spar and tower equal to $I_{66_{spar,tower}} \approx 45E6$ kg m².

9.4 Modelling of wind turbine generator

SIMA has the ability to implement WTGs in RIFLEX as a special module. The wind turbine is modelled with RIFLEX lines in the same manner as the spar and tower, and consist of a shaft, a hub, three blade connectors and three blades. The three blades are

identical and is built with 41 different cross-sections. These cross-sections are defined as airfoils, and each cross-section is given a geometry and a lift, drag and pitching moment coefficient which varies with the AOA. In Figure 9.6, an illustration of the coefficients variation with AOA is given for segment 12 of the blades.

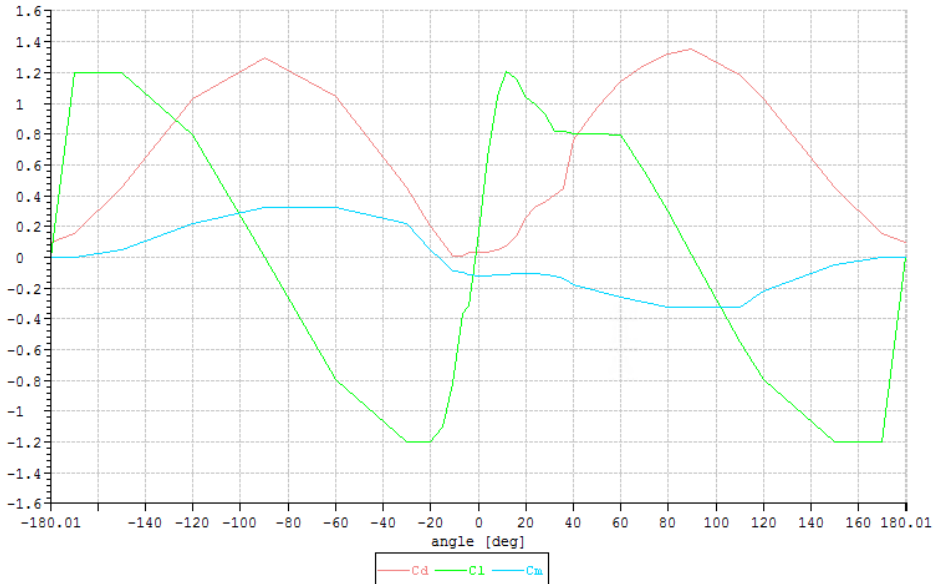


Figure 9.6: Aerodynamic coefficients for airfoil segment 10 as a function of angle of attack

The blade-pitch controller of a standard non-floating wind turbine regulates the pitch angle of the blades based on the rotational velocity of the rotor or the generator output, thus affecting the thrust force from the wind on the structure. For a FOWT, the blade-pitch controller also have to take the motion of the floater into account, as discussed in Section 5.5. A surge or pitch motion would give an altering relative velocity, which in turn would give a variation of the rotor velocity or generator power output. If a standard blade-pitch controller should control such a system, the system would amplify the natural motions of the floater by reducing the blade-pitch angle when the floater was moving against the wind, and increasing the blade-pitch angle when moving with the wind. The blade-pitch controller used in this thesis, provided in Bachynski 2016, is designed to be used with a spar FOWT, and will therefore prevent such tendencies.

To confirm that the WTG model is correct, a series of simulations with increasing wind velocity were run, from which the thrust force, generator power and blade pitch angle was extracted. The results are given in Figure 9.7-9.9.

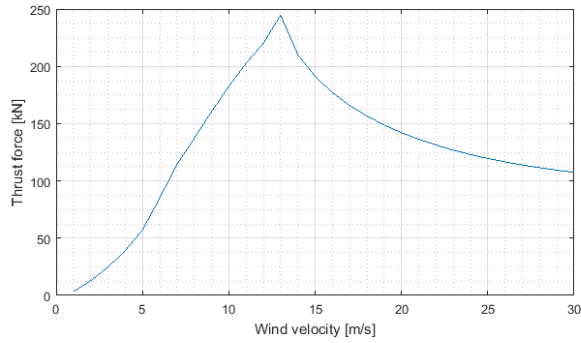


Figure 9.7: Rotor thrust force as a function of wind velocity

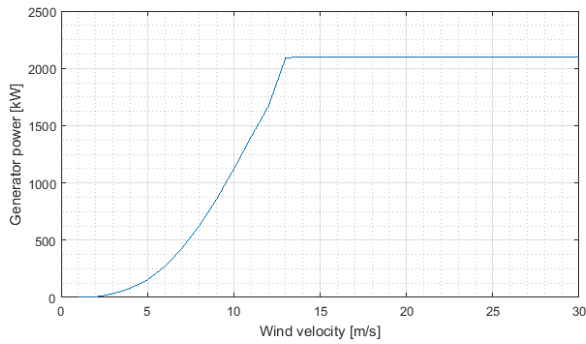


Figure 9.8: Generator power as a function of wind velocity

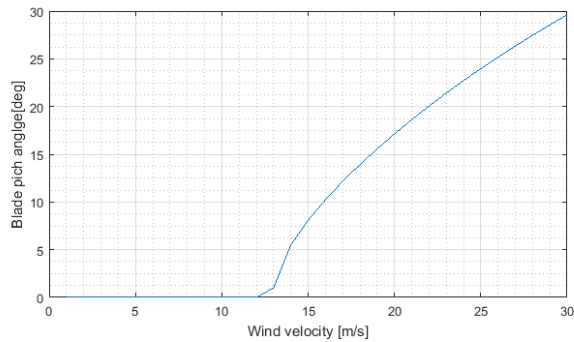


Figure 9.9: Blade pitch angle as a function of wind velocity

The thrust force results are consistent with that of Bjørnsen 2015, who's results are given in Figure 9.10, the blade pitch angle is seen to be 0 deg until the generator reaches it's rated

rotational velocity, which is where the power reaches it's maximum. From these results, the WTG is said to be verified.

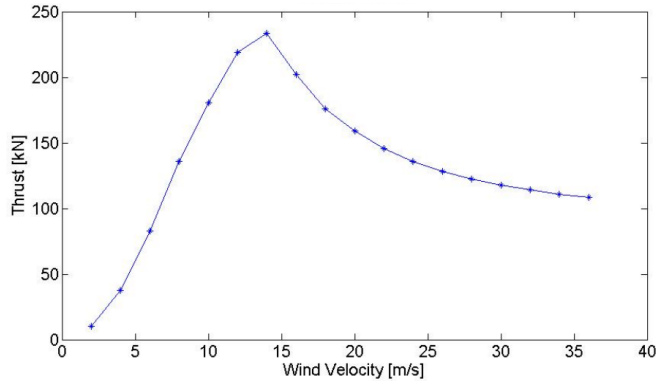


Figure 9.10: Rotor thrust force give in Bjørnsen 2015

9.5 Modelling of Mooring lines

In this section, the input data used in order to model the original, catenary, mooring system used in this thesis is given. All mooring lines are modelled as RIFLEX elements with supernodes representing the three anchors, the three bridle delta-plates and the three bridle connections at the spar. The number of elements per segment is adjusted so that no element is longer than 10 m.

The original, catenary, mooring system of Hywind Demo is illustrated in Figure 3.2. This system is governed by the geometric stiffness from the weight of the mooring lines. The technical data for a single mooring line is given in Table 9.5.

Component	Mass coefficient [kg m^{-1}]	Length [m]	External Area [m^2]	Hydrodynamic Diameter [m]
Bottom chain	125.94	320	0.016	0.152
Lower spiral strand rope	32.47	465	0.006	0.078
Lower link chain	127.03	37	0.016	0.152
Clump weight	66 645.00	1	19.83	5.000
Upper link chain	126.00	15	0.016	0.152
Upper spiral strand rope	32.00	75	0.005	0.078
Link adaptor	148.00	10	0.019	0.152
Bridle crow foot	126.00	50	0.016	0.152

The length given for the bridle crow foot is for one of the lines in the bridle. Each mooring line have a bridle with two of these crow feet.

Table 9.5: Mooring line input data to SIMA for Hywind Demo original mooring system

Using the data in Table 9.5 together with Lankhorst Ropes 2014 the *minimum breaking load* (MBL) of the original mooring system is found to be 650 t.

Drag coefficients for chain and spiral strand rope is taken from DNV-OS-E301 2013, and are given in Table 9.6. Due to confidentiality agreements with Statoil ASA, it is not given

Component	Transverse	Longitudinal
Stud chain	2.6	1.4
Spiral strand without plastic sheathing	1.6	N/A

Longitudinal drag forces on spiral strand ropes are neglected

Table 9.6: Mooring line drag coefficients for Hywind Demo original mooring system (DNV-OS-E301 2013)

whether or not the spiral strand rope has plastic sheeting, therefore this thesis utilize drag coefficient for ropes without sheeting to introduce some conservatism.

The pretension of the lines are 1.0×10^6 N and the line single mooring line characteristics are given in Figure 9.11

The footprint of the mooring system is given by the anchor positions and has a radius of 935 m.

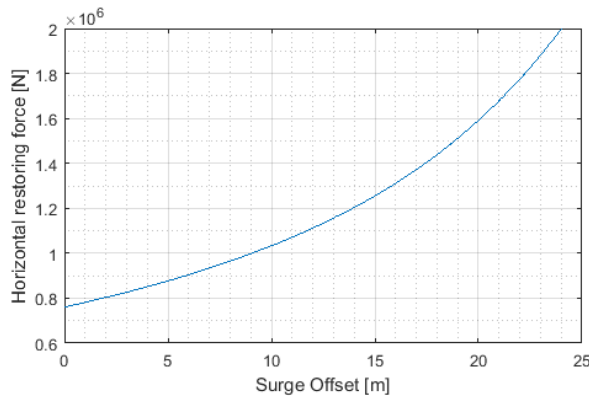


Figure 9.11: Single mooring line characteristics for original mooring system

9.6 Decay tests

A verification of the natural periods of the SIMO-RIFLEX model is done by performing decay tests in surge, heave, pitch and yaw. The decay tests were performed by applying a force at the COG of the model. The force was applied as a ramp, and then held constant for several seconds in order for the system to stabilize. To minimize the effect of the rotor blades, the WTG was parked for the decay tests. When released, the system will oscillate with its natural period back and forth, decaying as it is damped by the mooring system, drag force and skin friction, as discussed in Section 5.7.

Illustrations from the decay tests are given in Figure 9.12, the resulting natural periods are given in Table 9.7.

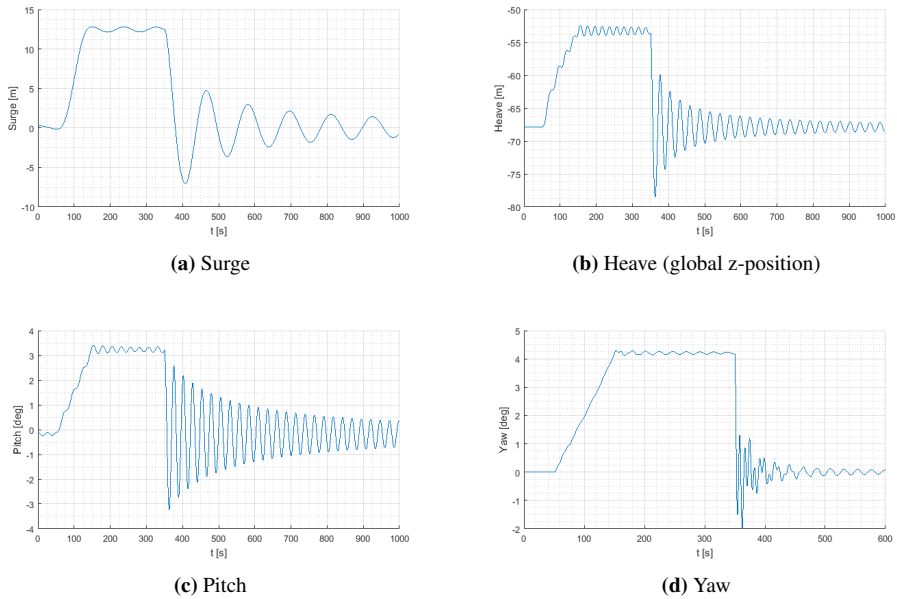


Figure 9.12: Decay tests, measured at center of gravity

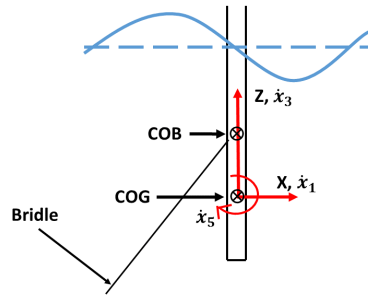


Figure 9.13: Coordinate system for decay tests

In Bjørnsen 2015, the results from decay tests performed on the full scale Hywind Demo is given. In Table 9.7 these are compared to the ones calculated from the decay tests run for this thesis' model.

	Surge	Heave	Pitch	Yaw
SIMO-RIFLEX model	115	28	26	18
Hywind Demo full scale	125	27	24	24

Table 9.7: Natural period of SIMO-RIFLEX model and full scale version

From the decay test results it is seen that the model's natural periods are in acceptable correlation with the results from the full scale system. It is noticed that for large yaw angles, the model has fluctuating positive and negative damping, this though to be due to the inertia of the mooring system. When the spar has reaches a maximum positive yaw angle, the mooring system has barely started to respond. When the spar has yawed back the other way, to the largest negative yaw angle, the mooring system is still applying a restoring force in the positive yaw direction. Thus, due to the sluggishness of the mooring system, the system will have altering positive and negative damping for large yaw angles. This is taken to be non-problematic, since it is not expected that this system will reach such large yaw angles during the simulations.

Chapter 10

Response analysis of original mooring system

In Borlet 2015, a frequency domain (FD) model of Hywind Demo was developed for use with the mooring system calculation software MIMOSA. In this chapter, the FD model from Borlet 2015 is compared against the TD model that was developed in Chapter 9. The comparison is comprised of the mean and maximum values of surge, heave, pitch and line tension from environments corresponding to rated wind velocity and 50-year return period, which are the ULS environmental conditions as described in Chapter 4. The establishment of the environmental conditions are given in Chapter 8.

All measurements are given with respect to the still water level.

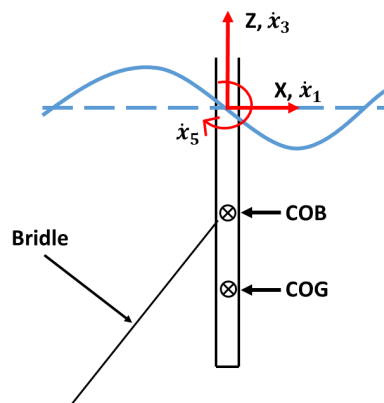


Figure 10.1: Coordinate system used for response analysis

10.1 Analytical differences between MIMOSA and SIMO-RIFLEX

MIMOSA is a software designed to calculate mooring system and vessel response in FD, SIMO-RIFLEX is, on the other hand, a response solver in TD.

To perform a FD analysis, the problem need to be linearised, and the force contributions need to be separated. In the case of Hywind Demo, that means that the the force contributions from waves, current, wind and thrust need to be given as a direct function of the wave frequency, current velocity and wind velocity. The WF motion of the floater is calculated using *response amplitude operators* (RAOs), while the LF motions is calculated by linearising the vessel and mooring model. This linearisation is done through an iterative process, but to minimize the computation time, MIMOSA only utilizes two iteration steps, which is expected to result in conservatism for LF motions (MARINTEK 2012). MIMOSA calculates the response from each of the force contributions and combines the results into a total response. For a FOWT, it is needed to adopt a linearised model of the thrust curve for wind region 3 that includes the negative damping that was discussed in Section 5.5, such a model is developed in Borlet 2015. As a result from the force separation, any coupling effect between the different force contributions are lost. In addition, the damping force from the mooring lines are lost since this contribution is highly dependant on the dynamic motion of the floater and the lines themselves, and is thus difficult to linearise.

The FD solution from MIMOSA is calculated from a response spectra, meaning that one has to assume the response to be Gaussian distributed in order to get the maximum responses calculated with the spectra's standard deviation. To account for the loss of dynamic effects, MIMOSA utilizes a *dynamic amplification factor* (DAF), this factor is generally known to be conservative, yielding conservative results (Larsen 2016). The big advantage of using FD analysis is the computational time. From the separation and linearisation of force contributions, and by neglecting any coupling between them, the computational time is usually in the range of a couple of seconds.

On the other hand, TD analysis solves the problem as a whole, performing time iterations step-by-step. This includes all non-linear effects such as stiffness, damping and non-linear contributions from the Morison equation, as well as all couplings between the different force contributions. In addition, the thrust force is included by an actual wind turbine control system. The downside of performing a TD simulation is the computational time. A FOWT provides a complex load system that need to be solved, and to acquire convergence in the step-by-step integration the time steps are usually required to be in the range of milliseconds, which often results in computational times that are longer than the simulated time length.

10.2 MIMOSA results

Using the FD model of Hywind Demo developed in Borlet 2015, calculations of line tension and motion responses for rated and 50-year environment is computed by MIMOSA. The motion results from MIMOSA are separated into an equilibrium position; WF motion; and LF motion, and are given in Table 10.1-10.3.

Equilibrium position		
	Rated	50-year
Surge [m]	14.25	14.25
Heave [m]	-0.20	-0.19
Pitch [°]	1.34	0.71

Table 10.1: Equilibrium position in surge, heave and pitch

WF motions						
	Rated			50-year		
	Surge	Heave	Pitch	Surge	Heave	Pitch
Max amplitude [m or °]	2.17	0.37	1.35	20.65	7.46	13.80
Sig [m or °]	0.56	0.10	0.35	5.52	2.04	3.70

Sig is the significant value, defined as two times the corresponding standard deviations

Table 10.2: Wave frequency motions

LF motions						
	Rated			50-year		
	Surge	Heave	Pitch	Surge	Heave	Pitch
Max amplitude [m or °]	3.48	0.07	0.88	6.67	0.16	2.12
Sig [m or °]	1.11	0.02	0.25	1.43	0.03	0.34

Sig is the significant value, defined as two times the corresponding standard deviations

Table 10.3: Low frequency motions

The results of the mooring line tension from MIMOSA are separated into a T_{base} and a T_{max} , where T_{base} represents the quasi-static line tension at a position that includes mean and LF offset and T_{max} represents the line tension at a position that also includes the maximum WF offset. The results are given in Table 10.4.

Line tension		
	Rated	50-year
T_{base} [N]	1.34E6	1.36E6
$T_{WF, max}$ [N]	0.18E6	1.03E6
T_{max} [N]	1.52E6	2.39E6

T_{base} is the quasi-static line tension due to mean and LF offset

$T_{WF, max}$ is the maximum tension from WF motion

T_{max} is the total maximum tension, given as $T_{max} = T_{base} + T_{WF, max}$

Table 10.4: Top tension of Line 3

To be able to compare the results from MIMOSA with those from SIMA, the results have to be presented with a mean value, and a maximum value. The equilibrium position from MIMOSA is taken as the mean position, and the maximum positions are found by combining the equilibrium position with the results from WF and LF motions, as described in MARINTEK 2012 and shown in Equation (10.1).

$$x_{max} = \bar{x} + \max \left\{ \begin{array}{l} x_{max}^{WF} + x_{sig}^{LF} \\ x_{sig}^{WF} + x_{max}^{LF} \end{array} \right\} \quad (10.1)$$

The results for the line tension is not directly comparable, since MIMOSA does not provide a true mean line tension, but T_{base} , which is the line tension at an offset including mean and LF motion. The results to be used in the comparison are given in Table 10.5.

	Rated				50-year			
	Surge [m]	Heave [m]	Pitch [deg]	Tension [N]	Surge [m]	Heave [m]	Pitch [deg]	Tension [N]
Mean	14.25	-0.20	1.34	1.34E6	14.25	-0.19	0.71	1.36E6
Maximum	18.29	0.19	2.94	1.52E6	36.33	7.30	14.85	2.39E6

Note that the mean value for line tension taken as the *base tension*, which is equal to tension including mean and LF offset

Table 10.5: Mimosa Results

10.3 SIMA results

Using the TD model of Hywind Demo, developed in Chapter 9, the mean and maximum values for motion and line tension responses was computed from time series for the two environmental conditions. The line tension was measured at the bridle tri-plate, since this is the part of the mooring system with steepest angle and thus largest tensions.

10.3.1 Mean values

The mean values for surge, heave, pitch and line tension was calculated from two 3-hour time simulation, corresponding to rated and 50-year environment. Sections of the time

series are given in Figure 10.2-10.5 for illustration purposes, the numerical results are given in Table 10.6.

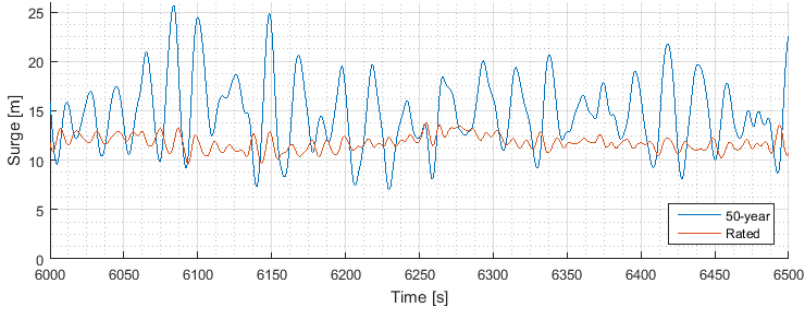


Figure 10.2: Time series of surge motion, original mooring

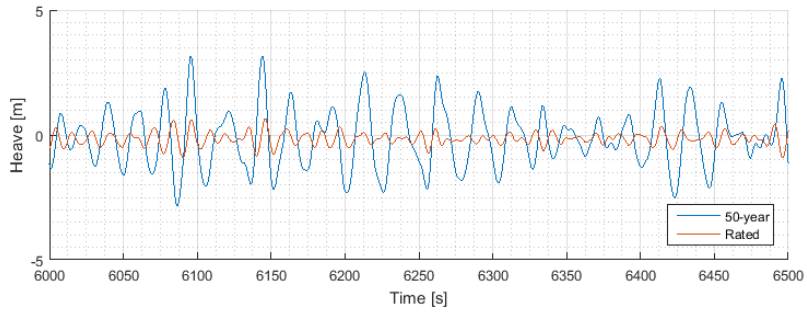


Figure 10.3: Time series of heave motion, original mooring

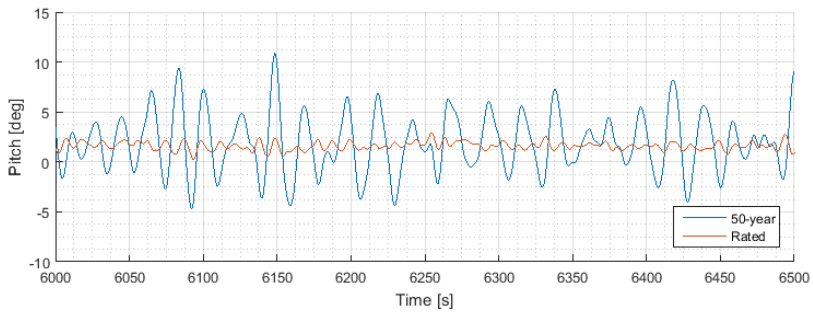


Figure 10.4: Time series of pitch motion, original mooring

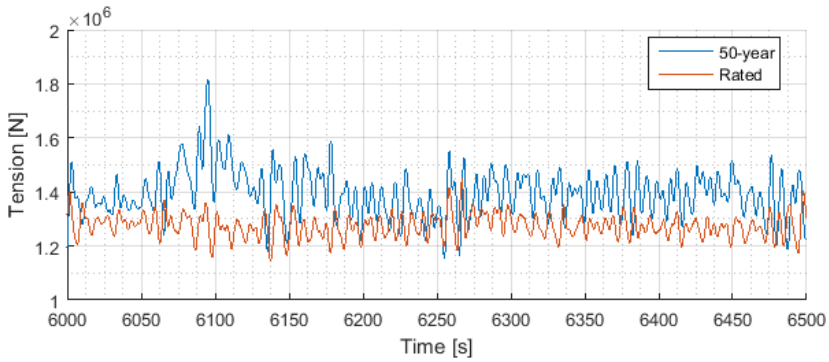


Figure 10.5: Time series of line tension, original mooring

	Rated				50-year			
	Surge [m]	Heave [m]	Pitch [deg]	Tension [N]	Surge [m]	Heave [m]	Pitch [deg]	Tension [N]
Mean	11.69	-0.15	1.94	1.27E6	14.39	-0.12	1.76	1.42E6
Std.	0.70	0.23	0.39	4.09E4	3.24	1.05	2.62	8.19E4

Std. is the standard deviation

Table 10.6: Mean values and standard deviation for motions and line tension for rated and 50-year environment from time-domain simulations

10.3.2 Maximum values

The maximum values of surge, heave, pitch and line tension were evaluated by the means of a 95% confidence interval and a distribution of largest maxima based on 20 different seed realizations of the same sea state. The sample set is given in Appendix B.

A Gumbel distribution was fitted to each of the sample sets for maxima of motion response and line tension. The probability density functions (PDF) are illustrated in Figure 10.6-10.9

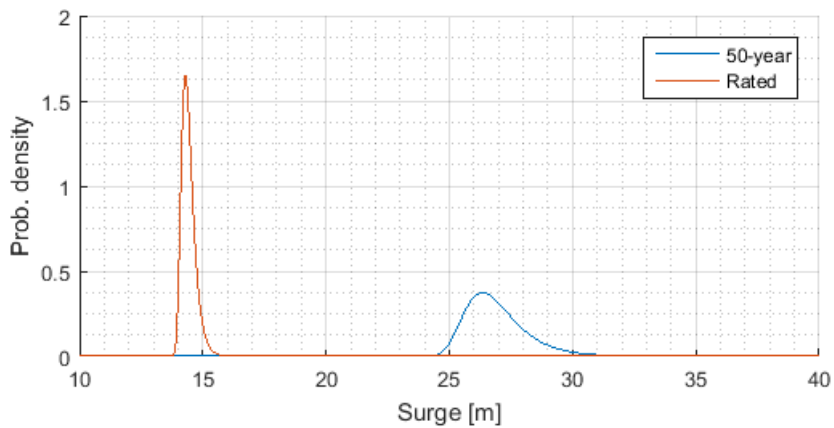


Figure 10.6: PDF of largest maxima, surge, original mooring

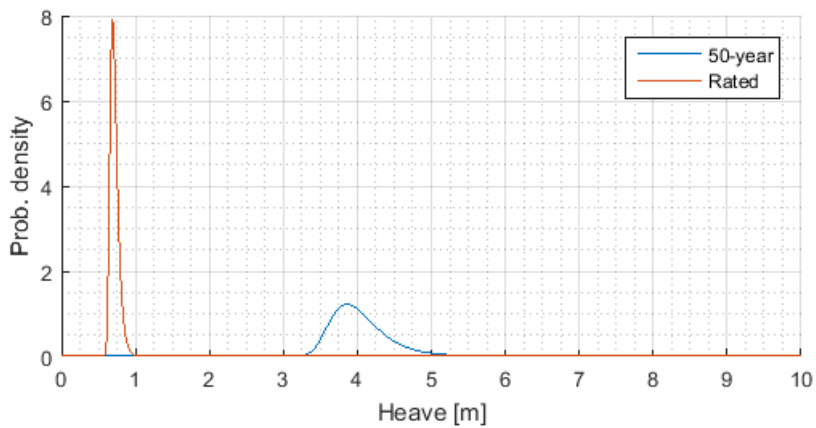


Figure 10.7: PDF of largest maxima, heave, original mooring

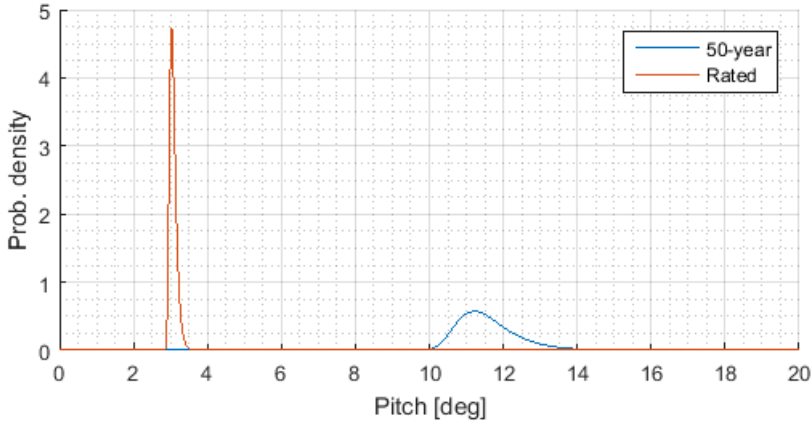


Figure 10.8: PDF of largest maxima, pitch, original mooring

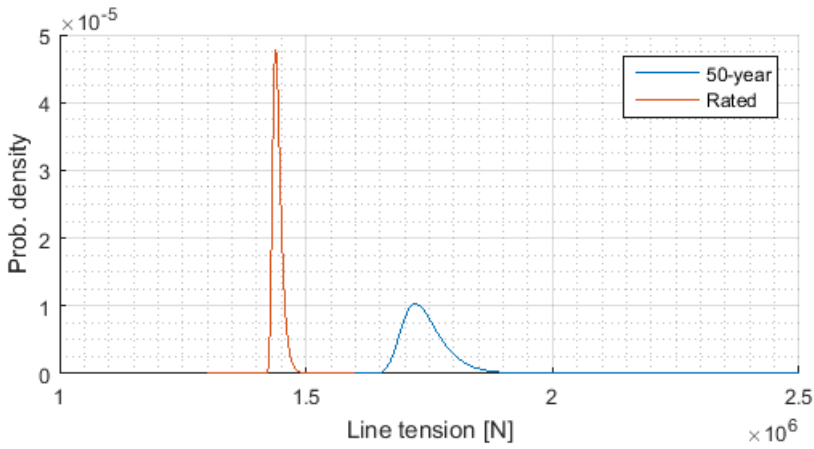


Figure 10.9: PDF of largest maxima, line tension, original mooring

The MPMs are identified as the peaks of the PDFs, and are given in Table 10.7. The upper limits of the confidence intervals, $R_{0.975}$, are found using the mean values and standard deviations given in Table 10.6.

	Rated				50-year			
	Surge [m]	Heave [m]	Pitch [deg]	Tension [N]	Surge [m]	Heave [m]	Pitch [deg]	Tension [N]
$R_{0.975}$	13.06	0.30	2.35	1.35E6	20.74	1.94	6.90	1.58E6
MPM	14.30	0.69	3.03	1.44E6	26.35	3.86	11.22	1.72E6

$R_{0.975}$ is the upper boundary of the 95% confidence interval
MPM is the most probable value

Table 10.7: Maximum values for surge, heave, pitch and line tension for rated and 50-year environment from time-domain simulations

10.3.3 Comparison and discussion MIMOSA/SIMA

The results from MIMOSA and SIMA, given in Section 10.2 and 10.3, are shown together in Figure 10.10.

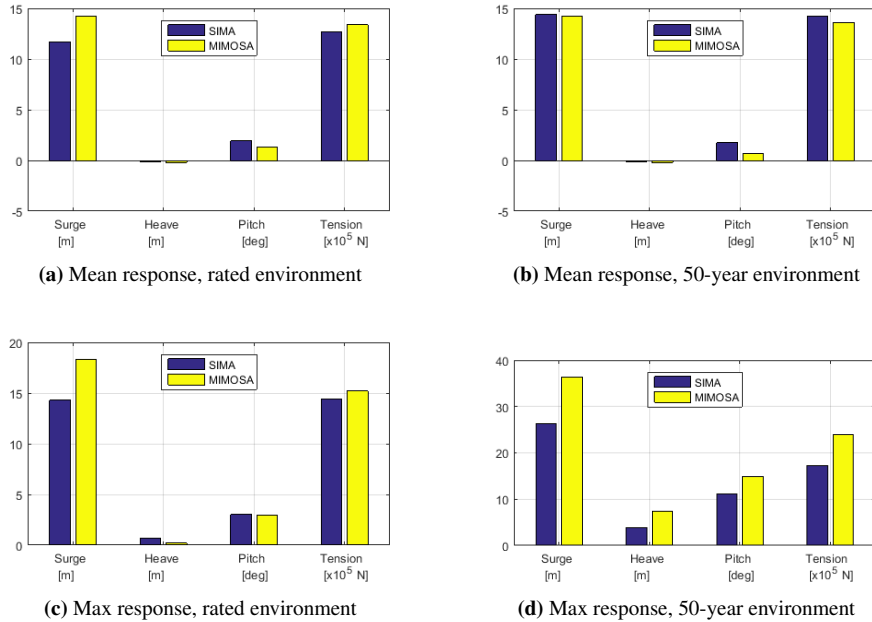


Figure 10.10: Response comparison between MIMOSA and SIMA

From the comparison, it is seen that the two models generally follow the same response trends. Note that several of the maximum responses from MIMOSA are larger than the results from SIMA. The reason for this can be the conservatism from the calculations in MIMOSA, which is known to yield conservative results. In Bjørnsen 2015, it is found that MIMOSA yields greater line tension response for Hywind Demo than SIMORIFLEX.

It is also noted that the mean pitch angle for the SIMA model is larger for 50-year environment than for rated environment. The pitch angle is usually seen to follow the thrust curve, Figure 9.7, since the rotor thrust force is the main contributor to the pitch angle for all operational wind velocities. However, at 50-year environment, the wind turbine is in a parked condition and has its blades feathered in order to minimize the lift force on the blades. In this condition, all force contributions from the WTG are neglected in the MIMOSA model from Borlet 2015. In the SIMA model, however, there are contributions to the pitch moment from both the nacelle and the three blades.

The nacelle has a larger diameter than the tower, and the inner sections of the blades has relatively large drag coefficients even while feathered. These contributions, which are

increasing quadratically with the wind velocity, can cause an increased pitch angle at 50-year environment. To verify that the large pitch angle is caused by the wind forces, a simulation of the 50-year environment without wind was compared to the regular 50-year environment with wind. The mean pitch angle standard deviation and upper limit of the 95% confidence interval for pitch angle with and without wind in 50-year environment is given in Table 10.8.

	Pitch, 50-year [deg]	Pitch, 50-year without wind [deg]
Mean	1.76	0.14
Std.	2.62	3.13
$R_{0.975}$	6.90	6.27

Std. is the standard deviation

$R_{0.975}$ is the upper boundary of the 95% confidence interval

Table 10.8: Pitch response in 50-year environment with and without wind loads

From the mean and standard deviation it is seen that the wind loads are the main contribution to the mean pitch angle, with some contribution to the dynamic pitch motion. It is also seen that the waves are the main contributor to the dynamic motion as the standard deviation is pushing the confidence interval limit to almost the same pitch value as the regular 50-year environment.

In conclusion it is seen that the MIMOSA model should be updated to include the pitch contributions from the WTG at 50-year environment.

10.3.4 Surge and tension spectra

A fast Fourier transformation (FFT) of the time series of surge motion and line tension was conducted to investigate the contributions to their responses. The spectra are given in Figure 10.11-10.13

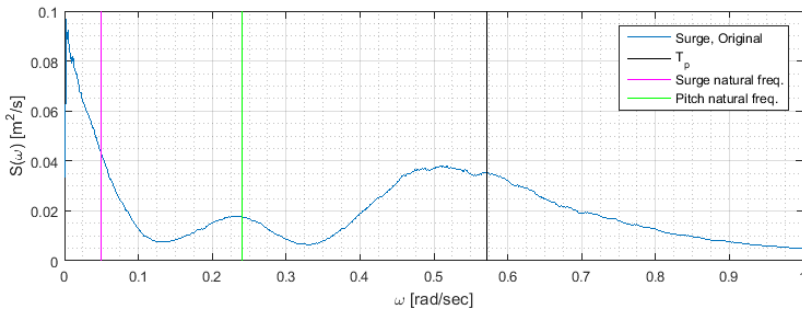


Figure 10.11: Spectrum of surge motion, rated environment, original mooring

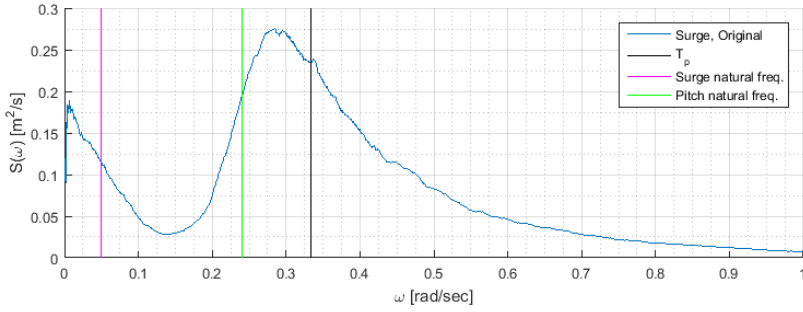


Figure 10.12: Sepctrum of surge motion, 50-year environment, original mooring

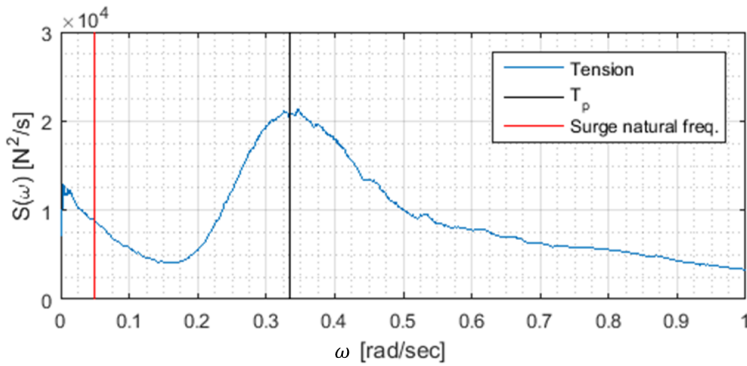


Figure 10.13: Spectrum of line tension, rated environment, original mooring

10.4 DNV compliance

Compliance with DNV regulations are investigated through the requirements given in Chapter 4. From the MBL of the original mooring system, given in Section 9.5 and Equation (4.4) the characteristic capacity of the rope is found as

$$\begin{aligned}
 S_{C_{Original}} &= 0.95 \cdot S_{mbs} \\
 &= 0.95 \cdot 650E3 \text{ kg} \cdot 9.81 \text{ m s}^{-2} = 6.06E6 \text{ N}
 \end{aligned}
 \tag{10.2}$$

The design tension is calculated using the results for mean and maximum line tension in Table 10.6 and 10.7 and Equation (4.1) together with the ULS safety factors for normal

safety class, given in Table 4.1.

$$\begin{aligned} T_{dOriginal} &= \gamma_{mean} \cdot T_{c,meanOriginal} + \gamma_{dyn} \cdot T_{c,dynOriginal} \\ &= \gamma_{mean} \cdot T_{meanOriginal} + \gamma_{dyn} \cdot [T_{maxOriginal} - T_{meanOriginal}] \quad (10.3) \\ &= 1.3 \cdot 1.42\text{E}6 \text{ N} + 1.75 [1.72\text{E}6 \text{ N} - 1.42\text{E}6 \text{ N}] = 2.37\text{E}6 \text{ N} \end{aligned}$$

Comparing the results from Equation (10.2) and (10.3), it is seen that

$$S_{COriginal} > T_{dOriginal}$$

which means that the original mooring system is in compliance with DNV regulation for mooring of FOWTs.

The utilization factor is

$$\frac{T_{dOriginal}}{S_{COriginal}} = \frac{2.37\text{E}6 \text{ N}}{6.06\text{E}6 \text{ N}} = 39.1\% \quad (10.4)$$

Fibre rope mooring system design for Hywind Demo

11.1 Introduction

This chapter investigates different fibre rope mooring configurations for Hywind Demo.

Compared with the original mooring system of Hywind Demo, which contain several different elements, the fibre rope systems discussed in this chapter are less complex. They contain for the most part a single fibre mooring line, either as plain taut mooring; with clump weight; or with a buoyancy element, as illustrated in Figure 2.11-2.13. In addition, all fibre rope mooring designs investigated in this chapter use the same bridle system as the original system.

The system that was chosen from these investigations utilizes a buoyancy element, the details of which are summarized in Table 11.6.

In order to maintain the correct draft of the system, the ballast in the bottom of the spar needed to be increased to accommodate the lighter mooring system. The details around the alterations of mass coefficient in order to provide the correct ballast is not given in this thesis due to confidentiality agreements with Statoil ASA. The increase in ballast, should in theory increase the stability of the spar since the COG was lowered, enlarging the distance between COG and COB. However, the increased distance was only 0.16 m for the final design, so it is not expected to provide any real improvements.

11.2 Goal

The purpose of this thesis is to perform an optimization of the mooring system for Hywind Demo based on synthetic fibre ropes, with the aim of developing a mooring configuration that gives the same horizontal restoring and mean offset as the original, but with reduced cost. In this chapter, the three different types of fibre mooring systems that were discussed in Chapter 2, i.e. fibre mooring with clump weights; fibre mooring with buoyancy elements; and plain taut mooring, are investigated for application to Hywind Demo at the original site with a water depth of 204 m. It is desirable to establish a system with a line characteristic that has the same stiffness at rated and 50-year environment as the original mooring system. The stiffness is visualized as the steepness of the slope of the line characteristic. The line characteristic for the original system is given in Figure 9.11.

11.3 Stiffness combination

A fibre rope mooring system with an attachment in the form of a buoy or a clump weight will have two stiffness contributions. One contribution from the fibre rope itself, i.e. elastic stiffness, and one from the attachment, i.e. geometric stiffness. By combining elastic and geometric stiffness' in a mooring system, the combined stiffness can be written as

$$\frac{1}{K_{TOT}} = \frac{1}{K_E} + \frac{1}{K_G} \quad (11.1)$$

where

- K_{TOT} = total stiffness
- K_E = elastic stiffness given as $K_E = \frac{EA}{L}$
- E = elastic modulus of the fibre rope
- A = cross-sectional area of the fibre rope
- L = length of rope
- K_G = geometric stiffness

Such a stiffness combination is illustrated in Figure 11.1

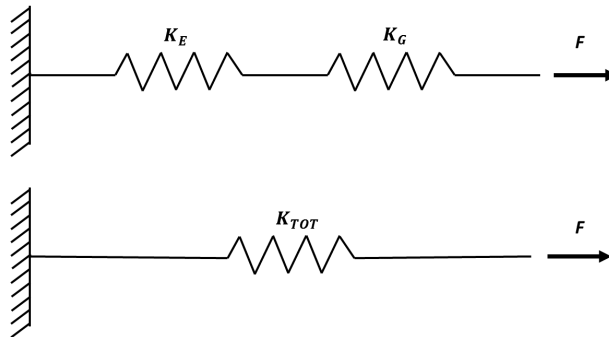


Figure 11.1: Combination of elastic and geometric stiffness

The relation between displacement and stiffness is given generally as

$$F = Kx \quad (11.2)$$

where

- F = force
- K = stiffness
- x = displacement

An important aspect when combining elastic and geometric stiffness is to design a system that make the two stiffness contributions work together. Since the elastic stiffness can be regarded as constant for a specific fibre rope with a given length, the geometric stiffness need to be tuned to work in tandem with the elasticity.

If the geometric stiffness is larger then the elastic stiffness, the system will utilize the elastic stiffness until the tension in the rope is large enough to begin to perform displacements with the geometric stiffness. This, naturally, results in a system stiffness larger then what the fibre rope would provide by itself. If the weight or buoy is severely over-dimensioned, the geometric stiffness will become so large that it can be regarded as a virtual anchor. On the other hand, if the buoy or weight is under-dimensioned, the geometric stiffness will be much lower than the elastic stiffness. The result of such a system will be large offsets even at low external loading, i.e. the spar will drift to a position where the geometric stiffness becomes equally large as the elastic stiffness. The only gain with such a system is the increased length of fibre rope within the footprint, which comes at the cost of large horizontal displacements.

The stiffness' need to be tuned so that the system initializes both the geometric and the elastic stiffness' together.

11.4 Challenges

11.4.1 Fibre rope challenges

The use of fibre mooring in shallow water yield several challenges. The largest and most important of which are to maintain the correct horizontal restoring stiffness. The floater need to be able to absorb the WF motions, meaning that the mooring system must be soft enough to give the floater the ability to move with the waves. In addition, the mooring system must provide sufficient resistance against the mean and LF loads so that the offset is reduced in order to avoid damage to the attached power cable and neighbouring installations. Fibre ropes have a stiffness that is inverse proportional with length, but a long mooring line will give a large footprint of the system, making it difficult to combine with other installations.

As discussed in Chapter 6, tensioning a fibre rope results in a compaction of the fibres, and as long as tension is maintained, the rope will follow the tension-elongation behaviour. On the other hand, if a fibre rope is to be subjected to compression, the behaviour of the fibres will diverge from the tension-elongation model. Such behaviour is not only difficult to model, but also very harmful to the fibres. Compression will force the sub-ropes to bend out normal to the compression force as shown in Figure 11.2. A cyclic force that causes tension-compression will dramatically increase the fatigue damage to the rope since the rope will cause great self-abrasion between the subropes and fibres. To avoid such damage, the pretension of the system must be of such magnitude that there is still tension in the leeward lines even when the floater is given an offset. However, it is also important to keep in mind that a large pretension will result in a higher stiffness in the rope, as discussed in Chapter 6. Since the stiffness of fibre ropes are softest when cycling the load in a range of 10-30% of MBS, this thesis aims to use a pretension in the lines of $T_0 \approx 0.1S_{mbs}$. It is also expected that the addition of either clump weights or buoyancy elements will help maintain tension in the leeward lines.



Figure 11.2: Fibre rope subjected to large compression forces (Smith 2011)

Fibre ropes has natural little abrasion resistance, and even though the industry is working towards a protective shielding that will provide a durable protection that is able follow the fibre rope's tension-elongation behaviour, there is doubt that such protection can cope with cyclic seabed contact. Hence, fibre ropes can not be allowed any seabed contact. To avoid this, one can either use a bottom chain, or provide a sufficient angle between rope and seabed at all times.

11.4.2 Clump weight challenges

If clump weights are utilized, these must also be designed to avoid seafloor contact. This is because if the weight is allowed to rest at the bottom, it might introduce snapping loads. In addition, if a weight is resting on the bottom, it means that the fibre rope between the weight and the anchor is also resting at the bottom, which will cause abrasion damage to the fibre rope.

11.4.3 Buoys challenges

If buoys are attached to the fibre ropes, it is important that these are below the sea surface at all times. This is because if the buoy reaches the surface, it's force on the line is reduced and snapping loads can occur if the buoy is pulled down rapidly. In practice this problem is similar to the one with a weight resting on the seafloor. In addition, a buoy that is close to the free surface will be subjected to large hydrodynamic forces and will be in risk of coming in contact with ships and service vessels.

11.4.4 Summary of challenges

The important factors for a fibre rope mooring system for Hywind Demo can be summarized as:

- Maintain acceptable restoring stiffness
- No seafloor contact of fibre ropes
- No seafloor contact of clump weights
- No sea surface contact of buoys
- Always maintain tension in all mooring lines
- Minimize pretension to maintain low stiffness in fibre ropes
- Minimize footprint
- Minimize offset of floater

11.5 Investigation of line characteristics

In order to investigate the three different mooring configurations, the following selection procedure was utilized as a screening process:

1. Generate line characteristics for different combinations of:
 - Line length

- Anchor position
 - Size of clump weight or buoy
 - Position of clump weight or buoy
2. For each of the three configurations, select line characteristics based on
 - Offset at rated and 50-year environment
 - Stiffness at rated and 50-year environment
 - Pretension
 3. Investigate the selected configurations for:
 - Seafloor contacts
 - Sea surface contacts

The anchor position was used to change the pretension of the system. For a given fibre rope length, the anchor position that matched the length of the rope was calculated and referred to as a reference point. From there, the anchor was moved along the seabed to alter the pretension. See Figure 11.3 for an illustration.

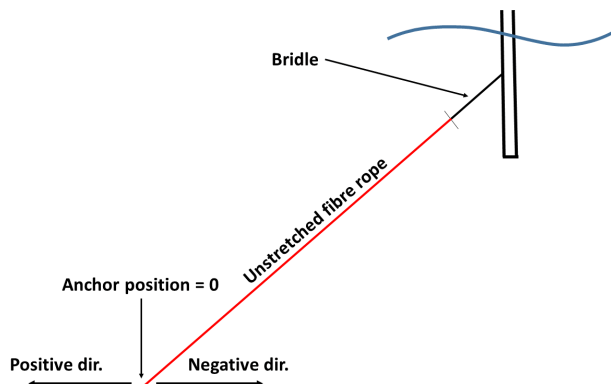


Figure 11.3: Pretension aquired by anchor position

11.5.1 Plain taut mooring

Plain taut mooring without any attachments are, due to it's simplicity, the most desirable solution. This is both due to less dynamic effects in the line and lower cost.

RIFLEX model

The choice of fibre rope was based on the MBL of the original mooring system, which is given in Section 9.5 as 650 t. Using Lankhorst Ropes 2015, a fibre rope with a MBL

of 700 t is selected to be used for fibre mooring of Hywind Demo. The chosen rope has a diameter of $D_{fibre} = 0.156$ m and a mass coefficient of $W_{air,fibre} = 16.7$ kg m⁻¹. This data is also given in Table 6.1. The given weight in water is $W_{w,fibre} = 4.3$ kg m⁻¹, but when calculating the net weight in water from the mass coefficient and diameter, the rope is found to be buoyant, as shown in Equation (11.3).

$$\begin{aligned}
 W_{w,fibre} &= W_{air,fibre} - \pi \cdot \left(\frac{D_{fibre}}{2} \right)^2 \cdot \rho_{water} \\
 &= 16.7 \text{ kg m}^{-1} - \pi \cdot \left(\frac{0.156 \text{ m}}{2} \right)^2 \cdot 1025 \text{ kg m}^{-3} \\
 &= 16.7 \text{ kg m}^{-1} - 19.6 \text{ kg m}^{-1} \\
 &= -2.9 \text{ kg m}^{-1}
 \end{aligned} \tag{11.3}$$

From the discrepancy between the given weight in water and the one found through hand calculations, it is realised that since a fibre rope consist of several sub-ropes, which again consist of several strands, as shown in Figure 2.3, water will penetrate the rope and fill the gaps between the different rope elements, thus lowering the volume that provides buoyancy. In order to account for this effect in RIFLEX, the rope was defined with a smaller external area than in reality, then the hydrodynamic diameter was altered back to the original of 0.156 m to maintain a correct computation of drag forces. By inverting Equation (11.3), and solving for a weight in water of 4.3 kg m⁻¹, it was found that an external area corresponding to a diameter of 0.124 m will yield the correct weight in water.

The stiffness of the fibre rope was calculated using Equation (6.4), and found to be

$$EA_{fibre} = 20 \cdot 700 \text{ t} \cdot 9.81 \text{ m s}^{-2} = 137.34 \text{ MN} \tag{11.4}$$

Drag coefficients for fibre ropes are taken from DNV-OS-E301 2013, and given in Table 11.1.

Component	Transverse	Longitudinal
Fibre rope	1.6	N/A

Longitudinal drag forces on fibre ropes are neglected

Table 11.1: Drag coefficients for fibre rope (DNV-OS-E301 2013)

Line characteristics

To evaluate the plain taut mooring, line characteristics base on combinations of the following single line parameters were inspected:

- Fibre rope length: 1000 m, 1500 m, 2000 m, 2500 m, 3000 m
- Anchor prescribed displacement: 5 m, 10 m, 20 m, 30 m, 40 m

By selecting the combinations that results in line characteristics that have desired pretension and stiffness, several mooring systems were found to be suitable. One of the best candidate were:

- Total fibre length: 2000 m
- Anchor prescribed displacement: 5 m

The line characteristics for this configuration is compared to the original one in Figure 11.4. The mean horizontal tension for rated and 50-year environment, based on the environmental response analysis in Chapter 10, are also plotted.

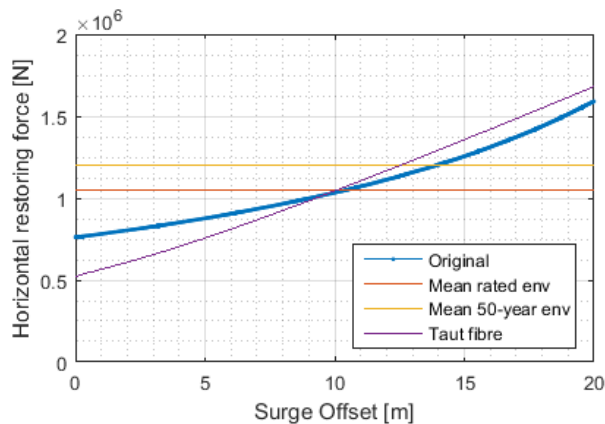


Figure 11.4: Line characteristics of plain taut mooring

From the different line characteristics that were studied, it was seen that a fibre length of 2000 m is needed to provide the desired stiffness. When analysing the lower parts of the leeward side when computing the line characteristics it was found that the leeward lines were subjected to bottom contact at an early stage. When subjected to a horizontal force corresponding to the mean force at 50-year environment, there are a significant amount of line resting on the bottom. This is due to the lines weight in water and the relative small angle between rope and seafloor, which is a direct result of the needed line length. This problem could be solved by increasing the pretension in the lines, however, the increase of pretension would have to be of such magnitude that it would effect the stiffness of the fibre rope, as discussed in Section 11.4. As a result, it is concluded that a plain taut mooring system for Hywind Demo at 204 m water depth is not a plausible solution for cost-reduction.

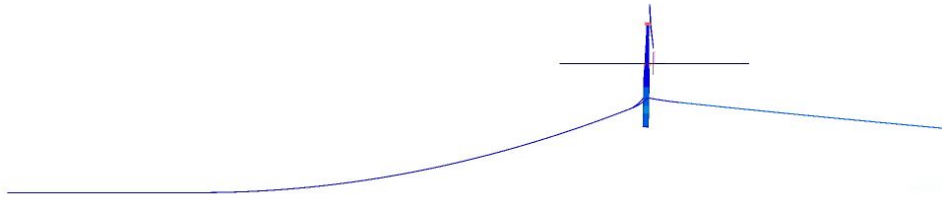


Figure 11.5: Taut mooring with line on bottom, subjected to 1000 kN, orthographic view

11.5.2 Taut mooring with clump weights

RIFLEX model

The concept of fibre mooring with clump weights were modelled using the same fibre rope as in Section 11.5.1.

The original Hywind Demo has clump weights that are hanging underneath the mooring line, as illustrated in Figure 3.2. In order to reduce fatigue from dynamic effects, an in-line weight consisting of three chains is proposed. The weight of the system is thus changed by altering the length of the chains. The chains used are of 120 mm, and the weight in water of all three is approximately $W_{w,weight} = 1 \text{ t m}^{-1}$. Drag coefficients are found by multiplying the drag coefficients for chain, given in Table 9.6, with 3. The results are given in Table 11.2.

Component	Transverse	Longitudinal
In-line clump weight of chains	7.2	3.45

Table 11.2: Drag coefficients for in-line clump weight (based on DNV-OS-E301 2013)

An illustration of the in-line, chain based, clump weights are given in Figure 11.6.

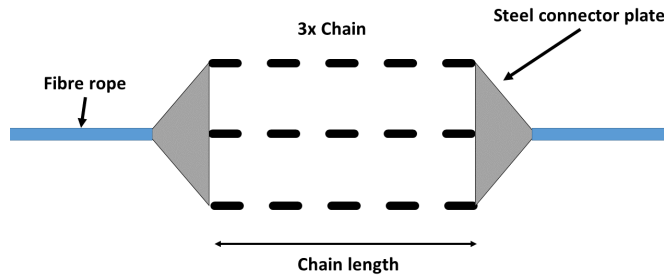


Figure 11.6: Clump weight made of chains

The clump weight was positioned so that the fibre rope was divided by a ratio of 1 : 2, as illustrated in Figure 11.7. This ratio was utilized as a compromise between maximizing the moment arm of the clump weight, as discussed in Section 2.3.1, and minimizing the chance of contact between seafloor and clump weight.

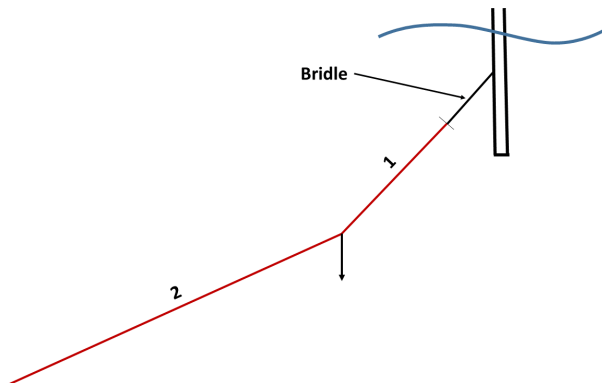


Figure 11.7: Example of 2 : 1 ratio of fibre mooring line on each side of a clump weight

Line characteristics

To evaluate the taut mooring with clump weights, line characteristics base on combinations of the following single line parameters were inspected:

- Fibre rope length: 1000 m, 1500 m, 2000 m, 2500 m, 3000 m
- Anchor prescribed displacement: -10 m, 0 m, 10 m, 20 m, 30 m, 40 m
- Clump weight chain length: 10 m, 30 m, 50 m

Similar to the plain taut mooring, the fibre mooring with clump weights were subjected to seafloor contact. This is because the angle between seafloor and fibre rope has been further reduced by the addition of the clump weight. It is concluded that none of the combinations of parameters give a line characteristic that is satisfactory while at the same time avoiding seafloor contact.

11.5.3 Taut mooring with buoyancy elements

RIFLEX model

The concept of fibre mooring with buoyancy elements were modelled using the same fibre rope as in Section 11.5.1.

The buoyancy elements used in this thesis are based on data from Lankhorst Mouldings 2016. These are moulded segments that are connected together around a steel shackle, and the net buoyancy can be altered by adding or removing segments. An illustration is given in Figure 11.8.



Figure 11.8: Mooring buoyancy elements (Lankhorst Mouldings)

Together with the steel shackle, the buoyancy elements have a density of $\rho_{buoy} = 563.25 \text{ kg m}^{-3}$ (Lankhorst Mouldings 2016), meaning that the net buoyancy of the buoys are 461.75 kg m^{-3} .

For this thesis, only symmetrical shaped buoyancy elements will be considered, but it is important to note that there are other designs for buoyancy elements. The use of elements such as shown in Figure 11.8 has to be investigated for dynamic motions since they can be prone to achieve a pendulum effect. Other elements that will not create their own dynamic systems are available, but these are limited in size, one design is pictured in Figure 2.5. This dynamic effect was, due to the scope of this thesis, not investigated.

A *nodal body* was used to model the buoyancy elements in RIFLEX. This is a way to model attachments to RIFLEX nodes in a way that incorporates the physical properties of bodies and calculates the dynamic effects this body has on the RIFLEX line. The nodal body is defined by volume, mass, drag force coefficient and added mass.

As opposed to the positioning of the clump weight along the fibre line, which was positioned relatively close to the spar, the buoy was positioned far away from the spar, as illustrated in Figure 11.9. This is to minimize the risk of contact with the sea surface and wave forces.

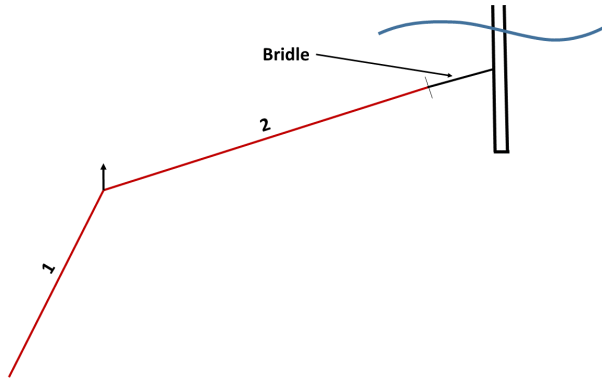


Figure 11.9: Example of 1 : 2 ratio of fibre mooring line on each side of a buoyancy element

The drag force coefficients used to define the nodal body in RIFLEX must include the dimensions of the body as well as the density of water, the drag coefficient and a factor of 0.5, as given in Equation (11.5).

$$C_{Buoy} = \frac{1}{2} \rho_{water} C_{D_{Buoy}} D_{buoy} L_{buoy} \quad (11.5)$$

where

- ρ_{water} = Density of water
- $C_{D_{Buoy}}$ = Drag coefficient of buoy
- D_{buoy} = Diameter of buoy
- L_{buoy} = Length of buoy

The drag coefficient of the buoy is found using DNV-RP-C205 2010, where drag coefficients of 2D bodies are given based on geometry. In Table 11.3, the drag coefficient of different rectangles are given.

4. Rectangle with rounded corners	L/D	R/D	C_D	L/D	R/D	C_D
		0.5	0	2.5	2.0	0
0.021			2.2	0.042		1.4
0.083			1.9	0.167		0.7
0.250			1.6	0.50		0.4
1.0			0	2.2		6.0
		0.021	2.0	0.5	0.29	
		0.167	1.2			
		0.333	1.0			
$Re \sim 10^5$						

Table 11.3: Drag coefficients for rectangles in steady flow (DNV-RP-C205 2010)

Using Table 11.3 for a cubic buoy, $\frac{L}{D} = 1$, with heavily rounded corners, $\frac{R}{D} = 0.333$, the drag coefficient of the buoy was found to be $C_{D_{Buoy}} = 1.0$. The assumption of heavily rounded corners is assumed valid due to the fact that the buoy elements can be moulded into any shape.

Using the drag coefficient, $C_{D_{Buoy}} = 1.0$, density of water, $\rho_{water} = 1025 \text{ kg m}^{-3}$, and the fact that the buoy is symmetrical, $D_{buoy} = L_{buoy}$, a drag force coefficient that is dependant solely on volume was created and added to the nodal body in RIFLEX as a script that changes value based on the volume of the buoy. The variable drag force coefficient is given in Equation (11.6).

$$C_{Buoy} = \frac{1}{2} \rho_{water} C_{D_{Buoy}} \sqrt[3]{V_{Buoy}} \sqrt[3]{V_{Buoy}} = \rho_{water} C_{D_{Buoy}} \sqrt[3]{V_{Buoy}} \quad [\text{N s}^2 \text{ m}^{-2}] \quad (11.6)$$

where

- V_{Buoy} = Volume of buoy

The added mass used to define the nodal body in RIFLEX must include the volume of the buoy, the density of water and the added mass coefficient, as given in Equation (11.7).

$$A_{M_{buoy}} = \rho_{water} C_{A_{buoy}} V_{Buoy} \quad (11.7)$$

where

- ρ_{water} = Density of sea water
- $C_{A_{buoy}}$ = Added mass coefficient
- V_{Buoy} = Volume of buoy

The added mass coefficient of square prisms is given in DNV-RP-C205 2010, as shown in Table 11.4.

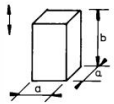
Square prisms		Vertical	b/a	C_A	$a^2 b$
			1.0	0.68	
	2.0	0.36			
	3.0	0.24			
	4.0	0.19			
	5.0	0.15			
	6.0	0.13			
	7.0	0.11			
	10.0	0.08			

Table 11.4: Added mass coefficients for square prisms in steady flow (DNV-RP-C205 2010)

By using the fact that the buoy is symmetric, $\frac{b}{a} = 1.0$, the added mass coefficient is found to be $C_{A_{buoy}} = 0.68$. Using this and the density of water, $\rho_{water} = 1025 \text{ kg m}^{-3}$, the

added mass as a function of volume is given in Equation (11.7). Note that the added mass coefficient provided in DNV-RP-C205 2010 is for a cube without rounded edges, this coefficient is therefore seen to be conservative.

Line characteristics

To evaluate the taut mooring with clump weights, line characteristics base on combinations of the following single line parameters were inspected:

- Fibre rope length: 1000 m, 1500 m, 2000 m, 2500 m, 3000 m
- Anchor prescribed displacement: -10 m, 0 m, 10 m, 20 m, 30 m, 40 m
- Buoy volume: 22 m³, 65 m³, 110 m³

Similar to the mooring with clump weights, there are several of the mooring systems with buoys that suffer from contact with the sea surface. The main challenge with this mooring configuration, and similarly with clump weights, was identified as achieving geometric flexibility, while at the same time keeping the buoys at leeward side at a decent depth. It was also seen that lines with a length of 2500 m and longer get large curvatures on each side of the buoys, which can lead to loss of tension in dynamic motion. There was, however, found a parameter combination that provide a satisfying line characteristic and at the same time does not suffer from curvature or sea surface contact. A list of the combinations that provide satisfactory line characteristics is given in Table 11.5 along with comments about their geometry.

Combination nr.	Fibre length [m]	Buoy volume [m ³]	Anchor displacement [m]	Comment
1	1000	65	-10	Good buoy depth
2	1000	110	-20	Possible wave interaction
3	2500	22	10	Large curvatures
4	3000	22	20	Large curvatures
5	3000	22	10	Large curvatures

Table 11.5: Possible taut mooring combinations with buoy

Combination 1, does not suffer from wave-interaction, and is the combination that contains the least amount of material, which is important for the total cost of the system. Combination 2 yields leeward side buoys that have insufficient depth when considering the large wave forces close to the surface. Combination 3, 4 and 5 all suffer from large slack curvatures at leeward side. An isotropic illustration of combination 1 is given in Figure 11.10, while orthographic illustrations of Combination 1, 2 and 4 under horizontal forces are given in Figure 11.11-11.13, respectively.

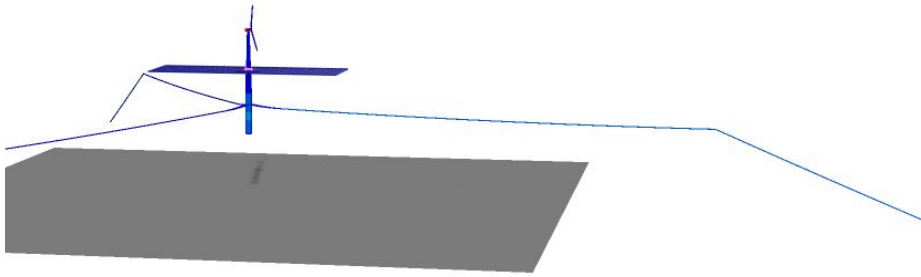


Figure 11.10: Isotropic view of combination 1 without horizontal load

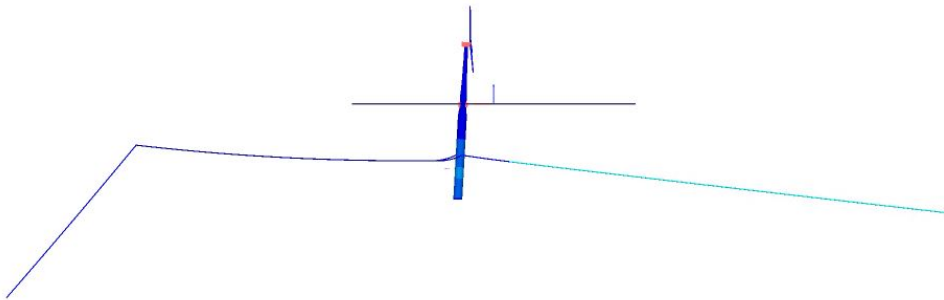


Figure 11.11: Orthographic view of combination 1 at 3000 kN horizontal load

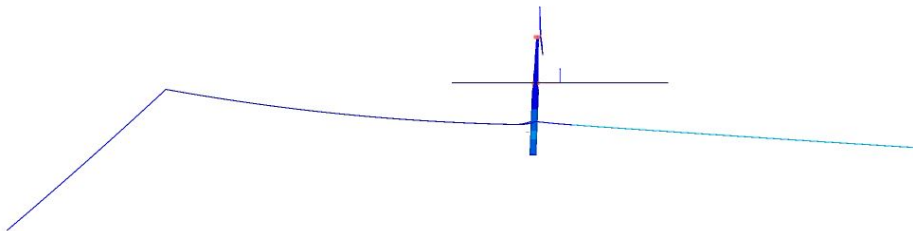


Figure 11.12: Orthographic view of combination 2 at 2000 kN horizontal load

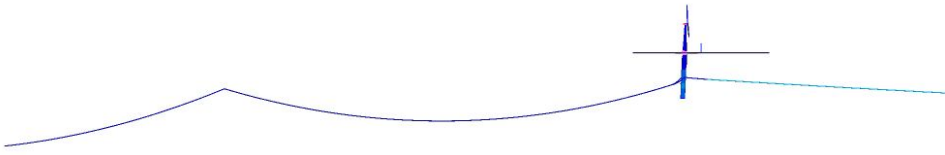


Figure 11.13: Orthographic view of combination 4 at 2000 kN horizontal load

The line characteristics of combination 1 is compared to the the original mooring system in Figure 11.14

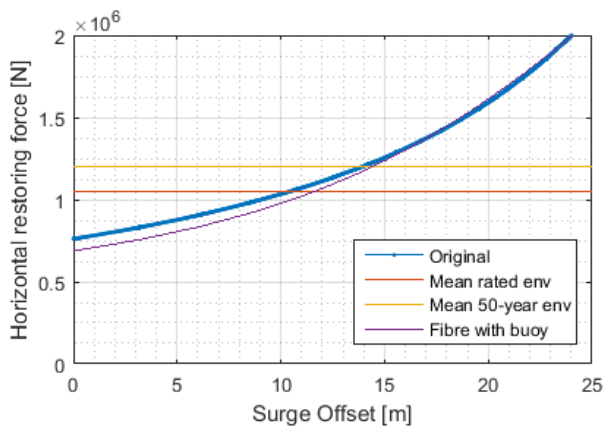


Figure 11.14: Single line characteristics of combination 1

From the line characteristic it is seen that that Combination 1 is indeed a good candidate as a mooring system for Hywind Demo in the way that it provides almost identical horizontal stiffness as the original mooring system. It was also found that the line has a pretension of 10% of the MBL, about 750 kN between anchor and buoy and 700 kN between buoy and bridle, which means that it has a good initial condition when considering compression forces in the leeward lines, while at the same time keeping the operational tension in the windward line at 10-30% of the MBL, which yields the lowest possible stiffness of the fibres.

The footprint of the system, given by the anchor positions, is a circle with a radius of 1030 m.

11.5.4 Buoy size and position sensitivity test

With the aim of reducing the volume of the buoy, and thereby reducing cost, a sensitivity test that investigates the possibility of maintaining the properties of Combination 1 while

reducing the buoy volume and altering the buoy placement and anchor displacement was conducted.

The parameters that was investigated was:

- Buoy volume: 8 m³, 16 m³, 27 m³, 40 m³, 53 m³, 65 m³
- Anchor displacement: -10 m, -8 m, -6 m, -4 m, -2 m, 0 m, 2 m, 4 m, 6 m, 8 m, 10 m
- Buoy placement: 0.10, 0.25, 0.33

Where buoy placement refers to the ratio of fibre between anchor and buoy. A ratio of 0 means that the buoy is located at the anchor and a ratio of 1 means that the buoy is connected at the bridle-fibre connection. A ratio of 0.33 correlates to the 1 : 2 ratio.

From the sensitivity study it was seen that a buoy volume of less then 65 m³ suffers from lack of geometric flexibility. This is because the decrease in buoyancy force introduces the need for the anchor to be positioned closer to the anchor’s reference point, decreasing the angle at the buoy and limiting the it’s range of motion. In Figure 11.15, the line characteristic of a system with the following parameters is given.

- Buoy volume: 53 m³
- Anchor displacement: -2 m
- Buoy placement: 0.33

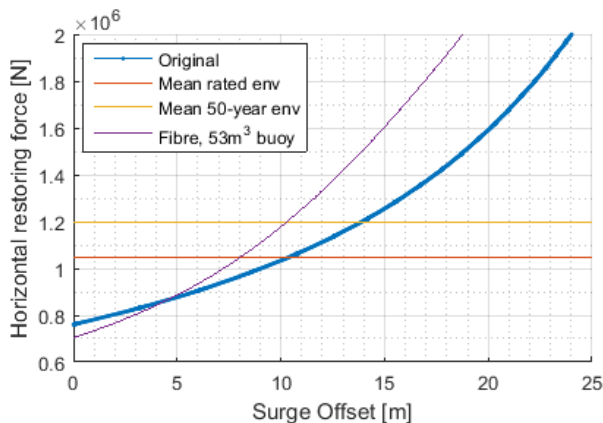


Figure 11.15: Single line characteristics of taut mooring with 53 m³ buoy

An illustration of the system with a 53 m³ buoy is given in Figure 11.16

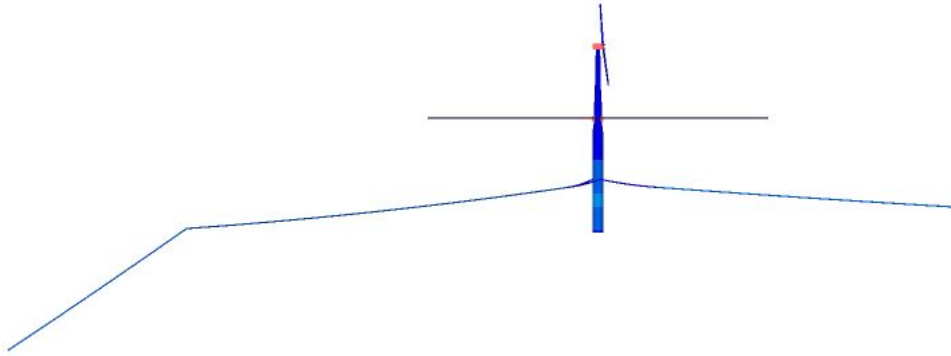


Figure 11.16: Orthographic view of taut mooring with 53 m³ buoy without horizontal load

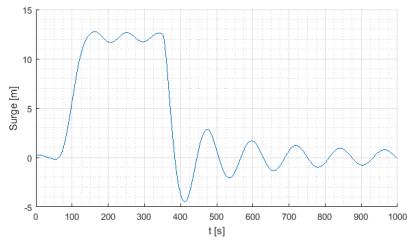
From the sensitivity study it was concluded that a buoy of 65 m³ is needed to achieve the geometric flexibility that match the original mooring systems characteristics. Combination 1 is therefore chosen to be the best configuration.

Fibre length [m]	Fibre ratio [-]	Buoy buoyancy [t]	Anchor radius [m]
1000	1 : 2	30	1030

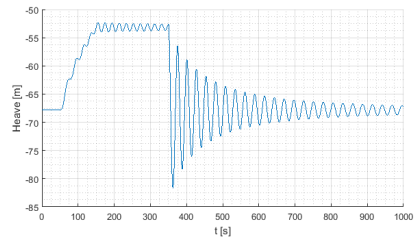
Table 11.6: Combination 1 parameters

11.6 Decay test

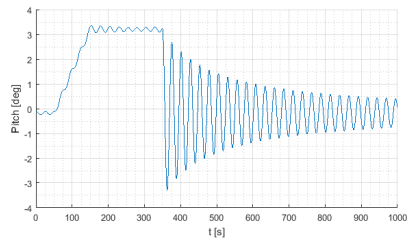
To be able to investigate the impact of natural periods from the new fibre mooring system, a set of decay tests were performed. The applied forces and moments applied are equal to the ones used for the original mooring system. The decay tests are plotted in Figure 11.17, and the calculated natural periods are given in Table 11.7 together with results from tests performed on the full scale Hywind Demo. The decay tests are measures at the COG, a coordinate system is given in Figure 9.13.



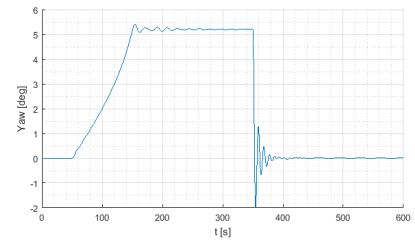
(a) Surge



(b) Heave (global z-position)



(c) Pitch



(d) Yaw

Figure 11.17: Decay tests, measured at center of gravity

	Surge	Heave	Pitch	Yaw
Fibre rope with buoy	123	27	26	23
Hywind Demo full scale	125	27	24	24

Table 11.7: Natural period of Hywind Demo with fibre rope mooring system

Chapter 12

Response analysis of fibre mooring system

12.1 Environmental simulations

From the positive outlook of Combination 1 from Chapter 11 based on line characteristics; pretension; leeward buoy position; and natural periods, environmental response analyses of rated and 50-year environment were run in order to determine the mean and maximum values of surge, pitch, heave and tension. From here on, the Combination 1 from Section 11.5.3 is referred to simply as “fibre mooring”, the parameters of which are given in Table 11.6.

All measurements are taken at still water level, a coordinate system is given in Figure 10.1.

12.1.1 Mean values

The same 3-hour environmental conditions that were used to determine the mean values of the original mooring were run against the fibre mooring system. Sections of the time series are given in Figure 12.1-12.4 and the numerical results are given in Table 12.1. The line tension is measured between the anchor and buoy, since this is the line segment with the steepest angle, and thus the largest tensions.

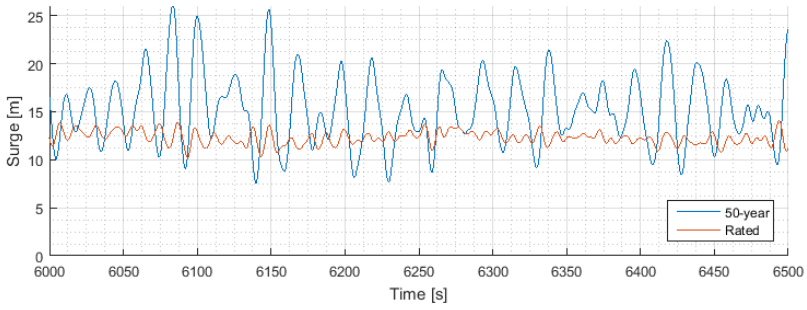


Figure 12.1: Time series of surge motion, fibre mooring

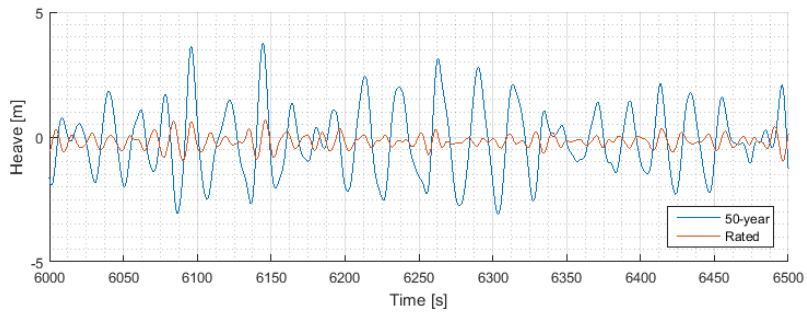


Figure 12.2: Time series of heave motion, fibre mooring

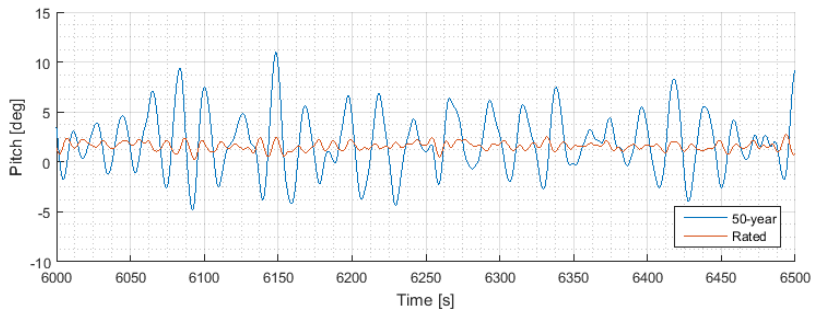


Figure 12.3: Time series of pitch motion, fibre mooring

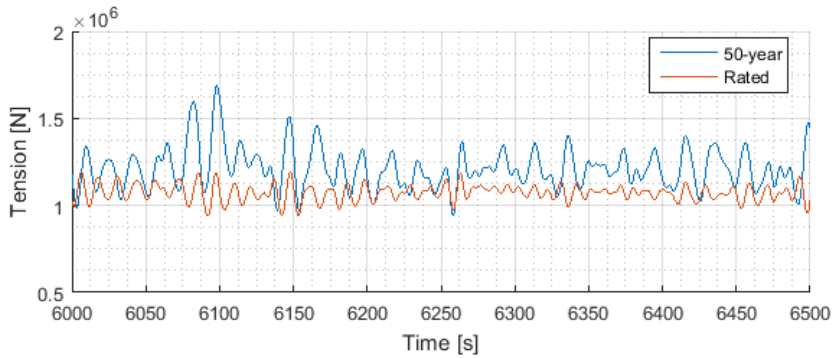


Figure 12.4: Time series of line tension, fibre mooring

	Rated				50-year			
	Surge [m]	Heave [m]	Pitch [deg]	Tension [N]	Surge [m]	Heave [m]	Pitch [deg]	Tension [N]
Mean	12.27	-0.18	1.58	1.07E6	14.89	-0.15	1.77	1.21E6
Std.	0.66	0.24	0.40	4.51E4	3.28	1.42	2.66	1.08E5

Std. is the standard deviation

Table 12.1: Mean values and standard deviation for motions and line tension for rated and 50-year environment for fibre mooring

12.1.2 Max values

Similar to the original mooring system, 95% confidence intervals and MPM values based on 20 seeds were obtained for the taut mooring with buoy. The PDFs are plotted in Figure 12.5-12.8, and the numerical results are given in Table 12.2. The sample set is given in Appendix C.

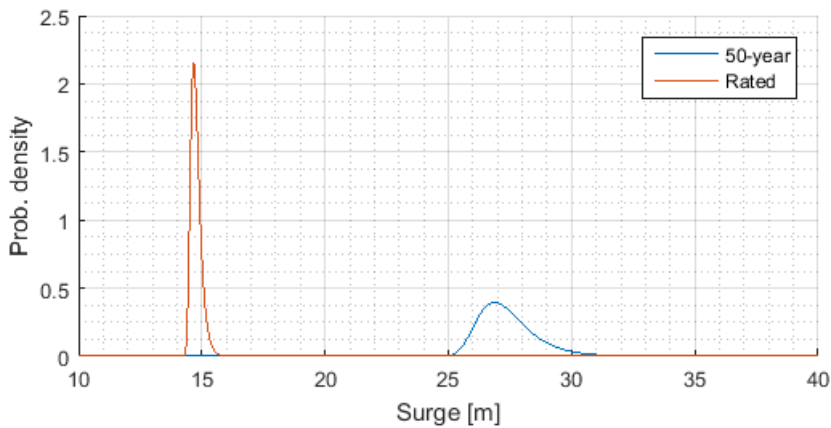


Figure 12.5: PDF of largest maxima, surge, fibre mooring

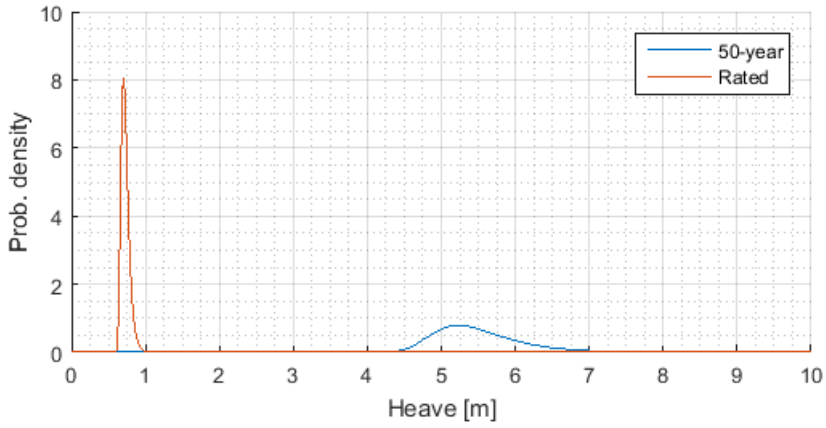


Figure 12.6: PDF of largest maxima, heave, fibre mooring

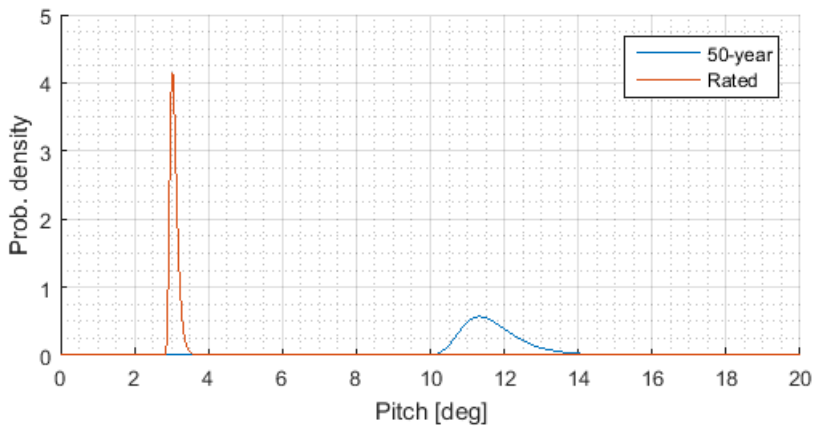


Figure 12.7: PDF of largest maxima, pitch, fibre mooring

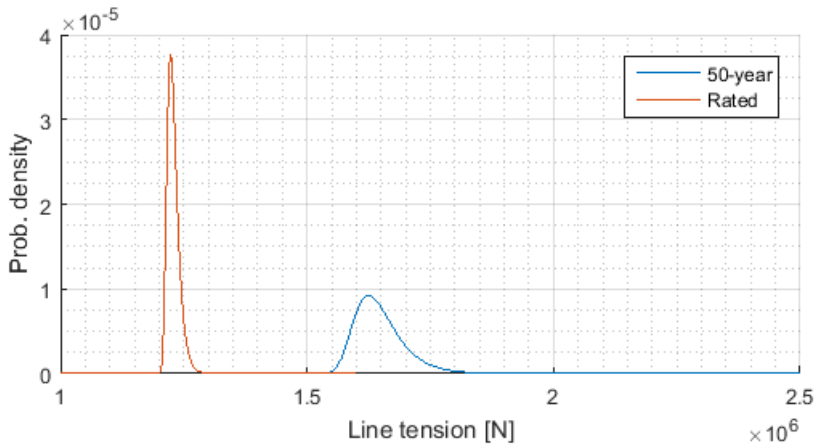


Figure 12.8: PDF of largest maxima, line tension, fibre mooring

	Rated				50-year			
	Surge [m]	Heave [m]	Pitch [deg]	Tension [N]	Surge [m]	Heave [m]	Pitch [deg]	Tension [N]
$R_{0.975}$	13.56	0.29	2.36	1.16E6	21.32	2.63	6.98	1.42E6
MPM	14.67	0.70	3.02	1.22E6	26.87	5.23	11.34	1.63E6

$R_{0.975}$ is the response at the upper boundary of the 95% confidence interval
 MPM is the most probable value

Table 12.2: Maximum values for surge, heave, pitch and line tension for rated and 50-year environment for fibre mooring

12.2 Surge and tension spectra

A FFT of the time series of surge motion and line tension was conducted to investigate the contributions to their responses. The spectra are given in Figure 12.9 and 12.11

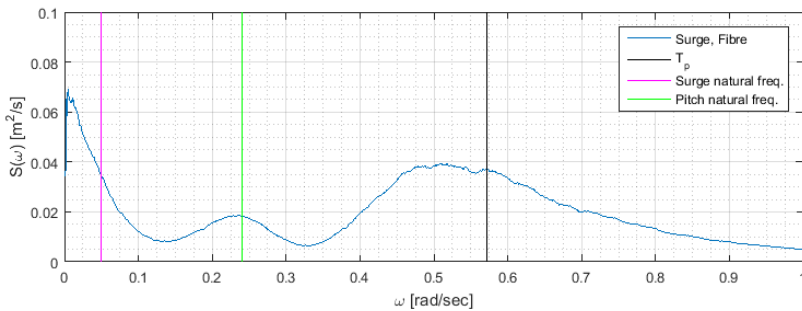


Figure 12.9: Spectrum of surge motion, rated environment, fibre mooring

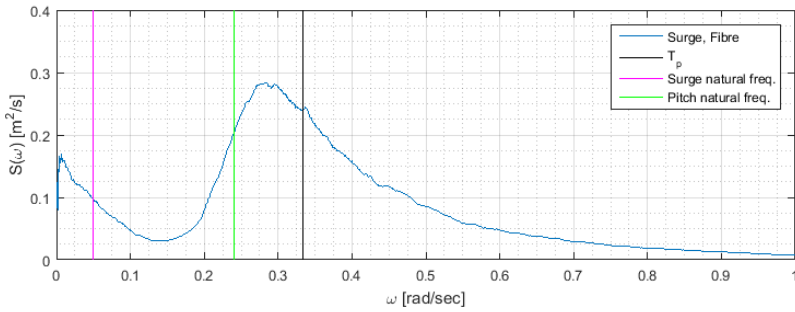


Figure 12.10: Spectrum of surge motion, 50-year environment, fibre mooring

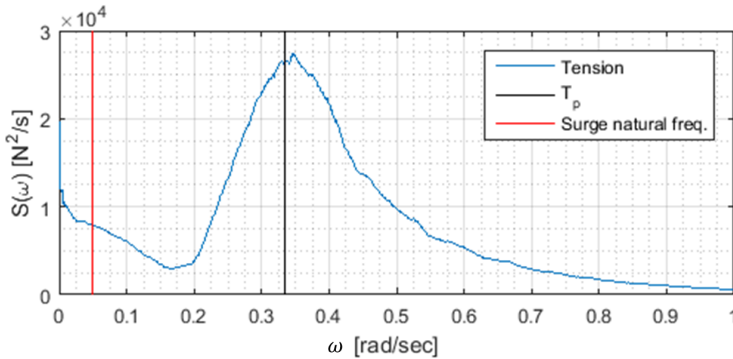


Figure 12.11: Spectrum of line tension, 50-year environment, fibre mooring

12.3 Leeward line behaviour

As discussed in Section 11.4, two of the challenges with fibre rope mooring with buoy is to maintain tension in the leeward line, and to avoid sea surface contact with the leeward buoy.

The mean value, standard deviation and corresponding 95% confidence interval of the vertical position of the leeward buoy and leeward line tension is given in Table 12.3 and 12.4, respectively. The leeward line tension refers to the tension between buoy and bridle, since this is the segment with lowest tension due to the gentle line angle.

Mean [m]	-63.31
Std. [m]	1.21
$R_{0.025}$ [m]	-65.68
$R_{0.975}$ [m]	-60.94

Std. is the standard deviation

$R_{0.975}$ is the response at the upper limit of the 95% confidence interval

$R_{0.025}$ is the response at the lower limit of the 95% confidence interval

Table 12.3: Leeward buoy vertical position in 50-year environment

Mean [N]	5.98E5
Std. [N]	3.70E4
$R_{0.025}$ [N]	5.25E5
$R_{0.975}$ [N]	6.71E5

Std. is the standard deviation

$R_{0.975}$ is the response at the upper limit of the 95% confidence interval

$R_{0.025}$ is the response at the lower limit of the 95% confidence interval

Table 12.4: Leeward line tension in 50-year environment

12.4 DNV compliance

Compliance with DNV regulations are investigated with the procedure given in Chapter 4. From the MBL of the fibre mooring system, given in Section 11.5.1, and Equation (4.4) the characteristic capacity of the fibre rope is found as

$$\begin{aligned}
 S_{C_{Fibre}} &= 0.95 \cdot S_{mbs} \\
 &= 0.95 \cdot 700\text{E}3 \text{ kg} \cdot 9.81 \text{ m s}^{-2} = 6.87\text{E}6 \text{ N}
 \end{aligned} \tag{12.1}$$

The design tension is calculated using the results for mean and maximum line tension in Table 12.1 and 12.2 and Equation (4.1) together with the ULS safety factors for normal safety class, given in Table 4.1.

$$\begin{aligned}
 T_{d_{Fibre}} &= \gamma_{mean} \cdot T_{c,mean_{Fibre}} + \gamma_{dyn} \cdot T_{c,dyn_{Fibre}} \\
 &= \gamma_{mean} \cdot T_{mean_{Fibre}} + \gamma_{dyn} \cdot [T_{max_{Fibre}} - T_{mean_{Fibre}}] \\
 &= 1.3 \cdot 1.21\text{E}6 \text{ N} + 1.75 [1.63\text{E}6 \text{ N} - 1.21\text{E}6 \text{ N}] = 2.31\text{E}6 \text{ N}
 \end{aligned} \tag{12.2}$$

Comparing the results from Equation (12.1) and (12.2), it is seen that the fibre mooring

system is in compliance with DNV regulations with a utilization factor of

$$\frac{T_{d_{Fibre}}}{S_{C_{Fibre}}} = \frac{2.31E6 \text{ N}}{6.87E6 \text{ N}} = 33.6\% \quad (12.3)$$

Chapter 13

Comparison of mooring systems, additional aspects and discussion of results

13.1 Introduction

This chapter brings the analysis results for the two mooring systems together for a comparison. Similarities and differences are discussed, and additional aspects that were in need of more in-depth studies are also presented here. Topics that only concern the fibre mooring system are also discussed.

13.2 Natural periods and damping

	Surge	Heave	Pitch	Yaw
Original mooring	115	28	26	18
Fibre mooring	123	27	26	23
Hywind Demo full scale	125	27	24	24

Table 13.1: Comparison of natural periods, original and fibre mooring

It is seen that the fibre mooring system does not introduce any significant changes to the natural periods of the system, the stiffness' are thus not altered significantly. However, by comparing the decay test time series, given in Figure 13.1, it is seen that the fibre system does alter the damping of the system.

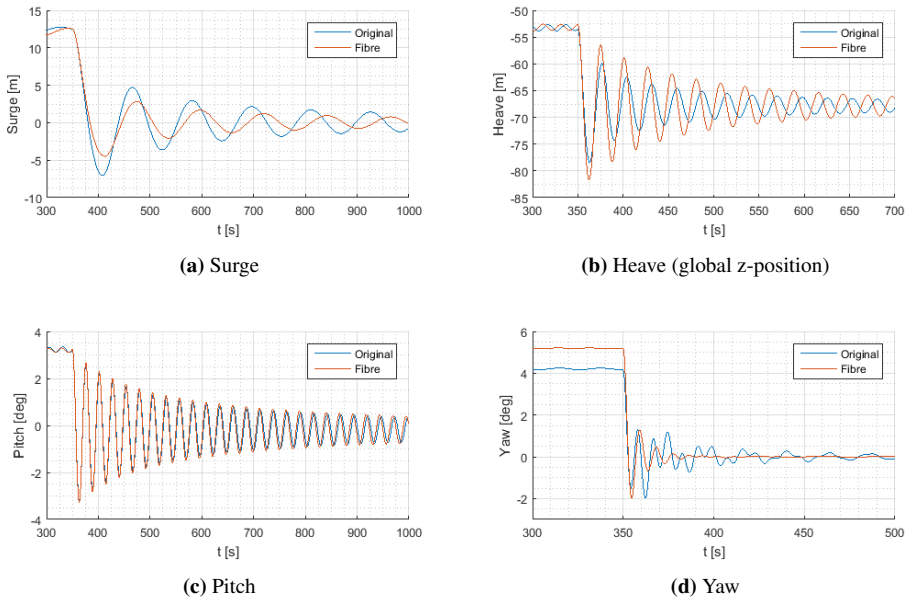


Figure 13.1: Comparison of decay tests, original and fibre mooring

The fibre mooring system has more damping in surge, but less in heave, when compared to the original system. In addition, the fibre system does not suffer from the negative damping in yaw, as is the case for the original mooring system. This is assumed to be a result of the decreased inertia of the fibre mooring system.

To provide comparable data for the two systems, damping ratios in surge and heave was calculated. The damping ratio, i.e. the ratio between actual damping and critical damping,

between two consecutive amplitudes is given in Larsen 2014 as

$$\xi = \frac{1}{2\pi} \ln \left(\frac{u_i}{u_{i+1}} \right) \quad (13.1)$$

where

- ξ = damping ratio
- u_i = first amplitude
- u_{i+1} = second amplitude

The damping ratio for the two mooring systems was calculated for two different intervals, one with large amplitudes and one with small. The damping ratio comparison is given in Table 13.2.

	Original	Fibre
$\xi_{surge_{1-2}}$	0.07	0.08
$\xi_{surge_{4-5}}$	0.03	0.03
$\xi_{heave_{1-2}}$	0.06	0.04
$\xi_{heave_{7-8}}$	0.02	0.02

Table 13.2: Comparison of damping coefficients, original and fibre mooring

The subscript notation indicates which amplitudes that were utilized, as illustrated in Figure 13.2. Note that these damping ratios are derived from the decay tests which were performed in still water condition. The damping ratios in an environment with wave, wind and current forces will deviate from these data and will most likely be higher due to dynamic effects from the mooring lines.

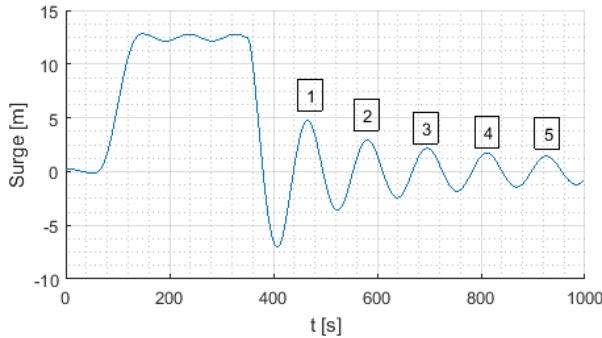


Figure 13.2: Illustration of amplitude notation for damping ratio

In agreement with the visual impression from the decay test comparison, it is seen that the fibre mooring system does provide an increase in surge damping, and a decrease in heave damping.

By comparing the physical properties of the original mooring system with the fibre system it is seen that the diameter of the fibre rope is two times as large as the diameter of the spiral strand rope, which constitutes most of the suspended length of the original mooring system. The drag coefficients for fibre rope and spiral strand rope are, on the other hand, identical. It is assumed that the increase in surge damping originates from an increase in drag force on the mooring system due to the increased diameter. In addition, due to the large size of the buoyancy element, this can also increase the damping of the fibre system. Note that due to the tension-elongation behaviour of the fibre lines, it is assumed that the line's velocity through the water is larger for the original system than for the fibre system. This would limit the increase in damping, and can be the reason why the difference in surge damping ratio between the two systems are not more prominent.

The decrease in heave damping for the fibre system is thought to be due to the loss of catenary effects with the fibre system. Heave motion with the original mooring system would generate large velocities in the mooring lines close to the sea floor. Part of the line that is set into motion is one end of the bottom chain, which has a high drag coefficient, the viscous drag on these lines will therefore generate a large damping force. The fibre mooring system, on the other hand, is assumed to experience less line displacement and velocity due to its non-catenary shape, and will thus provide inferior damping in heave.

Regarding both the surge, heave and pitch decay tests, it is seen that the dominating damping forces are quadratic in the way the damping appears to decrease with decreasing amplitude. This is also supported by the damping ratios, given in Table 13.2, which give larger damping ratios for the first amplitudes than for the later ones, whereas linear damping would yield equal damping ratios between all amplitudes. This quadratic damping is expected due to the drag force domination of slender elements, such as the mooring lines and spar.

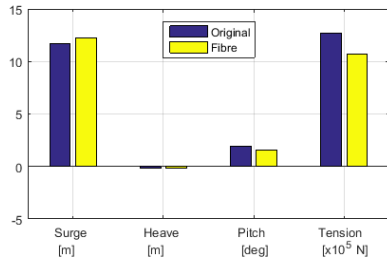
13.3 Response comparisons

An illustrated comparison of mean; upper limit of 95% confidence intervals; and maximum response values of the fibre rope system and the original mooring system is given in Figure 13.3.

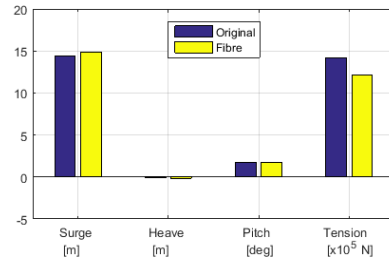
A time series comparison of surge, heave, pitch and line tension is given in Figure 13.4-13.7 and a comparison of gumbel distribution of largest maxima is given in Figure 13.8-13.11.

A comparison of the response spectra for surge motion and line tension are given in Figure 13.13 and 13.14.

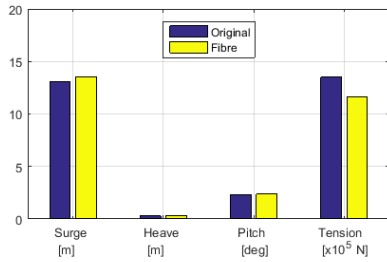
Note that the mean and maximum line tensions of the original system and fibre system was not taken at the same location along the line. The original system's line tension was measured at the bridle triplates, while the fibre system's tension was measured between the buoy and anchor. This is because the line tensions will be greatest in the segments that have the steepest angles.



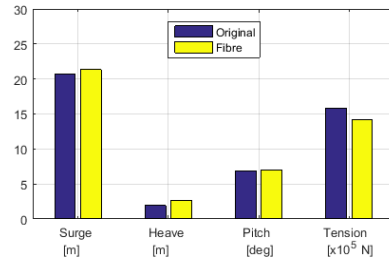
(a) Mean response, rated environment



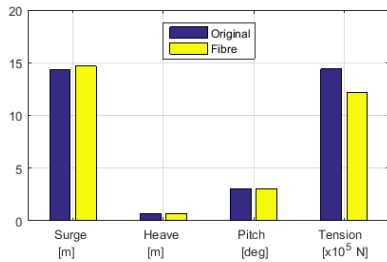
(b) Mean response, 50-year environment



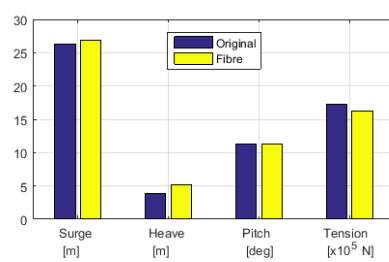
(c) Upper limit of 95% confidence interval, rated environment



(d) Upper limit of 95% confidence interval, 50-year environment



(e) Max response, rated environment



(f) Max response, 50-year environment

Figure 13.3: Response comparison, original and fibre mooring

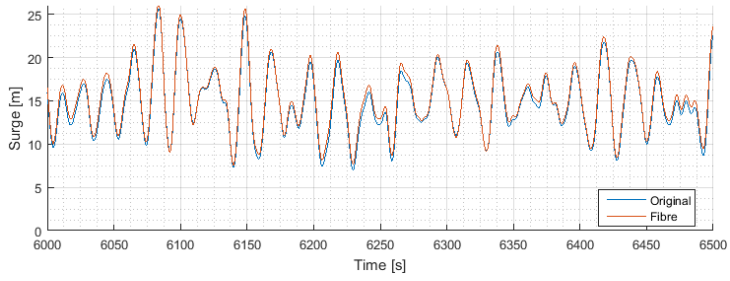


Figure 13.4: Time series of surge motion, comparison, 50-year environment

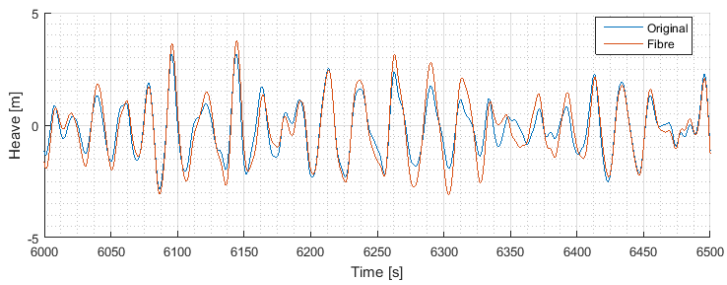


Figure 13.5: Time series of heave motion, comparison, 50-year environment

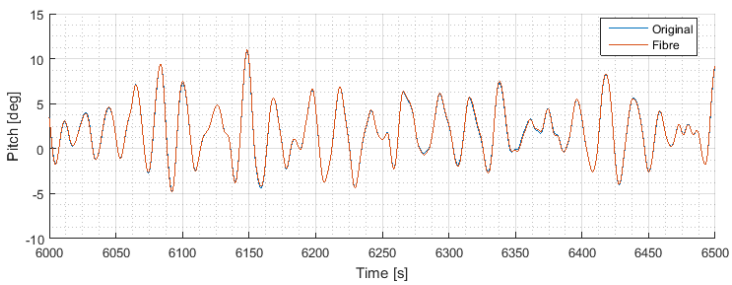


Figure 13.6: Time series of pitch motion, comparison, 50-year environment

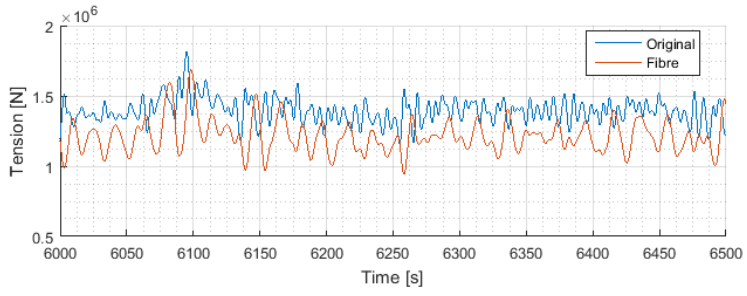


Figure 13.7: Time series of line tension, comparison, 50-year environment

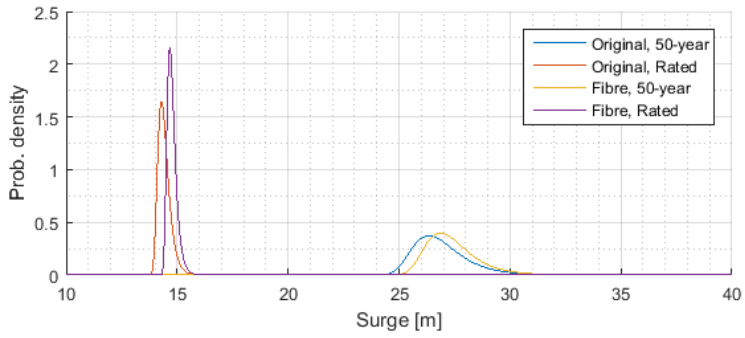


Figure 13.8: PDF of largest maxima, surge, comparison

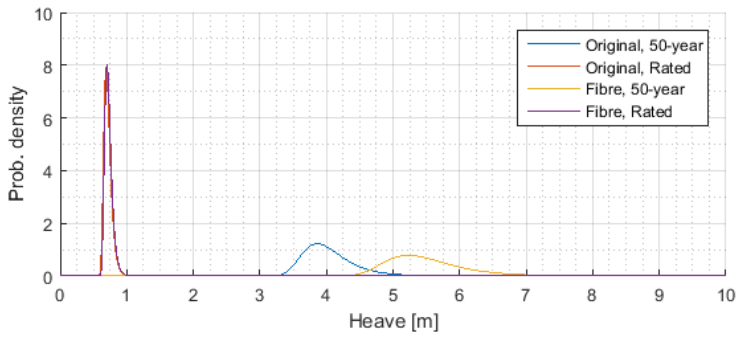


Figure 13.9: PDF of largest maxima, heave, comparison

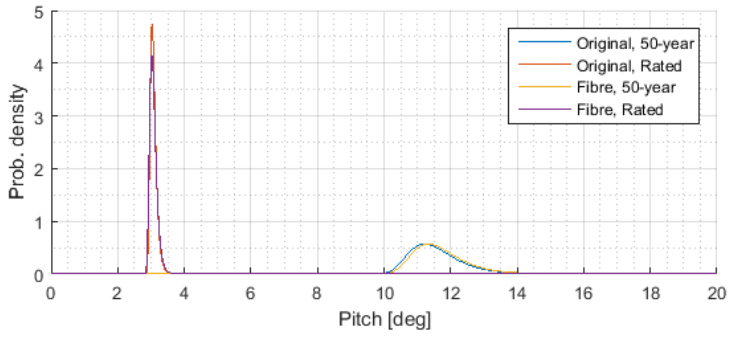


Figure 13.10: PDF of largest maxima, pitch, comparison

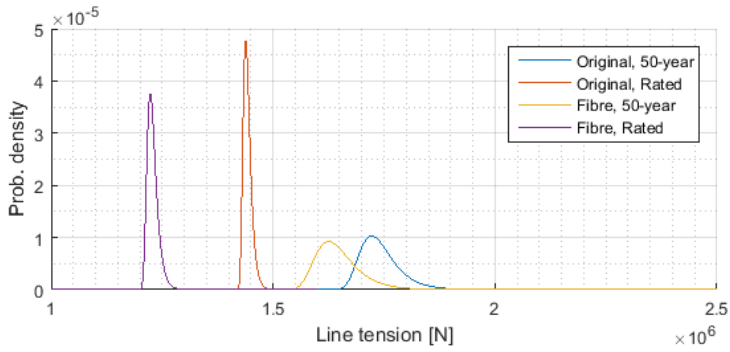


Figure 13.11: PDF of largest maxima, line tension, comparison

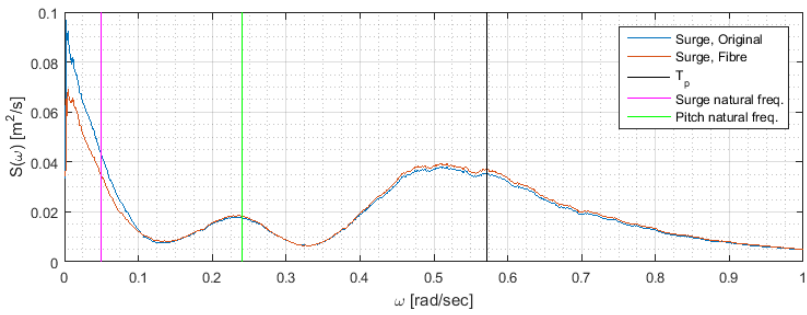


Figure 13.12: Spectrum comparison of surge motion, rated environment

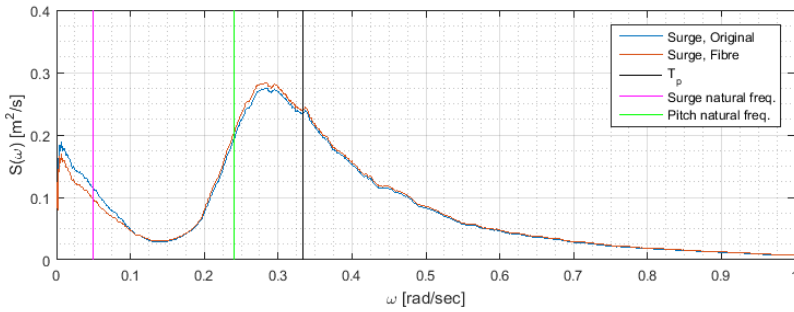


Figure 13.13: Sepctrum comparison of surge motion, 50-year environment

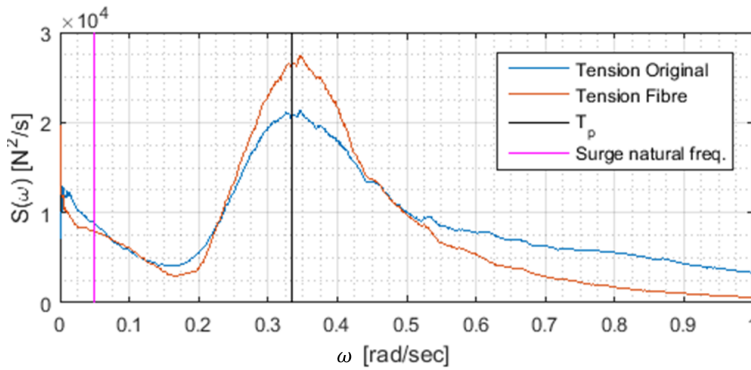


Figure 13.14: Spectrum comparison of line tension, 50-year environment

13.3.1 Surge

From the fibre mooring design in Chapter 11, a mooring system that mimicked the horizontal stiffness of the original system was designed. From the mean and maximum comparison, it is seen that the response from the fibre and original systems does indeed result in similar responses, meaning that the system was correctly designed.

In rated environment, the sea state is relatively mild, with a significant wave height of $H_s = 3.5$ m. It is therefore expected that the surge response is dominated by the wind force, with the thrust force as the main contributor. The surge response spectra for both original and fibre mooring in rated environment, given in Figure 13.12, indicates that most of the energy are located in the LF range, which corresponds to the wind spectra, given in Figure 8.5. There are also some WF energy, and some energy around the pitch natural period. Since the data used to generate the spectra are taken from the SIMO body “Watersurface”, it is expected to see some pitch-induced surge motions.

For 50-year environment, the WTG is parked, with blades feathered. In addition, the sea state is relatively harsh, with $H_s = 15.8$ m, it is thus expected that the surge motion has most of its energy located in the WF range. The spectra of surge motion in Figure 13.13 indicates that there are a significant amount of LF energy, which is seen to correlate well with the wind spectra in Figure 8.5, but the the main contribution is from the waves, both as a direct surge motion and as pitch-induced surge from wave forces.

It is noticed that the spectra does not have a prominent local maxima at the surge natural frequency. An explanation for this can be that the dynamic motions of the lines generate a damping force that hides the resonant behaviour.

By comparing the spectra for fibre mooring with original mooring in Figure 13.12 and 13.13, it is seen that these follow the same trends and are almost identical. In Section 13.2 it was found that the fibre mooring has a greater amount of damping in surge, this is also evident in the surge response spectra in the way that the fibre mooring system has less energy around the surge natural period.

13.3.2 Heave

The heave responses for the system with fibre mooring are, to a large degree, similar to the one for the original system. However, the MPM in 50-year environment yield a larger heave response for fibre mooring, 5.23 m against 3.86 m for the original system. From the results of the decay tests, it is seen that the system's stiffness' in heave has not change significantly, but the damping has been reduced, as given in Table 13.2. A spectrum analysis of the heave response in 50-year environment for the two mooring systems, illustrated in Figure 13.15, reveals that the fibre moored system has more energy around the heave natural frequency, which is seen to be a result of the fibre mooring system's inferior damping in heave.

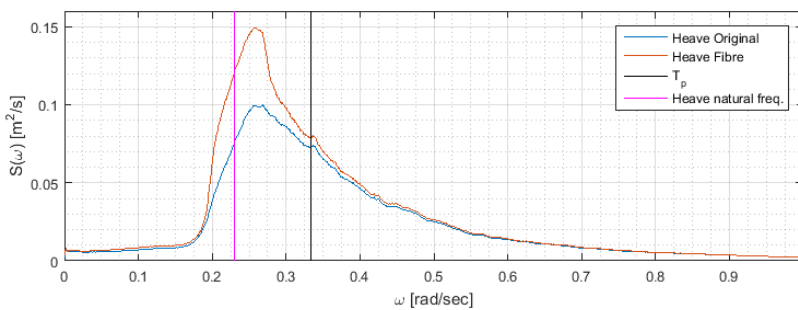


Figure 13.15: Spectrum comparison of heave motion, 50-year environment

13.3.3 Pitch

The change of mooring system was expected to have little effect on the pitch response of the spar. Any restoring contributions in pitch from the mooring system is thought to be directly linked to the mooring system's surge characteristics, which was designed to be similar to the original system. This expectation is verified by the results, which yield the same pitch response for both mooring systems.

It is seen that the tower has small pitch angles for rated environment, which is desired with respect to the hydraulic systems in the WTG. A general rule of thumb is to keep the pitch angle below 10 deg during operation. For 50-year environment it is seen that the larger wave forces contribute to larger pitch motions than for rated environment, which is deemed to be non-problematic since the WTG is parked.

13.3.4 Line tension

The line tension is consistently larger for the original mooring system than for the fibre system. This is in general due to the decreased pretension for the fibre system, 750 kN vs 1000 kN. However, from the distribution of maxima, in Figure 13.11, it is seen that this gap has decreased for 50-year environment. This can be a result of larger dynamic forces on the fibre mooring lines due to the increased line diameter.

From the spectra it is seen that the fibre mooring has more energy at T_p than the original mooring. By continuing the hypothesis that the fibre mooring introduces more viscous drag to the mooring system, due to the increased diameter, it is realized that this would increase the line tension for WF loading due to added resistance and more prominent dynamic line effects.

From the time series comparison in Figure 13.11 it is seen that the original system has more contributions from high frequency effects, which is also evident in the spectra in Figure 13.14. This difference is assumed to be from drag locking effects. At high frequency loading, the mooring line's ability to move through the water is limited due to large viscous drag forces from the rapid motions. In such a scenario, the stiffness in the mooring system is dominated by the elastic stiffness of the lines. Since the original mooring system have a larger axial stiffness, a drag locking scenario would lead to larger line tensions and tension spikes for the original mooring system compared to the fibre system, in accordance with Equation (11.2). Due to the difference in diameter between the original and fibre mooring lines, the two systems will initiate drag locking at different frequencies, which is not investigated in this thesis.

Note that any dynamic effect of buoy or clump weight attachment is neglected. Such dynamics could result in increased tension peaks.

13.3.5 Distributions of largest maxima

The distributions for largest maxima for the two mooring systems, given in Figure 13.8 -13.11, shows that the distributions for 50-year environment are consistently broader, and with longer tails, than the distributions for rated environment. It is assumed that this is because the response in rated environment is dominated by the wind loads, which is a linear effect, while the 50-year environment is dominated by wave loads, which is non-linear. To investigate this assumptions, the *coefficient of variation* (COV) is calculated for the different responses.

The COV is defined as

$$COV = \frac{\sigma}{|\mu|} \quad (13.2)$$

where

- σ = standard deviation
- μ = mean value

The COVs for the responses are given in Table 13.3 and 13.4

	Surge [-]	Heave [-]	Pitch [-]	Tension [-]
Rated	0.06	1.53	0.25	0.03
50-year	0.23	8.75	1.49	0.06

Table 13.3: Coefficient of variation, original mooring

	Surge [-]	Heave [-]	Pitch [-]	Tension [-]
Rated	0.05	1.33	0.25	0.04
50-year	0.22	9.47	1.50	0.09

Table 13.4: Coefficient of variation, fibre mooring

Note that the COV become very large for mean values that are close to zero, as for heave in this case. The COV for such processes provide little information.

From the fact that the COVs are larger for the responses in 50-year environment than the ones for rated environment, the hypothesis regarding wind-dominated response in rated and wave-dominated response in 50-year environment is further supported.

The maximum values that have been used are the MPM values, identified as the peaks of the distributions of largest maxima, which is the 37% percentile. The use of MPM can be discussed to be non-conservative, and that a design value taken further out in the tail of the distributions should be utilized, such as the 90% percentile. However, since this thesis utilizes the DNV rules and regulations, which is based on MPM, the utilization of MPM is seen to be justified.

13.3.6 Rotor air gap investigation

Due to the increased heave response with the fibre mooring system compared with the original mooring system, shown in Figure 13.3f, an investigation on the air gap between wave crest and rotor blade was conducted. The rotor air gap is crucial since the airfoils would without a doubt be damaged if they were to be struck by a wave crest. Even though the WTG would most likely be parked during an environmental condition that would result in a severely reduced air gap, it is possible that the rotor would be parked with one blade pointing straight downwards.

The rotor diameter is 82.4 m, and is positioned at a height of 65 m, as stated in Section 3.2, meaning that the still water air gap is $65 \text{ m} - \frac{82.4 \text{ m}}{2} = 23.8 \text{ m}$.

To investigate the air-gap process for the original and fibre mooring system, SIMA's post processor was used to establish a time series of the instantaneous rotor air-gap when the turbine was parked with one blade pointing straight down for both the original and fibre mooring system. The mean value of the process', along with the standard deviations and lower limits of the confidence intervals are given in Table 13.5.

	Original	Fibre
Mean [m]	22.12	22.08
Std. [m]	3.23	3.25
$R_{0.025}$	15.79	15.71

$R_{0.025}$ is the response at the lower limit of the 95% confidence interval

Table 13.5: Mean and standard deviation of air-gap process

From this investigation, it is seen that the mean response and standard deviation is almost identical for fibre and original mooring. For the scope of this thesis, the air gap it thus taken to be satisfactory.

13.4 Leeward line of fibre mooring

Due to fatigue damage of the fibre ropes, it is important to maintain tension in all mooring lines at all time, as discussed in Section 11.4. In addition, to avoid snapping loads and large wave-induced forces on the buoy, it is important that the buoy is not subjected to sea surface contact. The lower limit of the confidence interval of leeward line tension was calculated to be 525 kN, which is 70% of the pretension. During the design phase, it was expected that the leeward buoys would help maintain tension in the leeward lines, and this expectation is hereby confirmed. There was some uncertainty regarding how much the towards the sea surface the leeward buoys would stretch during a 50-year storm. The analysis yielded a mean depth of 63.31 m with a standard deviation of only 1.21 m, meaning that the vertical motion of the buoys are limited. The large depth of the buoy also

help limit the wave forces on the buoy. At 60 m depth, the wave induced particle velocity and acceleration are known to have decayed significantly, reducing the wave-induced drag and inertia forces on the buoy.

From the relatively large tension and deep buoy position for the leeward line, it is concluded that compression forces and sea surface contact are not issues that are likely to occur.

13.5 Economic comparison

To be able to compare the cost of the original and fibre mooring system, the cost of chain, steel spiral strand rope, clump weights, fibre rope and buoys were needed. In Larsen 2016 the following costs are recommended

Element	Cost [USD/kg]
Chain	6.0
Steel rope	7.2
Clump weight	4.8
Fibre rope	3.0
Buoy	4.2

The price of buoy are per kilogram of net buoyancy

Table 13.6: Cost of mooring system elements

Using the costs defined in Table 13.6 together with the mooring systems defined in Table 9.5 and 11.6, the following total expenses are found for the two mooring systems

Element	Length [m]	Mass coefficient [kg m ⁻¹]	Weight [kg]	Price [USD]
Link adaptor	10	148	1480	8880
Spiral strand rope	75	32	2400	17 280
Link chain	15	126	1890	11 340
Clump weight	1	66 645	66 645	319 896
Link chain	37	127	4699	28 194
Spiral strand rope	465	32.47	15 098.55	108 709.56
Bottom chain	320	125.94	40 300.80	241 804.8
SUM	923		132 513.35	736 104.36

Table 13.7: Cost of original mooring system

Element	Length [m]	Mass coefficient [kg m ⁻¹]	Weight [kg]	Price [USD]
Fibre rope	330	16.70	5511	33 066
Buoy		563.25	36 611	126 054.60
Fibre rope	670	16.70	11 189	67 134
SUM	1000		53 311	226 254.6

Since the buoy is not added as a RIFLEX element with length and mass coefficient, its cost is calculated directly for 30 000 kg of net buoyancy at a price of 4.2 USD/kg of net buoyancy

Table 13.8: Cost of fibre rope mooring system with buoy

From the total cost of the two mooring systems given in Table 13.7 and 13.8, it is seen that the fibre rope system provides a price reduction of $1 - \frac{226254.6\text{USD}}{736104.36\text{USD}} \approx 70\%$ of the original system. Note that the cost of each component is given only as a recommendation in Larsen 2016, and may not be accurate. The cost of anchor and anchor attachments are not taken into account for any of the mooring systems, neither is the cost of buoy attachments or fibre attachments to the bridle. Hence, there are some uncertainties in the cost comparison, but it is seen, without a doubt, that the fibre mooring system provide a significant cost reduction. The cost of the bridle system is not included, since the same bridle is used for both systems.

From Section 12.4, it is seen that the fibre mooring system that was designed in Chapter 11 yields a utilization factor of 33.6%, the original system had a utilization of 39.1%. Meaning that for the analyses performed in this thesis, both systems are over-engineered. It would, in many ways, be beneficial to utilize a thinner and weaker fibre rope in the mooring configuration. Not only would the material cost of the rope itself be reduced, but the rope would also become more flexible, since the stiffness is calculated from the MBS, as discussed in Section 6.3. A more flexible fibre rope could also permit a reduction in the volume of the buoy. It is therefore seen that the economic benefit of the fibre mooring system could go beyond the calculated cost reduction of 70%. However, due to the fact that the original mooring system also has a low utilization factor, it is thought that there are reasons behind this conservatism which go beyond the scope of this thesis, and the low utilization factor of the fibre systems is therefore deemed to be acceptable.

In addition to the cost reduction of the mooring system itself, the use of a fibre mooring system permits the use of smaller installation vessels due to the reduced weight of the system. The fibre mooring system introduces a weight reduction of about 60%, enabling lighter anchor handling tug supply (AHTS) vessels to perform the installation, which in turn reduces the cost of installation.

There are additional, possible, costs with the fibre mooring that is not an issue with the original mooring. Such costs can be to perform pre-stretching of the fibre rope to minimize fibre creep after installation. This, however, may not be necessary due to the buoy's ability to absorb the elongation. It may also be necessary to use a different anchor type, with higher resistance against vertical forces, but this is not discussed further in this thesis due to confidentiality agreements with Statoil ASA.

13.6 Footprint

The footprint of the original mooring system has a radius of 935 m, while the fibre mooring system's footprint has a radius of 1030 m, resulting in an increased footprint of 0.6 km². For use on Hywind Demo in a FOWT park scenario, such an increase in footprint is not significant, since the area will most likely not be used for fishing. For the use on Hywind Demo in today's situation, with its position along the coast of Norway as a sole installation, an increase in footprint will lead to a reduction in area that can be used for trawling. Due to the line geometry of the fibre mooring system, it will not be possible to make the system over-trawl-able, but this is also the case for the original mooring system (Skarbøvik 2016). The increase of footprint is not seen to be of significant proportion, but must be considered if the fibre mooring system is to be used in an area where there is trawling.

13.7 Limitations to the analyses

This thesis has focused on the design of a fibre rope mooring system for Hywind Demo that provide the same restoring capabilities as the original mooring system. The focus has therefore been primarily on surge, pitch and heave motion; and line tension responses. The motion response in yaw, sway and roll has not been analysed. This is, however, seen to be a justifiable method due to the 2-dimensionality of the problem.

In DNV-OS-J103 2013, it is stated that the mooring system should be designed for a 50-year return period environment, as discussed in Chapter 4. For the scope of this thesis, only a single 50-year condition, defined in Chapter 8, was analysed. To be in complete compliance of the DNV regulations, several 50-year conditions should be analysed. These can be found by utilizing a contour line of the 50-year combinations of H_s and T_p .

The analyses carried out in this thesis has been computed by SIMO and RIFLEX in SIMA. SIMO-RIFLEX does not perform calculations on vortex induced vibrations (VIV), for this SIMA has the module VIVANA. For the scope of this thesis, VIVANA was not utilized, and VIV is therefore not included in the response calculations. VIV can lead to higher tension in the mooring lines, but it is assumed that this effect would be limited. In addition, the mooring line drag coefficients taken from DNV-OS-E301 2013 does, to some degree, account for VIV (Larsen 2016).

This thesis has only focused on ULS analyses, and has not inspected the FLS or ALS conditions. However, it can in general be said that fibre ropes provides better endurance to cyclic load than steel wire and chain. The main focus on a FLS analysis should therefore be concerning the fibre rope's connection to the buoy. An ALS condition with one broken mooring line would result in a large horizontal offset which would most likely result in a power cable breakage. In such a condition, Hywind Demo would be moored with its two remaining mooring lines. Due to the low utilization factor of the mooring lines, it is assumed that the system can handle such an ALS condition. However, detailed analyses on the broken system need to be performed to provide a certain answer.

Chapter 14

Fibre mooring of Hywind Demo at 130m water depth

14.1 Introduction

This chapter provides a short feasibility study on fibre rope mooring of Hywind Demo in 130 m water depth, including mooring system design; system analysis; and discussion of results.

Hywind Demo is now positioned outside Karmøy, Norway, at 204 m water depth, and through the previous chapters of this thesis, a cost beneficial mooring system composed of fibre ropes and buoyancy elements has been proposed for this location. The proposed mooring system has been found to perform satisfactory, and to provided similar floater motion responses as the original mooring system.

As stated in Chapter 3, the purpose of Hywind Demo is not to generate electrical power for profit, but to be used as a research tool. In late 2015, Statoil ASA submitted a request to the Norwegian authorities to relocate Hywind Demo to the unmanned Valemon platform, located about 160 km west of Bergen, to study the possibility of using FOWTs to provide power to other offshore installations. The Valemon field has a water depth of about 130 m, and due to the possible relocation of Hywind Demo, this thesis has performed a short feasibility study on the possibility of utilizing the fibre mooring system designed for 204 m water depth in the new location.

14.2 Challenges

The use of fibre mooring in shallow water is generally regarded as a challenging task. As discussed in Section 11.4, one of the main challenge with shallow water mooring with fibre ropes is to maintain an acceptable level of horizontal flexibility. However, since a satisfactory design for fibre mooring in 204m is given in Chapter 11, it is assumed that this system is applicable for even shallower water and that it will yield similar horizontal stiffness in 130 m water depth as long as the angle at the buoy and the buoy placement is not significantly changed.

14.3 Design

The mooring system design is taken directly from the 204 m version, but in order to maintain the buoy at a satisfactory depth, i.e. roughly 50 m, the 1 : 2 ratio for buoy placement along the line had to be altered to a 1 : 5 ratio, as illustrated in Figure 14.1. It is expected that this will result in a reduction of the geometric flexibility.

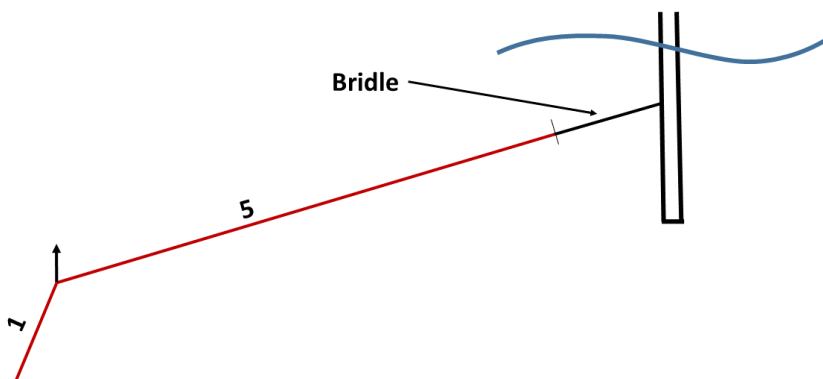


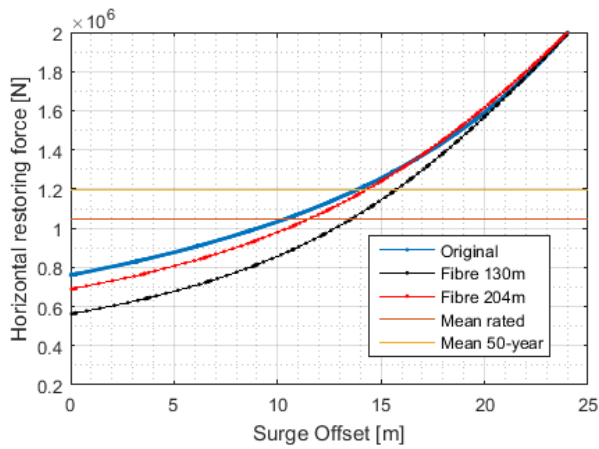
Figure 14.1: 1 : 5 ratio of fibre mooring line on each side of a buoyancy element

A mooring line characteristic was generated for the system using the same parameters as the 204 m, except for the new buoy placement.

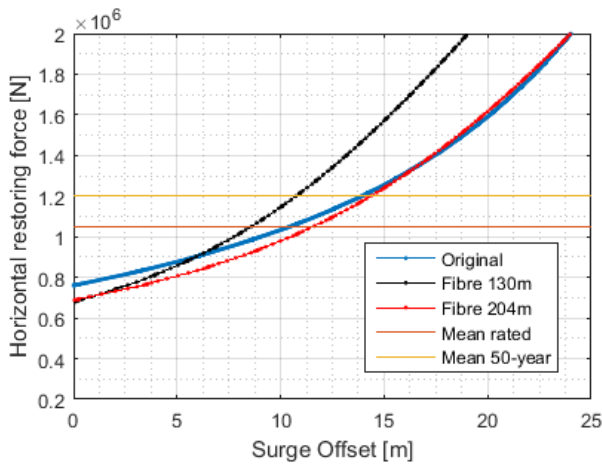
- Total length: 1000 m
- Buoy volume: 65 m^3
- Anchor displacement: -10 m
- Buoy placement: 0.165

where the buoy placement of 0.165 corresponds to the 1 : 5 ratio.

These parameters were seen to result in a system with a horizontal stiffness very similar to the case of 204 m, but with a pretension lower than initially desired. Therefore, a line characteristics for the same system, but with an anchor displacement of -5 m was investigated. This resulted in a reduction of geometric flexibility in the system, similar to the case of the buoy optimization in Section 11.5.4. From the leeward line tension investigation for 204 m, given in Section 12.3, it is seen that the system has relative large amount of tension in the leeward lines. Therefore, the reduced pretension was taken to be acceptable since this maintains a satisfactory amount of geometric flexibility. The system with anchor displacement of -10 m was thus chosen for further analysis. The pretension for the chosen system is 623 kN between anchor and buoy, and 559 kN between buoy and bridle. The footprint of the system is the same as 204 m version, i.e. 1030 meter radius. The line characteristics are given in Figure 14.2a.



(a) Anchor displacement: -10 m



(b) Anchor displacement: -5 m

Figure 14.2: Single mooring line characteristics for 130 m water depth

14.4 Natural periods and damping

To determine the natural periods of the system, the same kind of decay tests that were performed on the original mooring system, and on the fibre mooring in 204 m water depth, was utilized. Time series of the decay tests are given in Figure 14.3, and the natural periods are compared with the previously tested results in Table 14.1. The decay tests were measured at the COG, a coordinate system is given in Figure 9.13.

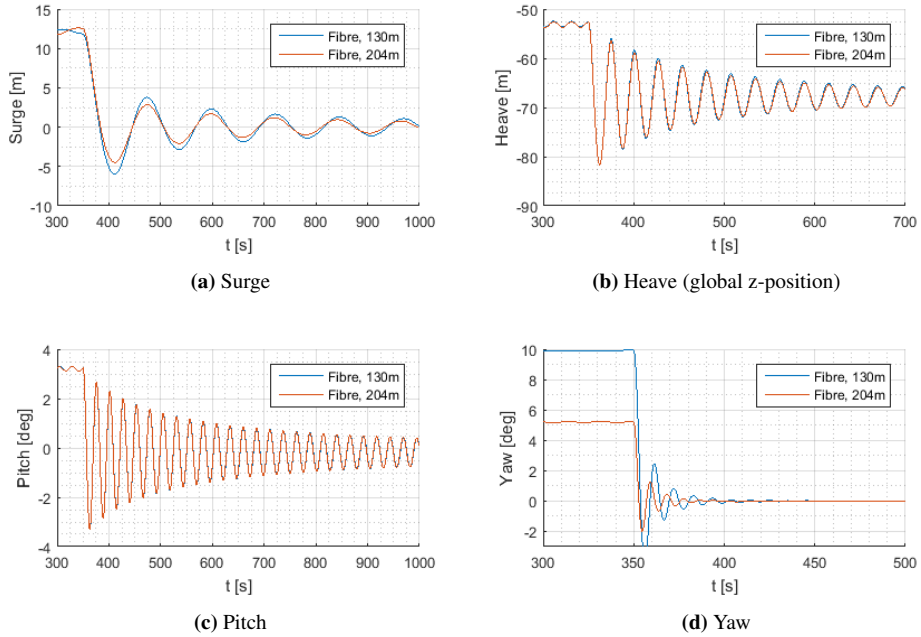


Figure 14.3: Decay tests, measured at center of gravity

	Surge	Heave	Pitch	Yaw
Fibre mooring, 130 m	124	27	26	27
Fibre mooring, 204 m	123	27	26	23
Original mooring 204 m	115	28	26	18
Hywind Demo full scale	125	27	24	24

Table 14.1: Natural period of Hywind Demo with fibre rope mooring system in 130 m water depth

From the decay tests and calculated natural periods, it is seen that the 130 m system have similar stiffness and damping in surge, heave and pitch as the 204 m fibre system. However, it is seen that the stiffness in yaw has decreased, which is thought to be in connection with the 1 : 5 fibre ratio. In Equation (2.2), it is evident that the stiffness in yaw will decrease if the distance to the mooring lines' horizontal rotation point is increased, and it is assumed that the buoy will function as the horizontal rotation point of the mooring line.

To compare the damping in yaw with the 204 m fibre system, the damping ratios were calculated in the same manner as described in Section 13.2. A comparison between the two fibre systems are given in Table 14.2.

	Fibre, 204 m	Fibre, 130 m
$\xi_{yaw_{1-2}}$	0.16	0.19
$\xi_{yaw_{4-5}}$	0.07	0.10

Table 14.2: Comparison of damping coefficients, original and fibre mooring

It is seen that the damping in yaw is larger for the 130 m version than for the 204 m version. This is in correlation to the assumption of the buoy acting as the rotation point, since this will lead to a longer length of line being set into motion for the 130 m system, resulting in more viscous damping from drag forces. Note that these damping coefficients are derived from the decay tests, which were performed in still water conditions. For an environmentally loaded system, the damping is assumed to increase due to dynamic line motion. In addition, since the yaw motion is of less interest in this thesis, assumptions regarding skin friction was made in Section 9.2 during the establishment of the model. The damping ratios are therefore not meant to be used in any design considerations.

14.5 Feasibility

The response of an FOWT can be described with the generalized dynamic equation given in Equation (5.1), i.e. a mass-spring-damper system. The response to an external load is thus dependant on the mass, stiffness and damping of the system. Knowing that the external load, i.e. the environmental forces are the same as for the 204 m system, and it has been found that the mass, stiffness and damping properties are also similar, it is assumed that the response of the 130 m system will also be similar.

There are, however, uncertainties to such an analogy. As previously stated, the damping for an environmentally loaded system will be different to the damping found from the still water decay tests. It is therefore necessary to perform a full set of analyses on the system to determine it's applicability. For the scope of this thesis, it is concluded that fibre mooring of Hywind Demo in 130 m water depth is feasible.

Chapter 15

Conclusions and recommendations

15.1 Concluding remarks

The work done in this thesis has resulted in an improved, fibre mooring system for Hywind Demo that reduce the cost of the mooring system with 70% while maintaining the same motion responses and utilization factors as the original, catenary system.

A comparison between frequency domain and time domain analysis was performed on the original mooring system, i.e. chain and spiral strand rope, revealing correlating results. The restoring properties of the original mooring system was set as the design goal for the fibre system, and several fibre mooring designs were investigated, including plain taut mooring and the utilization of clump weights and buoyancy elements. The system that was chosen for further studies utilized a buoyancy element of 65 m^3 and possessed a very similar restoring stiffness as the original system, without an significant increase in footprint. By analysing the fibre mooring system in environmental conditions, it was confirmed that the fibre system resulted in very similar motion responses of the floater.

It was found that the fibre mooring altered the damping of the system slightly in the way that the larger rope diameter provided an increase in surge damping, but the loss of catenary effect resulted in a decrease in heave damping.

Based on recent events, a feasibility study on the use of the fibre mooring system in 130 m water depth was performed. This feasibility study did not include environmental response analyses, but was based on the physical properties of the system. The study yielded positive results, and it is concluded that it is feasible to utilize the fibre mooring in 130 m water depth.

15.2 Recommendation for further work

This thesis has only analysed the global behaviour of the mooring system. Since the fibre mooring designed in this thesis includes a relatively large buoyancy element, it is necessary to perform an analysis on the local behaviour of the buoy, both with respect to ULS and FLS. In addition, an ALS analysis with a broken mooring line should be performed.

An investigation on the rotor air gap have been performed due to the decreased heave damping with fibre mooring. This investigation did, however, not include several time series realizations, and is therefore based solely on the mean and standard deviation of the process. It is recommended to simulate this process for several wave and wind seeds so that a distribution of the smallest air gaps can be established.

From the environmental data provided, the 50-year ULS environmental condition was established. However, only a single 50-year condition was utilized in this thesis, whereas there are several combination of H_s and T_p that can be associated with a 50-year return period. Therefore, it is recommended that ULS response analyses are performed with additional sea states that are related to the 50-year contour line.

To verify the feasibility of the fibre mooring system in 130 m, environmental response analyses on this system should be carried out. Similar to the 204 m system, these analyses should be based on several different 50-year sea states.

Fibre ropes are known to subject to irreversible elongation after installation due the compaction of fibres when they are tensioned for the first time. This can, for Hywind Demo, be solved by tensioning the ropes before installation, but this is not a cost effective solution. It is therefore recommended to perform studies on the possibilities of accommodating such creep with the buoyancy elements.

Bibliography

- AMC. *CLUMP*. Visited on 06/26/2016. <http://www.amc-cn.com>.
- Bachynski, Erin. *Basic aerodynamics for wind turbines (Lecture notes)*.
— . 2016. *Thesis-specific hand-outs*.
- Bjørnsen, Gaute. 2015. *A Comparison of Methods for Estimation of Fatigue and Extreme Mooring Response for a Floating Spar Wind Turbine*. Norwegian University of Science and Technology.
- Borlet, Rémi Marcel. 2015. *Optimization of Mooring system for Floating Wind Turbine*. Norwegian University of Science and Technology.
- Bridon. *Floating Production Mooring Systems*. Visited on 06/26/2016. www.bridon.com.
- Burton, T., et al. 2011. *Wind Energy Handbook*. Wiley.
- Carbon Trust. 2015. “Floating Offshore Wind : Market and Technology Review”, no. June. <http://www.carbontrust.com/media/670664/floating-offshore-wind-market-technology-review.pdf>.
- Deep Sea Anchors. *Deep Penetrating Anchors*. Visited on 06/26/2016. <http://www.deepseaanchors.com/>.
- DNV-OS-E301. 2013. “Position Mooring”.
- DNV-OS-J103. 2013. “Design of Floating Wind Turbine Structures”.
- DNV-RP-C205. 2010. “Environmental conditions and environmental loads”.
- DNV-RP-H103. 2014. “Modelling and Analysis of Marine Operations”.
- Falkenberg, Erik, et al. 2011. “GLOBAL PERFORMANCE OF SYNTHETIC ROPE MOORING SYSTEMS – FREQUENCY DOMAIN ANALYSIS”. *OMAE2011-49723*.
- Faltinsen, O.M. 1990. *Sea Loads on Ships and Offshore Structures*. Cambridge University Press. ISBN: 0-521-45870-6.

- Flory, John F, Vidar Ahjem, and Stephen J Banfield. 2007. "A New Method of Testing for Change-in-Length Properties of Large Fiber - Rope Deepwater Mooring Lines". *OTC 18770*.
- Ghao, Zhen. 2015. *Lecture: Introduction to offshore wind power and technology*.
- Godø, Sjur. 2013. *Dynamic Response of Floating Wind Turbines*. Norwegian University of Science and Technology.
- Green Rhino Energy. *Wind speed spectrum*. Visited on 06/06/2016. http://www.greenrhinoenergy.com/renewable/wind/wind{_}characteristics.php.
- Hagen, Per Chr. 2007. *Innføring i sannsynlighetsregning og statistikk*. 186. Cappelen Akademiske Forlag. ISBN: 978-82-02-26945-6.
- Hansen, Martin O.L. 2015. *Aerodynamics of Wind Turbines*. 3rd ed. Routledge. ISBN: 978-1-138-77507-7.
- Hordvik, Tore. 2011. *Design analysis and optimisation of mooring system for floating wind turbines*.
- Kaasen, Karl Erik, et al. 2014. "DEVELOPMENT OF TIME DOMAIN MODEL FOR SYNTHETIC ROPE MOORING". *OMAE2014-24180*.
- Lankhorst Mouldings. 2016. *E-mail correspondance*.
- . *Mooring Buoyancy Modules*. Visited on 05/19/2016. <http://www.lm-offshore.com/en/subsea-buoyancy-modules>.
- Lankhorst Ropes. 2014. *Offshore Steel Wire Ropes*. Visited on 06/18/2016. http://www.lankhorstropes.com/files/uploads/Offshore/brochures/Steel{_}Wire{_}Rope{_}brochure{_}{_}72dpi{_}{_}{_}{_}April{_}2014.pdf.
- . 2015. *Ropes for Deep Water Mooring*. Visited on 04/12/2016. http://www.lankhorstropes.com/files/uploads/Download/2015/Lankhorst{_}Ropes{_}Deep{_}Water{_}Mooring{_}0415{_}72dpi.pdf.
- Larsen, Carl Martin. 2014. *Marine Dynamics*. Kompendieforlaget.
- Larsen, Kjell. 2016. *Personal, thesis specific, conversation*.
- . 2015. *Thesis-specific hand-outs*.
- MARINTEK. 2012. *MIMOSA User's Documentation*.
- . 2015. "RIFLEX Theory Manual", no. V4.6v0.
- Moriarty, P. J., and A. C. Hansen. 2005. "AeroDyn Theory Manual (NREL/TP-500-36881)". *Renew. Energy*. ISSN: 00664189. <http://www.nrel.gov/docs/fy05osti/36881.pdf>.
- Moxnes, Simen. 2009. "Flytende vindmøller - Hywind (presentasjon)".
- Myrhaug, Dag. 2005. *Stochastic Theory of Sealoads*.
- NVE. 2012. "Vindkraft – Produksjonsstatistikk - 2011".

- Semar. *Removal of Suction Anchors at Shelley Field*. Visited on 06/26/2016. <http://www.semar.no>.
- Skarbøvik, Oddbjørn. 2016. *Uakseptabel plassering*. Visited on 06/24/2016. <http://www.fiskebat.no/default.asp?page=9242{\&}item=61912,1{\&}lang=1>.
- Smith, Bruce. 2011. *Synthetic winch line care*. Visited on 05/16/2016. <http://www.hardworkingtrucks.com/synthetic-winch-line-care/>.
- Statoil. 2004. *Heidrun Metocean Design Basis PTT NKG 0058*. Tech. rep.
- . 2009. *Hywind Demo*. Visited on 09/30/2015. <http://www.statoil.com/no/technologyinnovation/newenergy/renewablepowerproduction/offshore/hywind/pages/hywindputtingwindpowertothetest.aspx>.
- Vryhof. *Anchor Products*. Visited on 06/26/2016. <http://www.vryhof.com/>.

Appendices

Appendix A

Bridle details

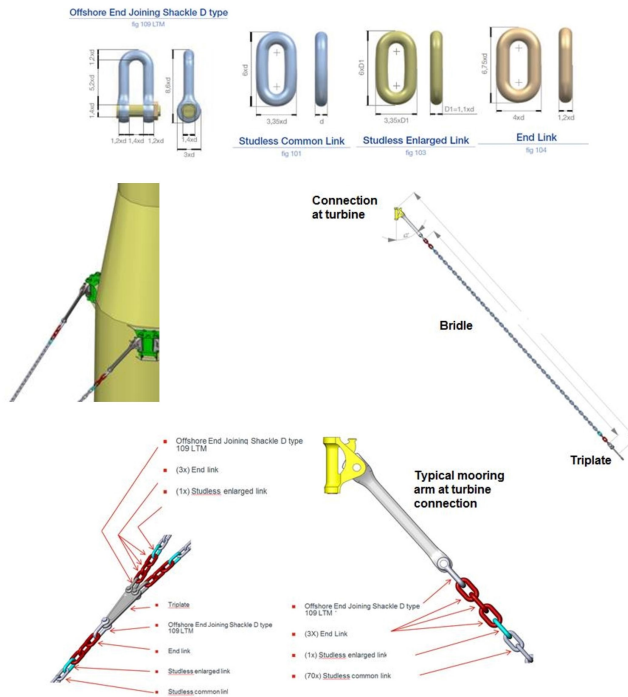


Figure A.1: Bridle details (Larsen 2015)

Appendix B

Original mooring response samples

	Rated				50-year			
	Surge [m]	Heave [m]	Pitch [deg]	Tension [N]	Surge [m]	Heave [m]	Pitch [deg]	Tension [N]
Sample 1	13.95	0.62	2.92	1.43E6	25.16	3.36	10.41	1.66E6
Sample 2	14.07	0.62	2.95	1.43E6	25.40	3.61	10.61	1.69E6
Sample 3	14.08	0.67	2.97	1.43E6	25.52	3.63	10.76	1.70E6
Sample 4	14.16	0.68	2.98	1.43E6	25.70	3.73	10.77	1.71E6
Sample 5	14.21	0.68	2.99	1.43E6	25.89	3.75	10.81	1.72E6
Sample 6	14.24	0.32	3.01	1.44E6	25.90	3.83	10.83	1.72E6
Sample 7	14.26	0.68	3.03	1.44E6	25.98	3.83	10.85	1.72E6
Sample 8	14.39	0.69	3.06	1.44E6	26.11	3.85	11.24	1.73E6
Sample 9	14.39	0.70	3.06	1.44E6	26.41	3.90	11.27	1.73E6
Sample 10	14.40	0.71	3.06	1.44E6	26.87	3.92	11.42	1.73E6
Sample 11	14.41	0.71	3.07	1.45E6	26.89	3.94	11.66	1.73E6
Sample 12	14.43	0.71	3.07	1.45E6	26.99	3.98	11.72	1.74E6
Sample 13	14.47	0.72	3.08	1.45E6	27.02	4.08	11.80	1.75E6
Sample 14	14.50	0.72	3.09	1.45E6	27.32	4.15	12.04	1.75E6
Sample 15	14.57	0.77	3.09	1.45E6	27.69	4.24	12.15	1.76E6
Sample 16	14.57	0.78	3.15	1.45E6	28.36	4.39	12.42	1.77E6
Sample 17	14.64	0.78	3.18	1.45E6	28.43	4.40	12.49	1.80E6
Sample 18	14.80	0.79	3.24	1.45E6	28.49	4.55	12.55	1.81E6
Sample 19	14.89	0.80	3.24	1.46E6	28.94	4.72	12.58	1.82E6
Sample 20	15.10	0.84	3.27	1.46E6	29.34	4.85	13.40	1.84E6

Note that this is collection of different data sets, and that each data set has been sorted by magnitude. Hence, there is no connection between the values that are placed on the same row in the table.

Table B.1: Response samples for Hywind Demo original mooring configuration

Appendix C

Fibre mooring response samples

	Rated				50-year			
	Surge [m]	Heave [m]	Pitch [deg]	Tension [N]	Surge [m]	Heave [m]	Pitch [deg]	Tension [N]
Sample 1	14.47	0.63	2.91	1.21E6	25.66	4.30	10.66	1.57E6
Sample 2	14.48	0.64	2.93	1.21E6	26.20	4.51	10.77	1.59E6
Sample 3	14.53	0.68	2.95	1.21E6	26.20	4.82	10.81	1.60E6
Sample 4	14.54	0.68	2.99	1.22E6	26.30	4.92	10.93	1.61E6
Sample 5	14.60	0.68	2.99	1.22E6	26.44	5.22	10.95	1.61E6
Sample 6	14.62	0.69	2.99	1.22E6	26.50	5.27	11.03	1.61E6
Sample 7	14.63	0.70	2.99	1.22E6	26.58	5.37	11.03	1.61E6
Sample 8	14.67	0.71	3.02	1.22E6	26.71	5.38	11.16	1.62E6
Sample 9	14.70	0.72	3.03	1.23E6	26.78	5.40	11.52	1.62E6
Sample 10	14.72	0.72	3.06	1.23E6	27.05	5.51	11.56	1.64E6
Sample 11	14.72	0.72	3.07	1.23E6	27.29	5.52	11.72	1.64E6
Sample 12	14.77	0.72	3.08	1.23E6	27.41	5.53	11.79	1.65E6
Sample 13	14.79	0.73	3.09	1.23E6	27.56	5.56	11.98	1.66E6
Sample 14	14.89	0.74	3.10	1.23E6	28.13	5.58	12.03	1.66E6
Sample 15	14.93	0.78	3.11	1.24E6	28.22	5.83	12.26	1.67E6
Sample 16	14.98	0.78	3.19	1.24E6	28.30	5.98	12.31	1.67E6
Sample 17	15.05	0.78	3.22	1.24E6	28.65	6.05	12.51	1.68E6
Sample 18	15.08	0.80	3.23	1.25E6	28.78	6.13	12.69	1.71E6
Sample 19	15.13	0.80	3.26	1.25E6	29.46	6.43	12.69	1.73E6
Sample 20	15.15	0.87	3.30	1.26E6	29.96	6.75	13.82	1.78E6

Note that this is collection of different data sets, and that each data set has been sorted by magnitude. Hence, there is no connection between the values that are placed on the same row in the table.

Table C.1: Response samples for Hywind Demo fibre mooring configuration